

Summer 2007

# Nonlinear dynamical analysis of brain electrical activity due to exposure to weak environmentally relevant electromagnetic fields

Erik Alfonso Nilsen  
*Louisiana Tech University*

Follow this and additional works at: <https://digitalcommons.latech.edu/dissertations>



Part of the [Electromagnetics and Photonics Commons](#), and the [Neurology Commons](#)

---

## Recommended Citation

Nilsen, Erik Alfonso, "" (2007). *Dissertation*. 496.  
<https://digitalcommons.latech.edu/dissertations/496>

This Dissertation is brought to you for free and open access by the Graduate School at Louisiana Tech Digital Commons. It has been accepted for inclusion in Doctoral Dissertations by an authorized administrator of Louisiana Tech Digital Commons. For more information, please contact [digitalcommons@latech.edu](mailto:digitalcommons@latech.edu).

NONLINEAR DYNAMICAL ANALYSIS OF BRAIN ELECTRICAL ACTIVITY  
DUE TO EXPOSURE TO WEAK ENVIRONMENTALLY  
RELEVANT ELECTROMAGNETIC FIELDS

by

Erik Alfonso Nilsen, B.S.E.E., B.S.Math., M.S.E.E.

A Dissertation Presented in Partial Fulfillment  
of the Requirements for the Degree  
Doctor of Philosophy

COLLEGE OF ENGINEERING AND SCIENCE  
LOUISIANA TECH UNIVERSITY

August 2007

UMI Number: 3270947

### INFORMATION TO USERS

The quality of this reproduction is dependent upon the quality of the copy submitted. Broken or indistinct print, colored or poor quality illustrations and photographs, print bleed-through, substandard margins, and improper alignment can adversely affect reproduction.

In the unlikely event that the author did not send a complete manuscript and there are missing pages, these will be noted. Also, if unauthorized copyright material had to be removed, a note will indicate the deletion.

**UMI**<sup>®</sup>

---

UMI Microform 3270947

Copyright 2007 by ProQuest Information and Learning Company.

All rights reserved. This microform edition is protected against unauthorized copying under Title 17, United States Code.

ProQuest Information and Learning Company  
300 North Zeeb Road  
P.O. Box 1346  
Ann Arbor, MI 48106-1346

LOUISIANA TECH UNIVERSITY

THE GRADUATE SCHOOL

5/10/2007

Date

We hereby recommend that the dissertation prepared under our supervision  
by Erik Alfonso Nilsen

entitled Nonlinear Dynamical Analysis of Brain Electrical Activity due to  
Exposure to Weak Environmentally Relevant Electromagnetic Fields

be accepted in partial fulfillment of the requirements for the Degree of  
Doctor of Philosophy (PhD)

Rays Nassar  
Supervisor of Dissertation Research  
Richard F. Greechie  
Head of Department  
Computational Analysis and Modeling (CAM)  
Department

Recommendation concurred in:

Ulizhong Dai  
Ali P.  
Richard F. Greechie  
Likun

Advisory Committee

Approved: Bob Srinivasan  
Director of Graduate Studies

Approved: William M. Conolly  
Dean of the Graduate School

Steve Napp  
Dean of the College

GS Form 13  
(5/03)

## **ABSTRACT**

The reports dealing with the effects of weak electromagnetic fields (EMFs) on brain electrical activity have been inconsistent. We suspected that the use of linear models and their associated methods accounted for some of the variability, and we explored the issue by using a novel approach to study the effects of EMFs on the electroencephalogram (EEG) from rabbits and humans. The EEG was embedded in phase space and local recurrence plots were calculated and quantified to permit comparisons between exposed and control epochs from individual subjects. Statistically significant alterations in brain activity were observed in each subject when exposed to weak EMFs, as assessed using each of two recurrence-plot quantifiers. Each result was replicated; a sham exposure control procedure ruled out the possibility that the effect of the field was a product of the method of analysis. No differences were found between exposed and control epochs in any animal when the experiment was repeated after the rabbits had been killed, indicating that a putative interaction between the field and the EEG electrodes could not account for the observed effects. We conclude that EMF transduction resulting in changes in brain electrical activity could be demonstrated consistently using methods derived from nonlinear dynamical systems theory.

## APPROVAL FOR SCHOLARLY DISSEMINATION

The author grants to the Prescott Memorial Library of Louisiana Tech University the right to reproduce, by appropriate methods, upon request, any or all portions of this Dissertation. It is understood that "proper request" consists of the agreement, on the part of the requesting party, that said reproduction is for his personal use and that subsequent reproduction will not occur without written approval of the author of this Dissertation. Further, any portions of the Dissertation used in books, papers, and other works must be appropriately referenced to this Dissertation.

Finally, the author of this Dissertation reserves the right to publish freely, in the literature, at any time, any or all portions of this Dissertation.

Author Erik Alfonso Nilsen 

Date 05/10/2007

## TABLE OF CONTENTS

<b>ABSTRACT</b> .....	iii
<b>LIST OF TABLES</b> .....	viii
<b>LIST OF FIGURES</b> .....	ix
<b>ACKNOWLEDGMENTS</b> .....	xvi
<b>CHAPTER 1</b>	
<b>ELECTROMAGNETIC FIELD BIOLOGICAL EFFECTS</b> .....	1
1.1- Introduction to Electromagnetic Field Biological Effects.....	1
1.2 - Electromagnetic Fields and Their Interaction with Matter.....	4
1.3 - Function and Structure of the Brain .....	8
1.3.1 - Neuron Structure.....	8
1.3.2 - Neuron Resting Membrane Potential .....	10
1.3.3 - Neuron Action Potential .....	11
1.4 - Electroencephalogram.....	13
1.5 - EMF Electroencephalogram Effects .....	15
<b>CHAPTER 2</b>	
<b>LINEAR TIME SERIES ANALYSIS</b> .....	16
2.1 - Stochastic Time Series .....	16
2.2 - Linear Stochastic Models.....	18
2.2.1 - ARIMA Modeling and Analysis .....	18
2.2.2 - Spectral (Fourier) Modeling and Analysis.....	20
2.3 - Summary of Linear EMF EEG Analysis .....	22
<b>CHAPTER 3</b>	
<b>NONLINEAR DYNAMICAL TIME SERIES ANALYSIS</b> .....	25
3.1 - Deterministic Chaos.....	25
3.2 - Dynamical Systems.....	27
3.3 - Phase Space Reconstruction.....	29
3.4 - Nonlinear Dynamical Quantifiers .....	32
3.4.1 - Global Measures .....	32
3.4.2 - Local Measures .....	35

3.5 - Surrogate Data Analysis.....	36
3.5.1 - Surrogate Data Construction.....	37
3.5.2 - Surrogate Data Analysis of the Lorenz System .....	39
3.5.3 - Surrogate Data Analysis of Human EEG.....	42
3.6 - Nonlinear Dynamical EEG Evoked Response Model .....	44
3.6.1 - The Experimental Model System.....	44
3.6.2 - The Basic Hypothesis.....	45

#### **CHAPTER 4**

<b>CHANGES IN RABBIT BRAIN ELECTRICAL ACTIVITY DUE TO 60 HZ ELECTROMAGNETIC FIELDS.....</b>	<b>46</b>
4.1 - Methods.....	46
4.1.1 - Exposure System.....	46
4.1.2 - Animals .....	51
4.1.3 - Procedure .....	52
4.1.4 - EEG Analysis.....	54
4.1.5 - Statistics .....	55
4.2 – Results .....	55
4.3 – Discussion .....	67

#### **CHAPTER 5**

<b>CHANGES IN RABBIT BRAIN ELECTRICAL ACTIVITY DUE TO CELL PHONE ELECTROMAGNETIC FIELDS .....</b>	<b>70</b>
5.1 - Methods.....	70
5.1.1 - Exposure System.....	70
5.1.2 - Animals .....	72
5.1.3 – Procedure.....	72
5.1.4 - EEG Analysis.....	73
5.1.5 - Statistics .....	75
5.2 – Results .....	76
5.3 – Discussion .....	80

#### **CHAPTER 6**

<b>CHANGES IN HUMAN BRAIN ELECTRICAL ACITIVIY DUE TO 60 HZ ELECTROMAGNETIC FIELDS.....</b>	<b>85</b>
6.1 - Methods.....	85
6.1.1 - Exposure system .....	85
6.1.2 - Human Subjects .....	86
6.1.3 - Procedure .....	87
6.1.4 - EEG Analysis.....	88
6.1.5 - Statistics .....	88
6.2 – Results .....	90
6.3 - Discussion .....	93

<b>CHAPTER 7</b>	
<b>CONSISTENT EMF EEG EFFECTS .....</b>	<b>96</b>
<b>APPENDIX A</b>	
<b>NUMERICAL INTEGRATION OF THE LORENZ SYSTEM.....</b>	<b>98</b>
<b>APPENDIX B.....</b>	<b>100</b>
<b>CALCULATION OF THE WILCOXON SIGNED RANK STATISTIC .....</b>	<b>100</b>
<b>APPENDIX C .....</b>	<b>103</b>
<b>COMPUTATION OF THE LOGISTIC MAPPING .....</b>	<b>103</b>
<b>BIBLIOGRAPHY .....</b>	<b>104</b>

## LIST OF TABLES

Table 3.1: Surrogate data analysis results for the Lorenz system.....	41
Table 3.2: Surrogate data analysis results for 100 baseline EEG epochs.....	43
Table 5.1: Comparison of low-frequency spectral power in rabbit # 9 with that of the other male rabbits.....	83

## LIST OF FIGURES

Figure 1.1. Examples sources of electromagnetic fields: A) Cell phone tower, B) Power transmission lines.....	2
Figure 1.2: Health effects of electromagnetic fields.....	2
Figure 1.3: Locus of weak EMF transduction is unknown.....	3
Figure 1.4: Governing equations for electric and magnetic fields.....	5
Figure 1.5: The electromagnetic spectrum.....	6
Figure 1.6: An electromagnetic field.....	6
Figure 1.7: Anatomy of a neuron.....	10
Figure 1.8: An action potential.....	11
Figure 1.9: The chemical attributes of an action potential.....	12
Figure 1.10: Brain electrical activity of a healthy human. ....	13
Figure 1.11: International 10-20 system for EEG electrode placement.....	15
Figure 2.1: Percentage of subjects that responded to light as a function of the frequency at which the responses were observed (n = 28).....	23
Figure 2.2: Percentage of subjects that responded to EMFs as a function of the frequency at which the responses were observed (n = 53).....	23
Figure 3.1: Signal A was obtained from the logistic equation and signal B was generated by a random process. Both signals (shown in arbitrary units) appear to be noise (broadband spectra), but an optimal method of analysis (return map) yields a well-defined curve for signal A, suggesting that whatever gave rise to the data was deterministic, not random.....	26

Figure 3.2: The solid line depicts the relative humidity time series Predicted by model (the Lorenz system equations) for a given set of conditions. The dotted line shows the humidity under exactly the same conditions except that the initial temperature was increased by 0.000001°C; this change in temperature is regarded as an input to the weather system. The change had no effect on the prediction for about 1300 minutes. Thereafter, the two cases differed markedly, showing that long-term predictability is impossible because unavoidably small differences in initial conditions (state of system during application of stimulus) have large long-term effects.....27

Figure 3.3: Block diagram illustrating the logic of a surrogate data analysis.....39

Figure 3.4: A) Displays the original signal. B) Displays a surrogate for the original signal. The surrogate signal was constructed such that both the mean and power spectrum is commensurate to that of the original signal, as evidenced by the graphs in C) and D). So if any other structure existed (e.g., in the Fourier phase relations), it was intentionally destroyed via this transformation.....41

Figure 3.5: Recurrence plots produced from 2 s of human EEG data derived from an occipital electrode. The plots are symmetrical about the diagonals, which were added. (A) Original EEG (bottom) and associated plot (top). (B) Signal formed by randomizing the EEG (bottom); the recurrence plot (top) of the randomized signal is less deterministic than the plot for the original EEG (A, top). Recurrent points form distinct patterns characterized by %R and %D which, unlike the mean and standard deviation, are sensitive to nonlinear determinism present in the signal. N is number of recurrent points.....43

Figure 3.6: A) EEG response during application of controlled external stimuli (EMF). B) EEG response during the absence of controlled stimuli (EMF).....45

Figure 3.7: The baseline EEG is viewed as a complex combination of signals from many regions of the brain. The combined signal, as characterized by recurrence quantification analysis, is altered as a consequence of field transduction.....46

Figure 4.1: Schematic representation of the experimental system. A computer generated timing signal controlled switching of the stimulus. The timing signal was also fed into one of the channels of the EEG amplifier to facilitate identification of the exposed (E), sham (S), and control (C) epochs of the EEG in each trial (the *i*th trial is illustrated). The location of the rabbit relative to the field-producing coils (shaded bars) is shown.....48

Figure 4.2: Four multiple-turn coils used for global EMF exposure (b = 33.4 cm; a = 8.5 cm; d = 66 cm).....49

Figure 4.3: Magnetic field used for full-body exposure. The coils (shown in a side view as shaded bars) were energized to produce a homogeneous field in the region occupied by the rabbit (drawn approximately to scale).....	50
Figure 4.4: Magnetic field used for half-body field exposure. The coils Were energized (shaded) to maximize the difference in average field between the halves of the body. For exposure of the cranial half-body region, the rabbit was positioned in the coil unit as shown. For exposure of the caudal region, the box containing the rabbit was reversed (drawn approximately to scale).....	50
Figure 4.5: Sensory deprivation apparatus.....	52
Figure 4.6: The EEG is recorded continuously. The stimulus is applied for 2-second intervals, separated by 5 seconds. The exposed epoch consists of the 2-second epoch during which the stimulus is applied, and the corresponding control epoch is the 2-second interval that commences 3 seconds after termination of the stimulus.....	53
Figure 4.7: Percent Determinism in the EEG of rabbit no. 1, average over 50 trials.....	56
Figure 4.8: Local recurrence plots from rabbit no. 1 obtained by concatenating the field (left) and corresponding control (right) segments. The recurrent points are shows as regions of increased density that occur symmetrically about the diagonal. N is the point index number.....	57
Figure 4.9: Effect of 2.5 Gauss, 60 Hz in five female rabbits, as assessed using two RQA quantifiers. For each rabbit and each quantifier, the difference between the exposed and control EEG epochs was evaluated using the Wilcoxon signed-rank test. EEG window centered at 250 ms, with width of 250 ms. The average values of the quantifiers ( $\pm$ SD) and the 95% confidence limits of the test metric are presented.....	58
Figure 4.10: Percent Determinism in the EEG of rabbit no. 1, average over 50 trials.....	58
Figure 4.11: Effect of light on the EEG in five female rabbits, as assessed using two RQA quantifiers. For each rabbit and each quantifier, the difference between the exposed and control EEG epochs was evaluated using the Wilcoxon signed-ranked test. EEG window centered at 175 ms, with width of 266 ms. The average values ( $\pm$ SD) and 95% confidence limits of the test metric are presented for each rabbit.....	59

Figure 4.12: Local recurrence plots from rabbit no. 1 obtained by concatenating the light (left) and corresponding control (right) segments. The recurrent points are shown as regions of increased density that occur symmetrically about the diagonal. N is the point index number.....59

Figure 4.13: Reproducibility of the effect of 2.5 Gauss, 60 Hz on two RQA quantifiers of brain electrical activity in rabbit no. 1. EEG windows centered at 250 ms, with width of 250 ms. The average values of the quantifiers ( $\pm$ SD) and the 95% confidence limits of the test metric) are presented for each rabbit.....60

Figure 4.14: Effect of 2.5 Gauss, 60 Hz on the EEG in five male rabbits, as assessed using two RQA quantifiers. For each rabbit and each quantifier, the difference between the exposed and control EEG epochs was evaluated using the Wilcoxon signed-ranked test. EEG window centered at 175 ms, with width of 266 ms. The average values ( $\pm$ SD) and 95% confidence limits of the test metric are presented for each rabbit..... 61

Figure 4.15: Sham exposure of the brain of rabbits (temperature control). The current through the coils was identical to that used in Figure 14, but it resulted in no detectable magnetic field ( $< 0.01$  Gauss). For each rabbit and each quantifier, the exposed and control EEG epochs were compared using the Wilcoxon signed-rank test ( $n = 50$  trials). A 250-ms segment of the data from each epoch (centered at 250 ms from the beginning of the epoch) was evaluated. The average values ( $\pm$ SD) of the quantifiers are shown. The average and 95% confidence limits of the test metrics are shown for each rabbit in the third bar.....61

Figure 4.16: Magnetic field used for half-body field exposure. The coils were energized (shaded) to maximize the difference in average field between the halves of the body. For exposure of the cranial half-body region, the rabbit was positioned in the coil unit as shown. For exposure of the caudal region, the box containing the rabbit was reversed (drawn approximately to scale).....62

Figure 4.17: Effect of exposure to 60-Hz magnetic field such that the cranial and the caudal half-body regions were exposed to  $2.2 \pm 0.6$  and  $0.5 \pm 0.3$  Gauss, respectively (see Figure 3). For each rabbit and quantifier, the exposed and control EEG epochs were compared using the Wilcoxon signed-rank test ( $n = 50$  trials). A 250-ms segment of the data from each epoch (centered at 250 ms from the beginning of the epoch) was evaluated. The average values ( $\pm$ SD) of the quantifiers are shown. The average and 95% confidence limits of the test metrics are shown for each rabbit in the third bar.....63

Figure 4.18: Effect of exposure to 60-Hz magnetic field such that the cranial and the caudal half-body regions were exposed to  $0.5 \pm 0.3$  and  $2.2 \pm 0.6$  Gauss, respectively (see Figure 3). For each rabbit quantifier, the exposed and control EEG epochs were compared using the Wilcoxon signed-rank test ( $n = 50$  trials). A 250-ms segment of the data from each epoch (centered at 250 ms from the beginning of the epoch) was evaluated. The average values ( $\pm$ SD) of the quantifiers are shown. The average and 95% confidence limits of the test metrics are shown for each rabbit in the third bar.....63

Figure 4.19: Magnetic field used for exposure of rabbit eye. The field was produced using one coil (shown on the right). The field (averaged over a circular area in the transverse plane 1 cm in diameter centered on the coil axis) is shown as a function of distance from the coil. The average field over the retina (assumed to be at 1.5–2 cm) was  $2.8 \pm 0.5$  Gauss, 60 Hz.....64

Figure 4.20: Effect of exposure to a 60-Hz field of  $2.8 \pm 0.5$  Gauss, averaged over a transverse plane through the retina. For each rabbit and quantifier, the exposed and control EEG epochs were compared using the Wilcoxon signed-rank test ( $n = 50$  trials). A 250-ms segment of the data from each epoch (centered at 250 ms from the beginning of the epoch) was evaluated. The average values ( $\pm$ SD) of the quantifiers are shown. The average and 95% confidence limits of the test metrics are shown for each rabbit in the third bar.....65

Figure 4.21: Magnetic field used for exposure of rabbit brain (shaded outline). The field (averaged over a circular area in the sagittal plane 4 cm in diameter centered on the coil axis) is shown as a function of distance from the mid-point between the generating coils. The average field in the brain (assumed to be at 1.5 to 1.5 cm) was  $2.5 \pm 0.3$  Gauss, 60 Hz. Common axis of coils is shown as a dashed line.....66

Figure 4.22: Effect of exposure of the brain to  $2.5 \pm 0.3$  Gauss, 60 Hz ( $n = 5$ ) (see Figure 6). For each rabbit and quantifier, the exposed and control EEG epochs were compared using the Wilcoxon signed-rank test ( $n = 50$  trials). A 250-ms segment of the data from each epoch (centered at 250 ms from the beginning of the epoch) was evaluated. The average values ( $\pm$ SD) of the quantifiers are shown. The average and 95% confidence limits of the test metrics are shown for each rabbit in the third bar.....66

Figure 4.23: Sham exposure of the brain of rabbits (temperature control). The current through the coils was identical to that used in Figure 22, but it resulted in no detectable magnetic field ( $< 0.01$  Gauss). For each rabbit and each quantifier, the exposed and control EEG epochs were compared using the Wilcoxon signed-rank test ( $n = 50$  trials). A 250-ms segment of the data from each epoch (centered at 250 ms from the beginning of the epoch) was evaluated. The average values ( $\pm$ SD) of the quantifiers are shown. The average and 95% confidence limits of the test metrics are shown for each rabbit in the third bar.....67

Figure 5.1: Schematic representation of the experimental system. The detail shows the location of the EEG electrodes relative to the head antenna. A computer-regulated RF switch controlled the connection with the base station. In each trial, the connection was maintained through the head antenna during 0-2 sec and through the distant antenna during 2-7 sec. The effects on the EEG were ascertained by comparing exposed (E) and control (C) epochs in each trial, using the Wilcoxon signed-rank test ( $N=50$ , the  $i$ th trial is illustrated). Sham (S) and control epochs were compared as a control procedure. Light was used as a positive control stimulus.....71

Figure 5.2: Effect of cell-phone field on the EEG in 10 rabbits, as assessed using, the nonlinear quantifiers, %Determinism and %Recurrence. For each rabbit, a 250-msec segment of the data from each E epoch (centered at 250 msec from the beginning of the epoch) was compared with the similar segment of the control epoch in the same trial ( $N=50$ ). The data was filtered in the frequency domain and in phase space after which the nonlinear quantifiers were calculated from the recurrence plots and compared using the Wilcoxon signed-rank test. The average values ( $\pm$ SD) of the quantifiers are shown. The average and 95% confidence limits of the test metrics are shown for each rabbit in the third bar.....77

Figure 5.3: Effect of light on the EEG in 10 rabbits, as assessed using, the nonlinear quantifiers, %Determinism and %Recurrence. For each rabbit, a 250-msec segment of the data from each E epoch (centered at 175 msec from the beginning of the epoch) was compared with the similar segment of the control epoch in the same trial ( $N=50$ ). The data was filtered in the frequency domain and in phase space after which the nonlinear quantifiers were calculated from the recurrence plots and compared using the Wilcoxon signed-rank test. The average values ( $\pm$ SD) of the quantifiers are shown. The average and 95% confidence limits of the test metrics are shown for each rabbit in the third bar.....78

Figure 5.4: Effect of relocating the head antenna to the thoracic region, 1 cm from the rabbit, as assessed using, the nonlinear quantifiers, % Determinism and % Recurrence. For each rabbit, a 250-msec segment of the data from each E epoch (centered at 250 msec from the beginning of the epoch) was compared with the similar segment of the control epoch in the same trial (N=50). The data was filtered in the frequency domain and in phase space after which the nonlinear quantifiers were calculated from the recurrence plots and compared using the Wilcoxon signed-rank test. The average values ( $\pm$ SD) of the quantifiers are shown. The average and 95% confidence limits of the test metrics are shown for each rabbit in the third bar.....79

Figure 5.5: Results of control experiments performed on dead rabbits, as assessed, using the nonlinear quantifiers, %Determinism and %Recurrence. For each rabbit, a 250-msec segment of the data from each E epoch (centered at 250 msec from the beginning of the epoch) was compared with the similar segment of the control epoch in the same trial (N=50). The data was filtered in the frequency domain and in phase space after which the nonlinear quantifiers were calculated from the recurrence plots and compared using the Wilcoxon signed-rank test. The average values ( $\pm$ SD) of the quantifiers are shown. The average and 95% confidence limits of the test metrics are shown for each rabbit in the third bar.....80

Figure 6.1: Schematic representation of the experimental system. A computer generated timing signal controlled switches for the magnetic field and the light (S1 and S2, respectively). The timing signal was also fed into one of the channels of the EEG amplifier to facilitate identification of the exposed (E), sham (S), and control (C) epochs of the EEG in each trial (the *i*th trial is illustrated). Circle, field-producing coils.....86

Figure 6.2: Recurrence plots produced from 2 s of EEG data derived from an occipital electrode. The plots are symmetrical about the diagonals, which were added. (A) Original EEG (bottom) and associated plot (top). B) Signal formed by randomizing the EEG (bottom); the recurrence plot (top) of the randomized signal is less deterministic than the plot for the original EEG (A, top). Recurrent points form distinct patterns characterized by %R and %D which, unlike the mean and standard deviation, are sensitive to nonlinear determinism present in the signal. N is the recurrent point index.....90

Figure 6.3: Effect of magnetic-field exposure on the EEG derived from central, parietal, and occipital electrodes, assessed using %R. The window (width of 190 ms) for comparison of the exposed and control epochs was centered at 215 ms from the beginning of the epoch. The average values ( $\pm$ SD) of the quantifiers are shown, \*P < .05.....92

Figure 6.4: Effect of magnetic-field exposure on the EEG derived from occipital electrodes, assessed using %D. The window (width of 190 ms) for comparison of the exposed and control epochs was centered at 215 ms from the beginning of the epoch. The average values ( $\pm$ SD) of the quantifiers are shown, \*P < .05.....92

Figure 6.5: Effect of a light stimulus on the EEG derived from occipital electrodes, assessed using %R and %D. The window (width of 190 ms) for comparison of the light and control epochs was centered at 175 ms from the beginning of the epoch. The average values ( $\pm$ SD) of the quantifiers are shown, \*P < .05.....93

## ACKNOWLEDGMENTS

The following dissertation, while an individual work, benefited from the insights and direction of several people. First, my Dissertation Chair, Dr. Raja Nassar, exemplifies the high quality scholarship to which I aspire. In addition, he provided timely and instructive comments and at all stages of the dissertation process. Next, I wish to thank the complete Dissertation Committee, and outside reader, respectively: Dr. Richard Greechie, Dr. Andrei Paun, Dr. Li-He Zou, and Dr. Weizhong Dai, and Mr. Rocky Angelucci. I want to also acknowledge Dr. Andrew Marino (LSU Medical Center in Shreveport, LA) for his assistance and use of his laboratories during this work.

In addition to the technical and instrumental assistance above, I received equally important assistance from my family. In particular, my wife, Stacey Johnson-Nilsen, provided seemingly never ending emotional support throughout the entire dissertation process. I love you. Finally, I want to thank my mother, Karen Nilsen, and father, Thomas Nilsen Jr. (passed away in 1997), who instilled in me, from an early age, the desire and skill to obtain the PhD.

This dissertation is dedicated to, my two precious daughters, Ashtyn Nicolle Nilsen and Addisyn Lily Nilsen. I love you.

## **CHAPTER 1**

### **ELECTROMAGNETIC FIELD BIOLOGICAL EFFECTS**

#### 1.1- Introduction to Electromagnetic Field Biological Effects

Innumerable artificial and natural sources (Figure 1.1) generate electromagnetic energy in the form of electromagnetic waves, which continually interact with both physical and biological systems [1, 13, 15, 16, 56, 59, 60, 61]. The question of whether or not weak, environmental electromagnetic fields (EMFs) enter the human body and cause health effects (Figure 1.2) became prominent in the 1960's and a resurgence of interest in this area has recently occurred. A wide range of experiments specifically designed to study proposed EMF biological effects (bioeffects) has been performed. Because the experiments were performed by a variety of researchers from various disciplines, the problem has been approached using diverse techniques and methodologies. Despite all the research, no consensus exists in the scientific community that weak EMFs enter the human body and cause a significant bioeffect [19, 59, 60, 61]. The ever present and increasingly energetic nature of environmental EMFs emphasizes the importance of determining EMF bioeffects and their impact on human health [1, 59, 61].

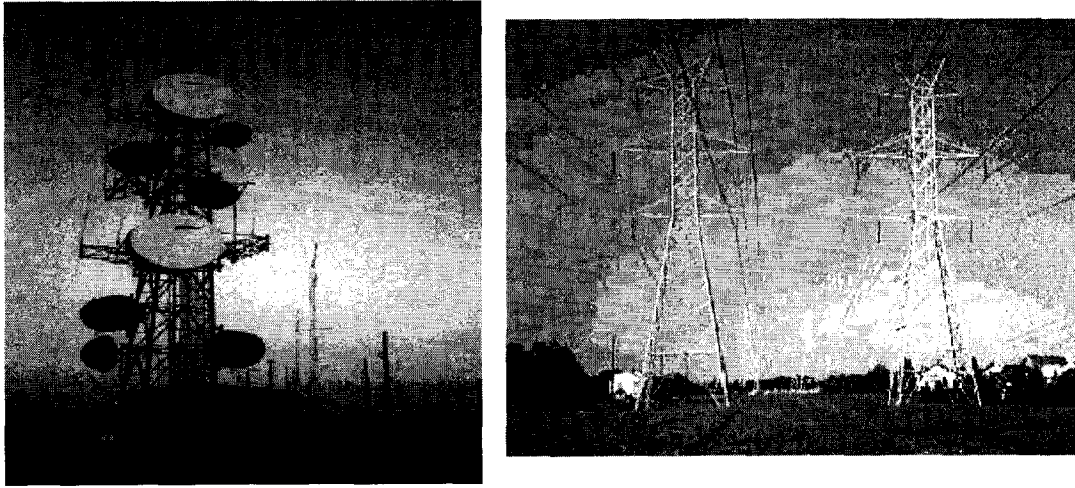


Figure 1.1: Examples sources of electromagnetic fields: A) Cell phone tower, B) Power transmission lines.

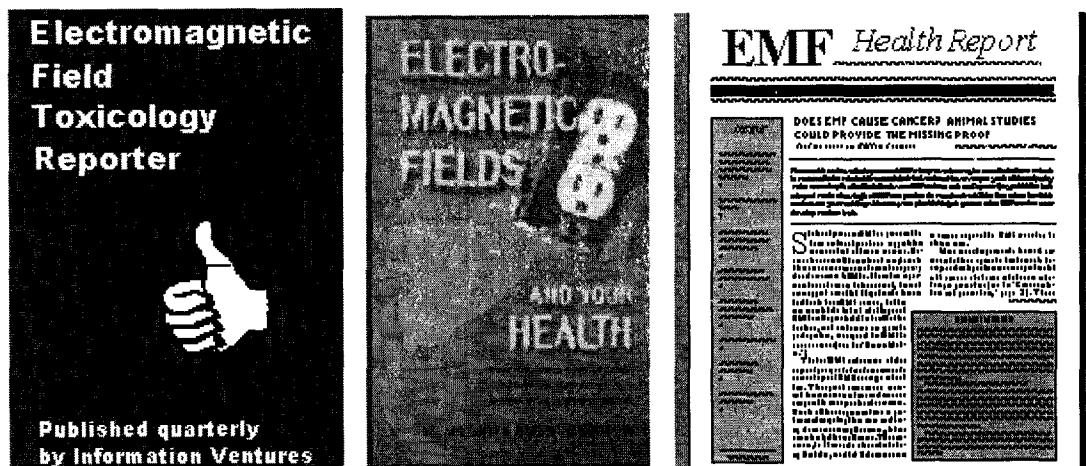
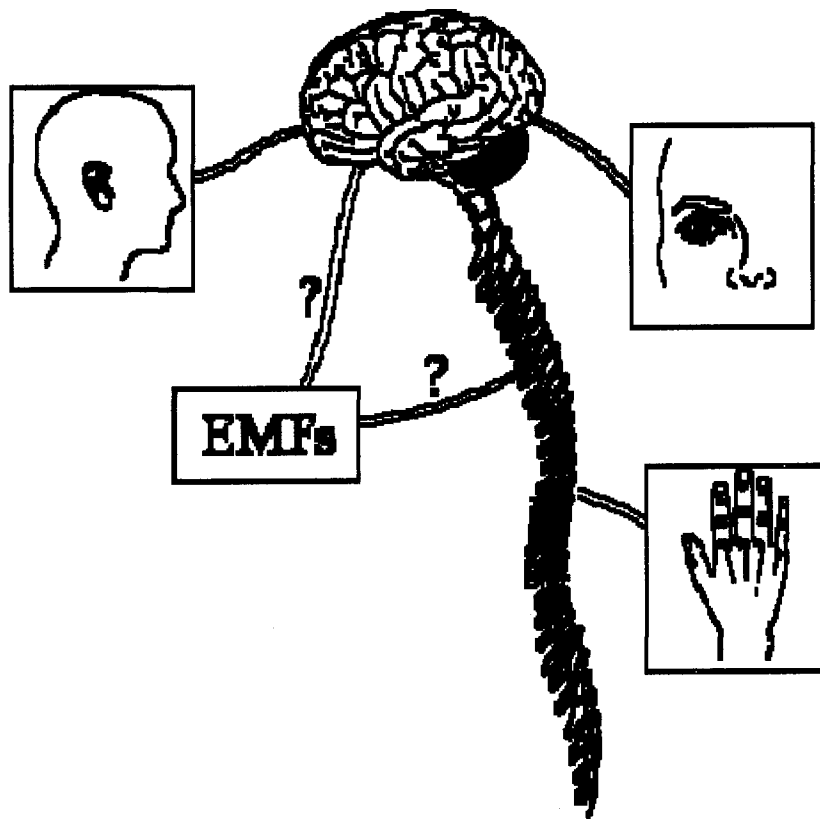


Figure 1.2: Health effects of electromagnetic fields.

Exposure to environmental EMFs has been linked to effects on the hematological, immunological, cardiovascular, and nervous systems of animals and humans, and with both the cure and cause of disease [6, 18, 21, 28, 22, 32, 39, 45, 50, 59]. The locus of EMF detection is unknown (Figure 1.3), but it is believed that the

induction of minute electric currents in the exposed system (transduction) is the first stage in a cascade of events that results in the reported biological effects [5, 6, 59].



**Figure 1.3:** Locus of weak EMF transduction is unknown.

Because environmental EMFs subject living tissues to currents that are much weaker than endogenous electrical activity (e.g., from the brain or heart), some scientists argue that it is improbable for environmental EMFs to have any important biological consequences [3, 4, 16, 18, 20, 56, 59, 61, 69]. Other scientists argue that, just as a trained ear can pick up a familiar voice in a crowd, a biological system can

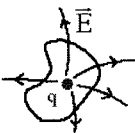
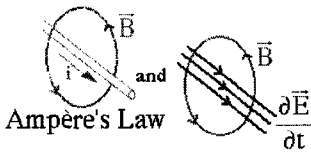
respond to minute current signals that are much smaller than the background noise arising from ongoing endogenous electrical activity [18, 24, 27, 30, 34, 38, 44, 62, 66, 76, 80].

There are many scientific publications describing both animal and human sub-systems, having highly specialized receptors, which are able to detect extremely weak signals in the presence of noise. One stark example can be found in the human eye, which can detect the presence of light by only a few photons landing on the retinal sub-system [60, 64].

### 1.2 - Electromagnetic Fields and Their Interaction with Matter

The effects of the electromagnetic waves upon systems are determined by the properties of the waves and the systems and the states of the exposed systems. Maxwell's equations (Figure 1.4) govern the interaction of EMFs with matter, but applying these equations to predict the EMF's interaction with biological matter has proved to be extremely difficult [1, 6, 60, 61, 69]. This difficulty results from the currently impossible task of completely specifying the properties and states of the biological system (e.g., a human); a task that is vital to accurately predict its interaction with a field [59].

## Maxwell's Equations

$\oiint \vec{E} \cdot \hat{n} \, dS = \frac{q}{\epsilon_0}$	Gauss's Law	
$\oiint \vec{B} \cdot \hat{n} \, dS = 0$	(no monopoles)	
$\oint \vec{B} \cdot d\vec{l} = \mu_0 \left( i + \epsilon_0 \frac{d\Phi_E}{dt} \right)$	Ampère's Law	
$\oint \vec{E} \cdot d\vec{l} = -\frac{d\Phi_B}{dt}$	Faraday's Law	
<hr style="width: 50%; margin: 0 auto;"/>		
$\nabla \cdot \vec{E} = \frac{\rho}{\epsilon_0}$	$\nabla \times \vec{B} = \mu_0 \left( \vec{j} + \epsilon_0 \frac{\partial \vec{E}}{\partial t} \right)$	
$\nabla \cdot \vec{B} = 0$	$\nabla \times \vec{E} = -\frac{\partial \vec{B}}{\partial t}$	
(Differential Forms)		

**Figure 1.4:** Governing equations for electric and magnetic fields.

In order to better understand EMF interactions with matter, it is essential to be familiar with the physical properties of the waves that make up the electromagnetic spectrum (Figure 1.5). Electromagnetic waves consist of electric (units of Volts per meter) and magnetic fields (units of Gauss) that oscillate in directions orthogonal to each other and to the direction of propagation (Figure 1.6). The waves are typically characterized by their amplitude, frequency (1 / wavelength), and propagation velocity [56]. The three parameters are interrelated and, hence, a change in any one of them influences the properties of the wave.

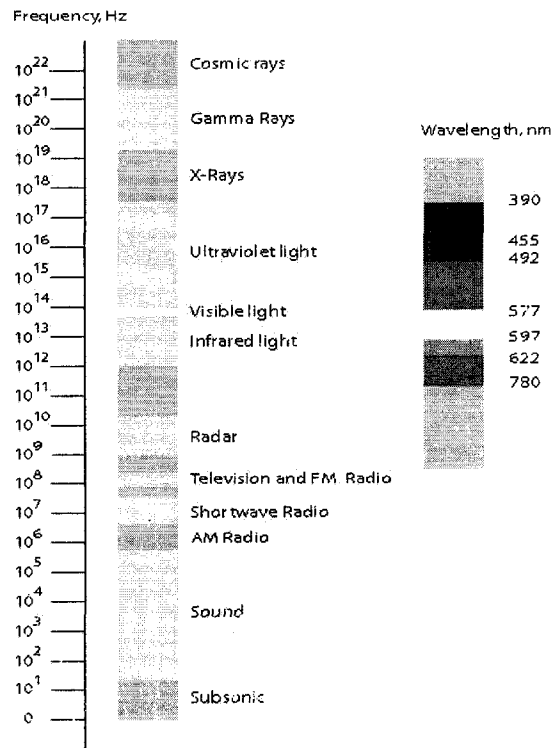


Figure 1.5: The electromagnetic spectrum.

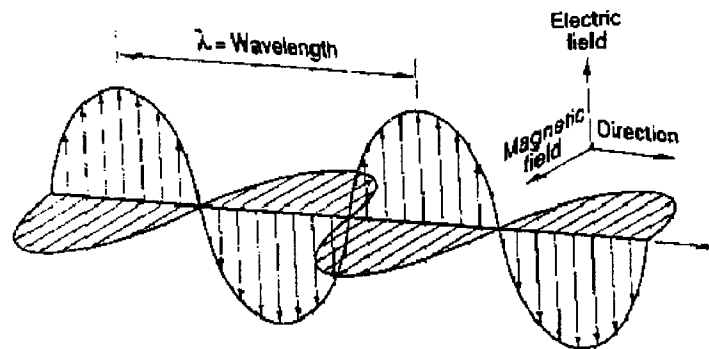


Figure 1.6: An electromagnetic field.

The frequency of an electromagnetic wave is simply the number of oscillations per unit of time and is measured in cycles per second, or Hertz (Hz). One cycle per

second equals one Hz. Large frequency divisions commonly used to describe waves include kilohertz (kHz), megahertz (MHz), and gigahertz (GHz). As the frequency of a wave increases, the distance (wavelength) between successive peaks decreases. Microwave ovens use a frequency of 2.45 billion hertz (2.45 GHz), which equates to a wavelength of 12.2 cm. The middle of the AM broadcast band operates at a frequency of one million hertz (1 MHz) and has an associated wavelength of about 300 meters. In the United States, power line distribution systems use a frequency of 60 Hz, which corresponds to a wavelength of 5000 km.

Electric and magnetic fields are composed of tiny packets of energy called photons. The energy in each photon is directly proportional to the frequency of the wave: the higher the frequency, the larger the energy in each photon. For example, a microwave field has more energy per photon than AM radio or power line fields. In the earth's atmosphere, the power of both electric and magnetic fields decreases as the distance between them and their source increases. Electric fields are easily shielded by conducting materials such as trees and buildings, whereas, magnetic fields are not significantly weakened when they pass through most materials, including humans [59, 61].

Electromagnetic waves at low frequencies are commonly called electromagnetic fields and those at much higher frequencies are called electromagnetic radiation. According to their frequency, electromagnetic waves can be classified as either ionizing or non-ionizing. Ionizing fields are extremely high-frequency electromagnetic waves that are capable of breaking atomic bonds. This phenomenon occurs when the photons absorbed by the atom have sufficient energy to free an electron from its attraction to the

nucleus [69]. It has been definitively shown that ionizing fields can cause irreversible damage to both biological and physical matter [1, 56, 59, 60, 61, 69]. Non-ionizing fields are EMFs with photon energies that are too weak to directly break atomic bonds. They include visible light, infrared radiation, microwave, radio frequency, extremely-low-frequency (ELF: frequencies below 3000 Hz) and static EMFs [59]. However, above a certain power-level, non-ionizing fields have also been conclusively shown to produce effects other than atomic bond breaking. For example, microwave fields, having wavelengths of several centimeters, possess enough energy significantly heat conducting materials [69]. Another example is that of visible light, which has been shown to influence the brain electrical activity in both humans and animals [64].

EMFs with energies low enough such that the change in temperature due to them is undetectable (e.g., a photon of visible light) are known as non-thermal (weak) electromagnetic fields [59]. Power (60 Hz) frequency fields have wavelengths of more than 5000 km and, consequently, have minute photon energy levels that do not cause measurable heating. However, these fields do create weak electric currents in conducting objects, including animals and humans [1, 56, 59, 60, 61, 66].

### 1.3 - Function and Structure of the Brain

#### 1.3.1 - Neuron Structure

The brain is the control center for the central nervous system and is responsible for the regulation of most vital biological functions and processes. Hence, an external stimulus that influences the brain electrical activity could potentially affect its subsequent control [2, 13, 15, 16, 25, 35, 42, 46, 47, 67, 79, 77].

The brain is composed primarily of living cells, namely neuronal and glial cells. Neurons transmit and receive electrochemical signals, whereas, the glial cells provide structural support for the ensemble of neuronal networks. The human brain contains about 100 billion neurons, each having a multitude of interconnections with other neurons, thereby allowing the brain to operate in massively parallel manner [70].

The neuron (Figure 1.7) consists of a cell body with branching dendrites (signal receivers) and a projection called an axon, which conducts the nerve signal. The axon, a long extension of a nerve cell, carries information away from the cell body. Bundles of axons are known as nerves, nerve tracts or pathways. Myelin coats and insulates the axon (except for periodic breaks, called nodes of Ranvier), increasing the transmission speed along the axon. Myelin is manufactured by Schwann's cells, and consists of 70-80% lipids (fat) and 20-30% protein. At the other end of the axon, the axon terminals transmit the electrochemical signal across a gap (synapse), between the axon terminal and the receiving cell. Dendrites branch from the cell body and carry information into the cell body. The cell body contains the neuron's nucleus (with DNA and typical nuclear organelles). A typical neuron has about 1,000 to 10,000 synapses, that is, it communicates with 1,000-10,000 other neurons [70].

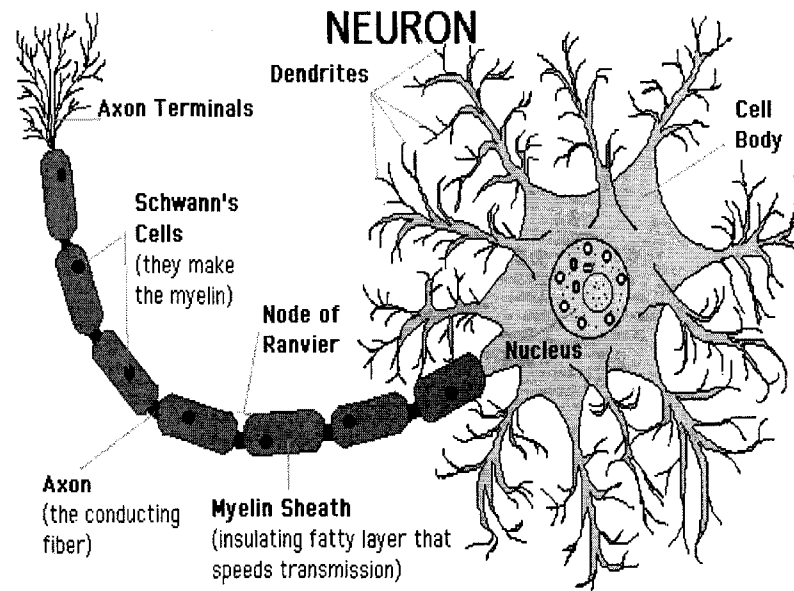


**Figure 1.7:** Anatomy of a neuron.

### 1.3.2 - Neuron Resting Membrane Potential

Neurons send messages using an electrochemical process. When chemicals in the body are electronically charged, they are called ions. The important ions in the central nervous system are sodium and potassium (both having a single positive charge), calcium (having two positive charges), and chloride (having a single negative charge). There are also some negatively charged protein molecules. Semi-permeable membranes encase neuronal cells, thereby allowing only certain ions to pass through. When a neuron is not sending a signal, it is said to be at rest or idle. For an idle neuron, the potential inside of the neuron is negative relative to the outside. The concentrations of the ions attempt to equate on both sides of the membrane, but are prevented from reaching an even density state by the membrane's ion channels, which allow only specific ions to pass. At rest, potassium ions ( $K^+$ ) can easily cross through the membrane, whereas chloride ( $Cl^-$ ) and sodium ions ( $Na^+$ ) are resisted. The

negatively charged protein molecules inside the neuron are also resisted by the cell membrane. In addition to these selective ion channels, the cell is programmed to transfer three sodium ions out of the neuron for every two potassium ions it receives. When all these forces are at equilibrium, the potential difference between the inside and outside of the neuron is approximately  $-70$  mV. This is the resting membrane potential of a neuron [59, 70].

### 1.3.3 - Neuron Action Potential

The initiation of an action potential begins with an exchange of ions across the neuronal membrane. A stimulus (e.g., from another neuron) first causes the opening of sodium channels. The high concentration of sodium ions outside of the cell in conjunction with the negative charge on the interior causes sodium ions to rush into the neuron via the membrane. This action results in the neuron becoming more positive and, consequently, depolarized. There is a small latency period before the potassium channels open, allowing  $K^+$  ions to leave the cell, thus reversing the depolarization. At this time, the sodium channels start to close. This causes the action potential to return to  $-70$  mV (a repolarization). The action potential actually exceeds  $-70$  mV (a hyperpolarization) because the potassium channels remain open for longer. Gradually, the ion concentration returns to equilibrium, returning the cell to its  $-70$  mV resting potential (Figures 1.8, 1.9) [71].

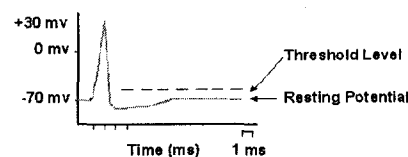


**Figure 1.8:** An action potential.

The action potential illustrates the activity of a neuron transmitting information from one cell to another. The action potential is a burst of electrical activity that is triggered by a depolarizing current. That is to say, a stimulus causes the resting potential to move toward 0 mV. When the depolarization reaches about -55 mV, a typical neuron's threshold, it will fire an action potential. If the neuron does not reach this critical threshold level, no action potential will fire. Furthermore, when the threshold level is reached, an action potential of fixed magnitude will typically fire; an exception always fire. For any given neuron, the size of the action potential is usually the same, thereby producing transmitted information that is mostly frequency encoded [59, 70, 71].

A simple analogy between digital logic gates and neuronal action potentials can be drawn: neurons can act as switches or logical decision units that direct the flow of information. Depending upon the pattern of signals arriving at its synapses (i.e., stimuli at neuron inputs) a neuron either does or does not send new signals along its axon. Thus, the brain can be thought of as a complex network of interconnected decision-making elements.

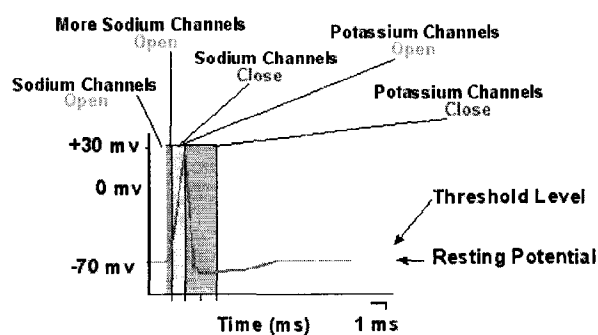
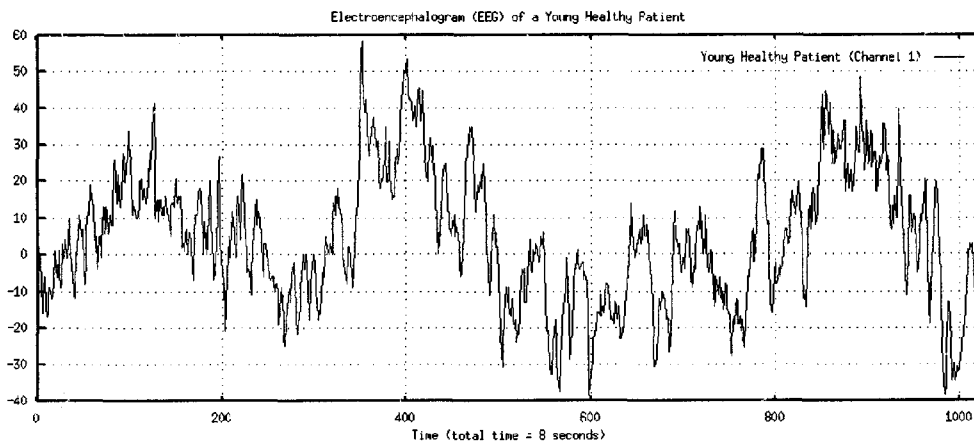


Figure 1.9: The chemical attributes of an action potential.

### 1.4 - Electroencephalogram

The brain is arguably the most complex system known to man. It is therefore not surprising that signals arising from the brain are also complex. Brain electrical signals measured from healthy animals and humans are aperiodic (irregular) and bounded (Figure 1.10) [24]. When these irregular waves are acquired using electrodes placed on the surface of the skull, the resulting potential fluctuations are time-dependent signals known as the surface electroencephalogram (EEG). When measuring the EEG, at least two electrodes are placed at different locations on the surface on the skull. The potential differences between the electrodes are filtered, amplified, digitized, and then transferred to memory in a digital computer. Subsequent digital signal analysis and processing can then be performed upon the EEG [78].



**Figure 1.10:** Brain electrical activity of a healthy human.

It is generally agreed upon that the electrical activity measured on the scalp is in most cases not the effect of the ion flows associated with action potentials themselves. These action potentials are too brief (1-2 ms) and irregular to produce any appreciable

net changes in ion concentration, with possible exceptions for brain stem and early evoked responses. Rather, the EEG originates mainly from the summed dendritic extracellular changes in ion concentrations that result from chemically mediated EPSPs and IPSPs (increased outflow of potassium together with even more increased inflow of sodium, and inflow of chloride, respectively), and last for about 10-250 ms. The mechanism of this source is therefore much more akin to the summation of dendritic inputs within the cell, which integrates over time as well as over inputs, than to single axonal discharges. The accumulations of charge outside the dendrite cause electric currents that flow through the surrounding media (brain tissue, dura mater, cerebrospinal fluid, skull, and skin). These electric currents finally change the electrical potentials on the scalp by Ohm's law, due to the electrical resistance of the tissue [59].

To facilitate a standardized approach in performing brain wave studies, the international 10-20 electrode system was established (Figure 1.11) [26]. The values 10 or 20 refer to the 10% or 20% interelectrode distance. The 10-20 system dictates the relationship between the location of an electrode and the underlying area of cerebral cortex. Each point on the accompanying figure indicates a possible electrode position. Each site has a letter to identify the lobe and a number or another letter to identify the hemisphere location. The letters F, T, C, P, and O stand for Frontal, Temporal, Central, Parietal, and Occipital. Even numbers (2, 4, 6, 8) refer to the right hemisphere and odd numbers (1, 3, 5, 7) refer to the left hemisphere. The z refers to an electrode placed on the midline. Also note that the smaller the number, the closer the position is to the midline.

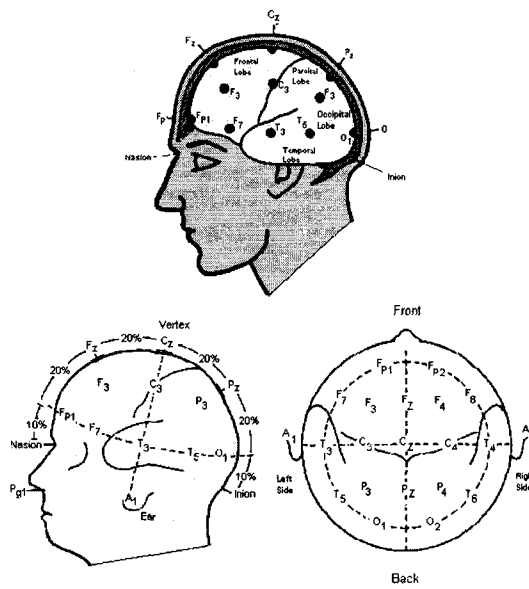


**Figure 1.11:** International 10-20 system for EEG electrode placement.

### 1.5 - EMF Electroencephalogram Effects

A deeper understanding of the changes in brain electrical activity produced during application of electromagnetic fields (EMFs) is the goal of different lines of research including transcranial stimulation (TS) [40, 43, 72] and evaluation of the public-health significance of fields in the environment [59]. The major unresolved issues regarding TS relate primarily to therapeutic consequences, because the detection process is reasonably well understood. For environmental EMFs, however, which typically are 3 or more orders of magnitude smaller than those used for TS, the central question concerns whether the fields are actually detected by subjects.

Group effects of low-strength EMFs on brain electrical activity were found in some studies; for example, subjects exposed to 3 Hz, 1 Gauss, and to 50 mGauss, pulsed at 6–20 Hz exhibited significantly reduced spectral power, on average [8, 9, 12, 14, 20, 31, 46]. In another studies, however, no average effect on spectral power was

found after exposure to 100 mGauss, 60 Hz [31, 45]. Mixed results also occurred when the effect of EMFs on brain electrical activity was assessed within individual subjects [10, 11, 14, 22, 37]. Exposure to 0.25–5.0 Gauss, 35–40 Hz produced changes in the EEG in only 7 of 14 subjects [10, 11]. Application of 10–40 Gauss DC altered the epileptiform spike activity in only 5 of 10 patients in the period immediately following application of the field [21]. Eleven subjects exposed to 0.8 Gauss, 1.5–10 Hz exhibited increased spectral power, but 8 subjects exhibited no effect [50]. These and other pertinent studies have been reviewed recently [18].

Various explanations could account for why EMFs altered the EEG in some studies or subjects, but not others. The apparent inconsistencies could have arisen from inter-subject variations in sensitivity to the EMF; that is, some subjects may not be sensitive to the EMF. The spectral properties of the EMF may be important in determining its biological effect, with the result that field effects occur only within particular windows of frequency or field strength [30]. Another possibility is that the absence of an effect in some subjects or some groups of subjects was due to a relative insensitivity of the methods used to analyze the EEG, which in all the previous studies were linear methods.

## CHAPTER 2

### LINEAR TIME SERIES ANALYSIS

#### 2.1 - Stochastic Time Series

A stochastic time series is defined as a random phenomenon that is a function of time. The time series, denoted by

$$\{ X(t), t \in T \} \text{ or } \{ X_t, t \in T \},$$

is called a discrete time series, and the set  $T$  (called the time domain) is a subset of all integers  $\{0, \pm 1, \pm 2, \dots, \pm N\}$ .

Traditionally, aperiodic (stochastic) time series, such as the EEG, have been modeled as linear, stochastic processes in both the time and frequencies domains. Under these models, the irregular signal is assumed to arise from a linear, deterministic system that is continually perturbed by external, stochastic driving forces. The stochastic driving forces are required because without external perturbations, a linear system can only display behavior that, in the limit, grows to infinity, decays to zero, or oscillates forever; that is to say, irregular behavior can not exist in a linear deterministic system [41,86].

## 2.2 - Linear Stochastic Models

### 2.2.1 - ARIMA Modeling and Analysis

An important class of stochastic models for discrete time series  $\{X_t, t \in T\}$  is the autoregressive model. In this model, a present value of the process is expressed as a finite linear combination of the past values of the process plus a random shock. An example of this model is given by

$$X_t = \phi_1 X_{t-1} + \phi_2 X_{t-2} + \dots + \phi_p X_{t-p} + a_t. \quad (2.1)$$

Where  $\{a_t, t \in T\}$  is a set of independent and identically distributed random variables with mean 0 and a finite common variance  $\sigma^2$ , and  $\phi_1, \phi_2, \dots, \phi_p$  are parameters to be estimated from the data. The set  $\{a_t\}$  is usually referred to as white noise. A stochastic time series which satisfies the model (2.1) is called as autoregressive process of order  $p$  or an AR( $p$ ) process [86].

Another model is the moving average model. In this model the value of the time series at time  $t$ ,  $X_t$ , is assumed to be a finite weighted sum of past random shocks  $a_t, a_{t-1}, \dots$ . For instance, the model

$$X_t = a_t - \theta_1 a_{t-1} - \theta_2 a_{t-2} - \dots - \theta_q a_{t-q}, \quad (2.2)$$

is called a moving average model of order  $q$ .  $\theta_1, \dots, \theta_q$  are parameters to be estimated. A stochastic time series which satisfies (2.2) is called a moving average process of order  $q$  or an  $MA(q)$  process [86].

The previous two classes of models can be combined to form an autoregressive moving average (ARMA) model. This model includes both autoregressive (feed back) and moving average (feed forward) components. An example of an ARMA model is given by

$$X_t = \phi_1 X_{t-1} + \dots + \phi_p X_{t-p} + a_t - \theta_1 a_{t-1} - \dots - \theta_q a_{t-q}. \quad (2.3)$$

A stochastic time series  $\{X_t, t \in T\}$  which satisfies the model (2.3) is called an autoregressive moving average process of order  $(p, q)$  or an  $ARMA(p, q)$  process [86].

In practice, some time series seem to be generated by probabilistic mechanisms which stay the same over time. In this case, the time series vary around a fixed mean and the dependence between the members of the series tends to be a function of the time difference between the members rather than their particular position in time. These kinds of stochastic processes are called weakly stationary (w-stationary) process. The ARMA model may represent a w-stationary process under certain conditions [86].

Many time series encountered in practice exhibit non-stationary behavior; however, some of these non-stationary time series may be transformed into w-stationary series by differencing them several times. More specifically, if the time series  $\{X_t, t \in T\}$  is non-stationary, one may be able to obtain a w-stationary time series by considering instead the differenced process  $\{W_t = X_t - X_{t-1}, t \in T\}$ . This kind of process is usuall

called autoregressive integrated moving average process of order (p,d,q) or an *ARIMA* (*p,d,q*) process, where p and q are defined as before, and d is the number of times the process is differenced in order to produce a w-stationary one [86].

### 2.2.2 - Spectral (Fourier) Modeling and Analysis

Spectrum analysis is concerned with the detection and exploration of cyclical patterns of data. A complex time series is decomposed into its sinusoidal (sine and cosine) functions of particular amplitudes and wavelengths. This analysis can uncover recurring cycles of different lengths in the time series, which at first looked more or less like random noise [41, 86].

To contrast this technique with ARIMA analysis, this analysis identifies the periodic fluctuations of different lengths (frequencies), while in the former types of analysis, the length of the periodic component is usually known (or guessed) *a priori* and then included in some theoretical model of moving averages or autocorrelations.

The periodogram is the simplest spectrum and it is commonly used estimate the amplitude of the largest sine component within the time series. In order to illustrate the calculation of the periodogram, suppose that the number of observations is odd. If we fit the Fourier series model

$$X_t = \alpha_0 + \sum_{i=1}^{\frac{N-1}{2}} (\alpha_i c_{it} + \beta_i s_{it}) + e_t ,$$

where

$X_t$  (is a w-stationary time series)

$$c_{it} = \cos(2\pi f_i t)$$

$$s_{it} = \sin(2\pi f_i t)$$

$e_i$  (is the residual or error)

$f_i = i/N$  (is the  $i$ th harmonic of the fundamental frequency  $1/N$ ).

Then the least squares estimates of the parameters  $\alpha_0, (\alpha_i, \beta_i)$  will be

$$\left. \begin{aligned} \hat{\alpha}_0 &= \bar{z} \\ \hat{\alpha}_i &= \frac{2}{N} \sum_{t=1}^N z_t c_{it} \\ \hat{\beta}_i &= \frac{2}{N} \sum_{t=1}^N z_t s_{it} \end{aligned} \right\} i = 1, 2, \dots, \frac{N-1}{2}.$$

And the periodogram then consists of the  $(N-1)/2$  values

$$I(f_i) = \frac{N}{2} (\hat{\alpha}_i^2 + \hat{\beta}_i^2), \quad i = 1, 2, \dots, \frac{N-1}{2},$$

where  $I(f_i)$  is called the intensity or amplitude at frequency  $f_i = i/N$ . The definition of the periodogram assumes that the frequencies  $f_i = i/N$  are harmonics of the fundamental frequency  $1/N$ . If this assumption is relaxed and the frequency is allowed to vary continuously in the range  $0-F$  Hz, the definition of the periodogram may be modified to

$$I(f) = \frac{2}{N} (\hat{\alpha}_f^2 + \hat{\beta}_f^2), \quad 0 \leq f \leq F$$

and  $I(f)$  is then referred to as the sample spectrum. It is used to detect and estimate the amplitude of sinusoidal components of unknown frequencies  $f$ . The power spectrum is defined by

$$p(f) = \lim_{N \rightarrow \infty} E[I(f)],$$

where  $E$  is the expectation operator [86].

Because the autocorrelation function and the spectrum are transforms of each other, they are mathematically equivalent and therefore any discussion on their advantages and disadvantages turns not on mathematical questions, but on their representational value [86].

### 2.3 - Summary of Linear EMF EEG Analysis

The reports dealing with the effects of weak electromagnetic fields (EMFs) on brain electrical activity have been inconsistent [59, 18]. Our review of these studies suggested that the inconsistencies were due to the use of linear methods. For example, a recent report showed that both weak low-frequency EMFs and visible light inconsistently affected the EEG in rabbits and humans. However, the rate of detection of the effects in the EEG due to the two stimuli differed, but in both cases was fewer

than all of the subjects (Figures 2.1, 2.2) [50]. Because all subjects were cognizant of their exposure to light and awareness is a centrally-mediated phenomenon, the experimental results suggest that at least some of the negative responses consisted of false negatives.

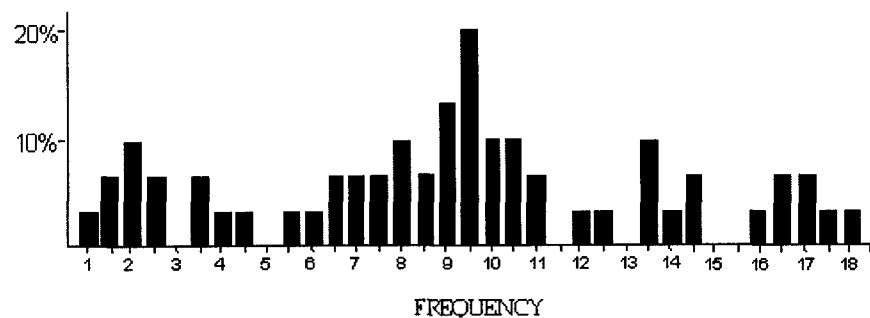


**Figure 2.1:** Percentage of subjects that responded to light as a function of the frequency at which the responses were observed ( $n = 28$ ).

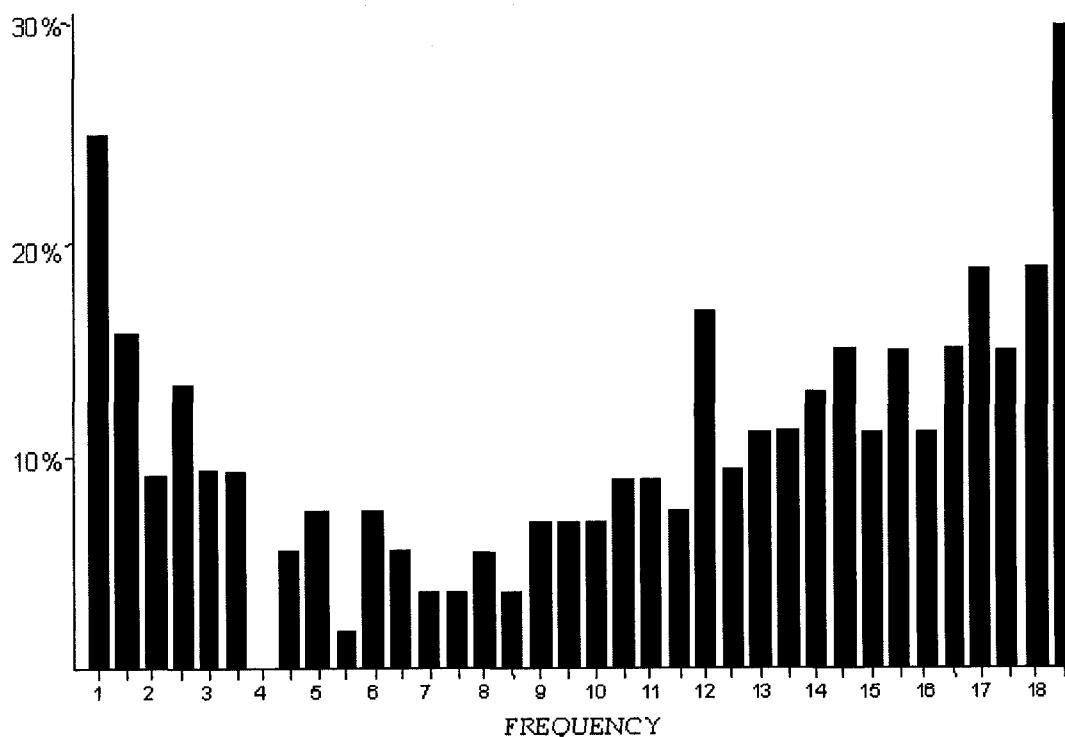


**Figure 2.2:** Percentage of subjects that responded to EMFs as a function of the frequency at which the responses were observed ( $n = 53$ ).

For many years, researchers did not have a choice of analyses for irregular behavior other than those derived from linear, stochastic models [37, 41, 85]. Recent studies suggested that the EEG can exhibit nonlinear determinism (law-like behavior) due to low-dimensional chaotic sources [2, 43, 55]. An analytical approach that also took nonlinear effects into consideration might lead to a more consistent picture of the changes in brain electrical activity produced during application of EMFs.

## **CHAPTER 3**

### **NONLINEAR DYNAMICAL TIME SERIES ANALYSIS**

#### 3.1 - Deterministic Chaos

Deterministic chaos theory offers a striking explanation for irregular behavior and in both physical and biological systems [55, 74]. The most direct link between chaos theory and the real world is the analysis of time series in term of nonlinear dynamics. The framework of deterministic chaos constituted a new approach to the analysis of time series. It has been shown that simple (low dimensional) chaotic dynamical systems can exhibit irregular time evolution even without random inputs (Figure 3.1) [85]; see APPENDIX C for code for computing Logistic mapping.

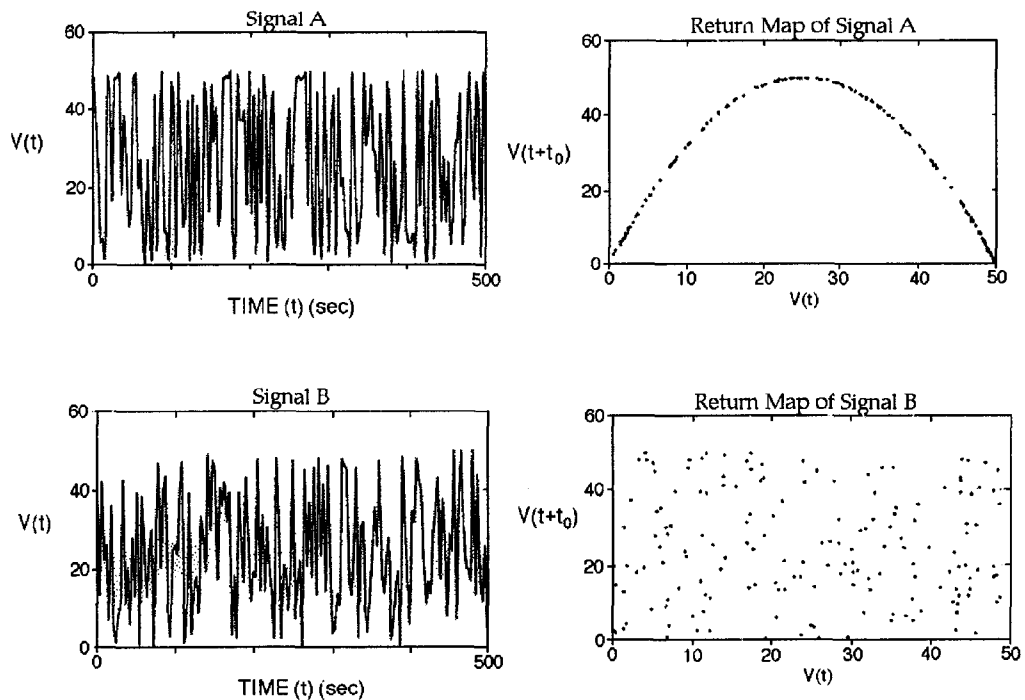


**Figure 3.1:** Signal A was obtained from the logistic equation and signal B was generated by a random process. Both signals (shown in arbitrary units) appear to be noise (broadband spectra), but an optimal method of analysis (return map) yields a well-defined curve for signal A, suggesting that whatever gave rise to the data was deterministic, not random.

One potential benefit of the nonlinear approach is that it may be capable of extracting determined features in the EEG even when linear methods are not successful in doing so [51, 75]. For example, nonlinear analysis allows discrimination between two complex dynamical states that do not differ significantly in their ARIMA or spectral properties [41]. Another advantage of a nonlinear model is that it is capable of responding to extremely weak stimuli, such as an environmental EMF. An example of a physical dynamical system that displays this type of sensitivity to initial conditions can be found in a simplified model of the weather (Figure 3.2) [85]; see APPENDIX A for MATLAB code for numerical integration of Lorenz system.

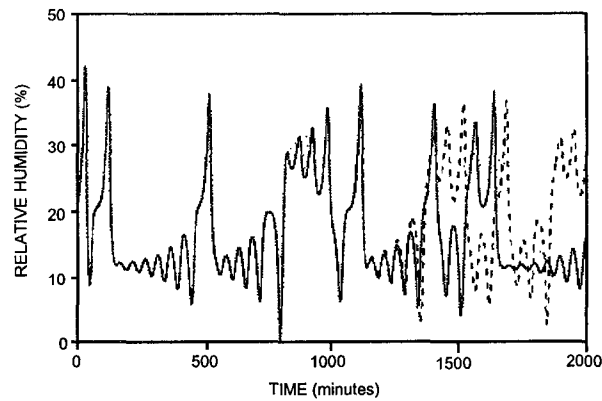


**Figure 3.2:** The solid line depicts the relative humidity time series predicted by a model (the Lorenz system equations) for a given set of conditions. The dotted line shows the humidity under exactly the same conditions except that the initial temperature was increased by  $0.000001^{\circ}\text{C}$ ; this change in temperature is regarded as an input to the weather system. The change had no effect on the prediction for about 1300 minutes. Thereafter, the two cases differed markedly, showing that long-term predictability is impossible because unavoidably small differences in initial conditions (state of system during application of stimulus) have large long-term effects.

### 3.2 - Dynamical Systems

In dynamical systems theory it is a common problem to analyze a discrete set of observed quantities (a time series). Consider for example the dynamical system defined by the differential equation

$$\frac{dy}{dt} = F(y),$$

where  $y(t) = (y_1, y_2, \dots, y_s)^T \in S$  is a vector representing the state of a the system at time  $t$  in some  $s$ -dimensional phase space  $S$ . The vector field (or evolution function)  $F : S \rightarrow TS$  (TS is the tangent space of  $S$ .) induces the flow

$$\begin{aligned} \mathcal{G}_t : S &\rightarrow S \\ y(t) &= \mathcal{G}_t(y_0); \end{aligned} \quad (3.1)$$

here,  $y_0$  comes from the initial condition  $y(t=0) = y_0$  [87].

Alternatively, one might have a discrete dynamical system, defined by the mapping

$$y_{n+1} = \mathcal{G}(y_n), n = 0, 1, 2, \dots, \quad (3.2)$$

where  $y_n \in S, \mathcal{G} : S \rightarrow S$ , and get the time  $\{v_n \equiv v(y_n)\}_{n \in \{0, 1, 2, \dots\}}$ .

As the system evolves, the trajectory in the phase space  $S$  approaches an attractor  $A$  which lies within some submanifold  $M$  of  $S$ :

$$A \subseteq M \subseteq S,$$

where  $\dim A \leq \dim M \leq \dim S$ . The dynamical system is dissipative; that is, the phase flow (trajectory) or map contracts volume in phase space [41, 87].

Often, when one analyzes a system, the analytic solution of  $y(t)$  (3.1) or  $y_{n+1}$  (3.2) is not known. Instead, only a time series is available, a series of values of one single quantity sampled at regular intervals:

$$v(y_0), v(\mathcal{G}_\tau(y_0)), v(\mathcal{G}_{2\tau}(y_0)), \dots \equiv v_0, v_1, v_2, \dots$$

$v(\mathcal{G}_t(y_0)) = v(y(t))$  is the value of some observable  $v$  of the system at time  $t$ .

The time interval  $\tau$  between two successive measurements of  $v$  is the sampling time or delay time.  $\tau$  need not be fixed; it is possible to consider the sequence

$$v(\mathcal{G}_{t_0}(y_0)), v(\mathcal{G}_{t_1}(y_0)), v(\mathcal{G}_{t_2}(y_0)), \dots \equiv v_0, v_1, v_2, \dots$$

as well, where the times  $t_0 < t_1 < t_2 < \dots$  are not equidistant [87].

### 3.3 - Phase Space Reconstruction

As described in the previous section, a dynamical system can be represented by a phase space model, where the states of the system evolve in accordance with a deterministic evolution operator (transfer function) and the measurement function maps the states to the observables [41]. To characterize the governing dynamical system from an observed time series, it is necessary to reconstruct a phase space from the time series.

The simplest method for phase space construction is known as time-delay embedding. In this method, a phase space is reconstructed, from an observed scalar time series, by using delayed copies of the original time series as components of the reconstructed phase space (RPS). The embedding theorem of Takens [87] guarantees that the RPS space portrays the dynamics of the true phase space; that is, there exists a diffeomorphism that maps the RPS to the true phase space. The interaction among the variables in the system allows embedding technique to reveal the mapping of the true state vector to the reconstructed state vector [41]. In other words, one variable carries

the information of all other variables that played a role in the generation of the observed signal.

Time-delay embedding involves sliding a window of length  $m$  through the data to form a series of vectors, stacked row-wise in the matrix. Each row of this matrix is a point in the RPS. Letting  $\{x_i\}$  represent the time series, the RPS is represented as:

$$X = \begin{pmatrix} x_0 & x_\tau & \cdots & x_{(m-1)\tau} \\ x_1 & x_{1+\tau} & \cdots & x_{1+(m-1)\tau} \\ x_2 & x_{2+\tau} & \cdots & x_{2+(m-1)\tau} \\ \vdots & & & \vdots \end{pmatrix},$$

where  $m$  is the embedding dimension and  $\tau$  is the embedding delay [87].

Schuster [35] proposed to base the choice of  $\tau$  and  $m$  on the idea that an embedding using delay coordinates is a topological mapping that preserves neighborhood relations. This means that points on the attractor in  $M$  which are near to each other should also be near in the embedding space  $\mathfrak{R}^m$ .

The distance of any two points  $x_i, x_j \in \mathfrak{R}^m$  cannot decrease but only increase when one increases the embedding dimension  $m$ . But if this distance increases under a change from  $m$  to  $m+1$  then  $m$  is not sufficiently large.  $m$  being too small means that the attractor is projected onto a space of lower dimensionality  $m$  and this projection possibly destroys neighborhood relations, resulting in some points appearing nearer to each other in the embedding space than they actually are. For example,  $x_j$  may be the nearest neighbor of  $x_i$  in  $\mathfrak{R}^m$  although this is not true in the proper embedding space

$\mathfrak{R}^{m+1}$ . If  $m$  is sufficiently large, then the distance of any two points of the attractor in embedding space should stay the same when one changes  $m$  into  $m+1$ .

Applying this geometrical point of view, one can find the proper embedding dimension by choosing initially a small value of  $m$  and then increasing it systematically. One knows that the proper value of  $m$  is found when all distances between any two points  $x_i$  and  $x_j$  do not grow any more when increasing  $m$ . Practically, one constructs the quantity

$$Q(i,k,m) = \frac{d_{m+1}(x_i(m+1), x(i,k,m+1))}{d_m(x_i(m), x(i,k,m))},$$

where  $x_i(m)$  is the  $i$ -th reconstructed vector in  $m$ -dimensional embedding space,

$$x_i(m) = (v_i, v_{i+1}, \dots, v_{i+m+1})^T \in \mathfrak{R}^m, \text{ and}$$

$$x(i,k,m) = \left\{ \begin{array}{l} \text{the } k\text{-th nearest neighbor } x_{j \neq i}(m) \text{ of } x_i(m) \\ \text{in } m\text{-Dimensional embedding space} \end{array} \right\}$$

$Q(i,k,m)$  measures the increase of the distance between  $x_i$  and its  $k$ -th nearest neighbor, as  $m$  increases.  $d_m(.,.)$  is some appropriate, fixed metric in  $\mathfrak{R}^m$ . According to the observations stated above  $Q$  should be greater than or equal to one. To get a notion what happens not only to the single point  $x_i$  and its neighbors but to all the  $x_i$  the next step is to calculate

$$W(m) = \frac{1}{\tau N(N-1)} \sum_{i=1}^N \sum_{k=1}^{N-1} \log Q(i, k, m), \quad (3.3)$$

which considers all  $N$  reconstructed points in the embedding space and all the  $N-1$  neighbors of these and adds up the logarithms of the ratios of the respective distances. The number of the  $x_i$ 's increase linearly with  $\tau$ , such that there would be a trivial linear  $\tau$ -dependence in  $W(m)$ . This is removed by dividing by  $\tau$  [87].

Clearly, for  $m$  equal to the proper embedding dimension and for the right sampling time  $\tau$ ,  $W(m)$  (3.3) should approach zero (within the experimental and numerical errors). Thus, systematic variation of  $m$  and  $\tau$  enables us to find sensible values for these quantities.

### 3.4 - Nonlinear Dynamical Quantifiers

#### 3.4.1 - Global Measures

Invariants of a system's attractor are measures that quantify the topological or geometrical properties of the attractor that remain constant under smooth transformations of the space. These smooth transformations include coordinate transformations such as phase space reconstruction of the observed time series [87].

Lyapunov exponents associated with a trajectory provide a measure of the average rates of convergence and divergence of nearby trajectories. For a system whose evolution function is defined by a function  $F$ , we need to analyze

$$\Delta x(t) \approx \Delta x(0) \frac{d}{dx} (F)x(0) .$$

To quantify this separation, we assume that the rate of growth (or decay) of the separation between the trajectories is exponential in time. Hence we define the exponents,  $\lambda_i$  as

$$\lambda_i = \lim_{n \rightarrow \infty} \frac{1}{n} \ln(\text{eig}_i \prod_{p=0}^n J(p)) , \quad (3.3)$$

where,  $J$  is the Jacobian of the system as the point  $p$  moves around the attractor. These exponents are called Lyapunov exponents, and are calculated by applying (3.3) to points on the reconstructed attractor. The exponents read from a reconstructed attractor measure the rate of separation of nearby trajectories averaged over the entire attractor [41].

Fractal dimension is a measure that quantifies the number of degrees of freedom (of the governing dynamical system) and the extent of self-similarity in the attractor's structure. Fractals are objects which are self-similar at various resolutions; self-similarity in a geometrical structure is a strong signature of a fractal object [41, 85].

Correlation dimension is a popular choice for numerically estimating the fractal dimension of the attractor. The power-law relation between the correlation integral of an attractor and the neighborhood radius of the analysis hypersphere can be used to provide an estimate of the fractal dimension:

$$D = \lim_{N \rightarrow \infty} \lim_{\varepsilon \rightarrow 0} \frac{\partial \ln C(\varepsilon)}{\partial \ln \varepsilon} , \quad (3.4)$$

where  $C(\varepsilon)$ , the correlation integral is defined as:

$$C(\varepsilon) = \frac{2}{N*(N-1)} \sum_{i=1}^N \sum_{j=i+1}^N \Theta(\varepsilon - \|\vec{x}_i - \vec{x}_j\|), \quad (3.5)$$

where  $\vec{x}$  is a point on the attractor (which has  $N$  such points). The correlation integral (3.5) is essentially a measure of the number of points within a neighborhood (hypersphere) of radius  $\varepsilon$ , averaged over the entire attractor. To avoid temporal correlations in the time series from producing an underestimated dimension, we use Theiler's correction for estimating the correlation integral [73, 74].

Kolmogorov entropy, defined over a state space, measures the rate of information loss or gain over the trajectory. Entropy is a well known measure used to quantify the amount of disorder in a system. It has also been associated with the amount of information stored in general probability distributions [34, 41, 85]. Numerically, the Kolmogorov entropy can be estimated as the second order Renyi entropy ( $K_2$ ) and can be related to the correlation integral of the reconstructed attractor as:

$$C_d(\varepsilon) \sim \lim_{\substack{\varepsilon \rightarrow 0 \\ d \rightarrow \infty}} \varepsilon^D \exp(-\tau d K_2),$$

where  $D$  (3.4) is the fractal dimension of the system's attractor,  $d$  is the embedding dimension and  $\tau$  is the time-delay used for attractor reconstruction. This leads to the relation

$$K_2 \sim \frac{1}{\tau} \lim_{\substack{\varepsilon \rightarrow 0 \\ d \rightarrow \infty}} \ln \frac{C_d(\varepsilon)}{C_{d+1}(\varepsilon)} .$$

The values of  $\varepsilon$  and  $d$  are restricted by the resolution of the attractor and the length of the time series [1].

### 3.4.2 - Local Measures

Recurrence quantification analysis (RQA) gives a local view of dynamical system behaviour. It analyzes distances of pairs of points in phase space rather than a distribution of distances. Therefore, unlike the fractal dimension, Lyapunov exponents, and Kolmogorov-Sinai Entropy, RQA is able to analyse fast transients and to localize in time the features of a dynamical variation.

To obtain a recurrence diagram, following the procedure introduced by Eckmann and colleagues [23], a point is plotted in 2-dimensional space at the location addressed by (i,j) each time state  $X_j$  is near  $X_i$ . In other words, each of the points (i,j) in an  $N \times N$  array, which comprise the recurrence diagram, implies that  $X_j$  is close to  $X_i$ . A state  $X_j$  is defined to be near to the state  $X_i$  only if both states are contained within a  $M$ -dimensional hyper-sphere; a hyper-sphere with radius 0 will result in a recurrence diagram containing zero points (no states are close to one another) and a hyper-sphere with a large radius will result in a recurrence diagram containing every point in the  $N \times N$  array. In this study, the recurrence diagrams will be quantified using percent recurrence (%R) and percent determinism (%D). %R is defined as the number of recurrent points divided by the possible number of recurrent points; %R is a measure of the extent to which the signal is correlated with itself in phase space. %D is

defined as the number of recurrent points located on lines parallel to the main diagonal of the plot divided by the number of recurrent points [80, 83, 84]; %D characterizes the tendency of the system to smoothly evolve through some volume of the attractor, and is therefore a measure of the amount of rule-obeying (deterministic) structure in the signal.

### 3.5 - Surrogate Data Analysis

Before we attempt to discriminate between two states of a system using nonlinear dynamical quantifiers (NDQs), it is wise to check whether or not there is any structure in the data that motivates such the endeavor. If the chosen nonlinear quantifier is unable to detect information which is not redundant to that detected by the optimal quantifiers for the linear, surrogate system, then little (if any) gain is to be expected through its use [74]. On the other hand, if the quantifier is able to capture information that is invisible to those associated with the surrogate system, then much can be gained through its use.

For example, suppose the surrogate data are constructed so that both the mean and power spectrum of the original is preserved in all the surrogates. If the value of the NDQ for the original data falls outside of the surrogate quantifier distribution, we can be confident that the quantifier is detecting information that is different from what is extracted by the mean or power spectrum. In this situation, it will be possible to distinguish between two states even if the mean and spectral properties of the states are identical [74]. In other words, when two states appear to be the same when analyzed using autocorrelation, mean or variance as quantifiers, it is not necessarily true that the

two states are indistinguishable [83]. Also, in a less extreme case, that is, when a spectral or ARIMA analysis is able to detect changes between two complex states, but not consistently, and a surrogate data analysis reveals the existence of nonlinear structure, an application of nonlinear quantifiers may improve the deficiency. Next, the mathematical details behind a surrogate data analysis will be given, in turn, followed by surrogate data analyses of signals obtained from various complex systems.

### 3.5.1 - Surrogate Data Construction

Surrogate data sets are constructed in a manner consistent with the null hypothesis being tested. In this study, we wish to address the following null hypothesis: the signal is nothing more than linearly filtered (covers both the ARIMA and spectrum analyses in Chapter 2) noise. Surrogate data sets that are consistent with this hypothesis must be phase-randomized versions of the original signal [74].

The most convenient procedure for generating phase-randomized surrogates makes use of the Fourier transform. Given a time series,  $x(t)$ , of  $N$  values taken at regular intervals of time  $t = t_0, t_1, \dots, t_{N-1} = 0, \Delta t, \dots, (N-1)\Delta t$ , apply  $F$ , the discrete Fourier transform operator, to obtain

$$X(f) = F\{x(t)\} = \sum_{n=0}^{N-1} x(t_n) e^{2\pi i f n \Delta t} .$$

Further, write this complex valued Fourier transform as:

$$X(f) = A(f) e^{i\phi(f)}, \quad (3.6)$$

where  $A(f)$  is the amplitude and  $\phi(f)$  is the phase.  $X(f)$  (3.6) is evaluated at the discrete frequencies  $f = -N\Delta f / 2, \dots, -\Delta f, 0, \Delta f, \dots, N\Delta f / 2$ , where  $\Delta f = 1/(N\Delta t)$  [86].

A phase-randomized Fourier Transform  $\tilde{X}(f)$  is obtained by rotating the phase  $\phi$  at each frequency  $f$  by an independent random variable  $\mathcal{G}$  that is chosen uniformly in the range  $[0, 2\pi)$ . That is,

$$\tilde{X}(f) = A(f)e^{i(\phi(f)+\mathcal{G}(f))} \quad (3.7)$$

The phase-randomized surrogate time series is given by the inverse Fourier transform of  $\tilde{X}(f)$  (3.7), that is  $\tilde{x}(t) = F^{-1}\{\tilde{X}(f)\} = F^{-1}\{X(f)e^{i\mathcal{G}(f)}\}$ . By construction,  $\tilde{x}(t)$  will have the same mean and power spectrum as the original data  $x(t)$ , whereas all other structure, if any existed, was intentionally annihilated.

After  $N$  surrogate data sets are created, a candidate NDQ is utilized to quantify the original signal and all of the surrogates, resulting in  $N+1$  such quantifications. Then, the distribution of the  $N$  surrogate NDQ values is formed. Following the creation of the surrogate distribution, the next step is to determine if the NDQ for the original data lies outside of the surrogate NDQ distribution. The final step in the analysis is to determine whether or not the null hypothesis should be rejected or accepted. Assuming that the NDQ values obtained from the surrogates form a Gaussian distribution, the probability that the surrogate NDQ will be less than the original NDQ can be obtained using a standard Z-score approach [41]. However, because the distribution of the surrogate NDQs is, in general, unknown, it is advisable to use a distribution-free approach, such

as the Monte Carlo method, to gauge significance [41]. Employing the Monte Carlo method, the probability that the NDQ of the surrogate is difference from the NDQ of the original is  $p_{MC}$ , where  $P_{MC} = \frac{\text{Number\_of\_Cases}_{NDQ_{surr} \neq NDQ_{orig}}}{\text{Number\_of\_Cases}}$ .  $p_{MC}$  can vary from 0% to 100% The block diagram in Figure 3.3 illustrates the logic of a surrogate data analysis.

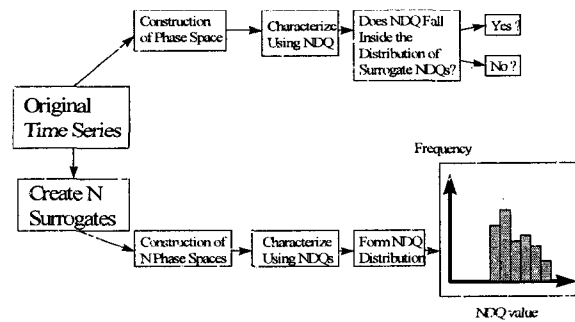


Figure 3.3: Block diagram illustrating the logic of a surrogate data analysis

### 3.5.2 - Surrogate Data Analysis of the Lorenz System

The Lorenz system is a simplified model of weather and it is governed by a set of nonlinear, deterministic equations that is capable of producing irregular behavior and exhibiting extreme sensitivity to initial conditions. The set of equations is

$$\begin{aligned}
 \frac{dx}{dt} &= \sigma(y - x) \\
 \frac{dy}{dt} &= rx - y - xz \\
 \frac{dz}{dt} &= xy - bz
 \end{aligned}
 \tag{3.8}$$

, where  $\sigma, r, b$  are positive, real parameters. For this study, the system parameters were tuned such that it was operating in the chaotic regime [85]. After setting the initial conditions, the governing equations (3.8) were numerically solved (see MATLAB code in APPENDIX A) using a 4<sup>th</sup>-order Runge-Kutta (time step = .01 seconds) numerical scheme. Figure 3.4 A displays the x-component of the solution for a specific time period and Figure 3.4 B shows one of its corresponding phase-randomized surrogates (obtained as described above). Notice that the corresponding spectra for, which are displayed in Figure 3.4 C, D, respectively, are indistinguishable.

After 1000 surrogate data sets were created, various NDQs (fractal dimension, Lyapunov exponents, Kolmogorov entropy, %R, and %D) were utilized to characterize the original signal and each of the surrogates, resulting in 1001 characterizations for each NDQ. Then, the distributions of the 1000 surrogate NDQ values, for each NDQ, were formed. Upon creation of the surrogate distributions, the next step is to determine if a NDQ for the original data lies outside of the corresponding surrogate NDQ distribution. The analysis was replicated 100 times in order to gauge its statistical power for each NDQ (Table 3.1). All statistical calculations were performed using MINITAB (Minitab, State College, PA).

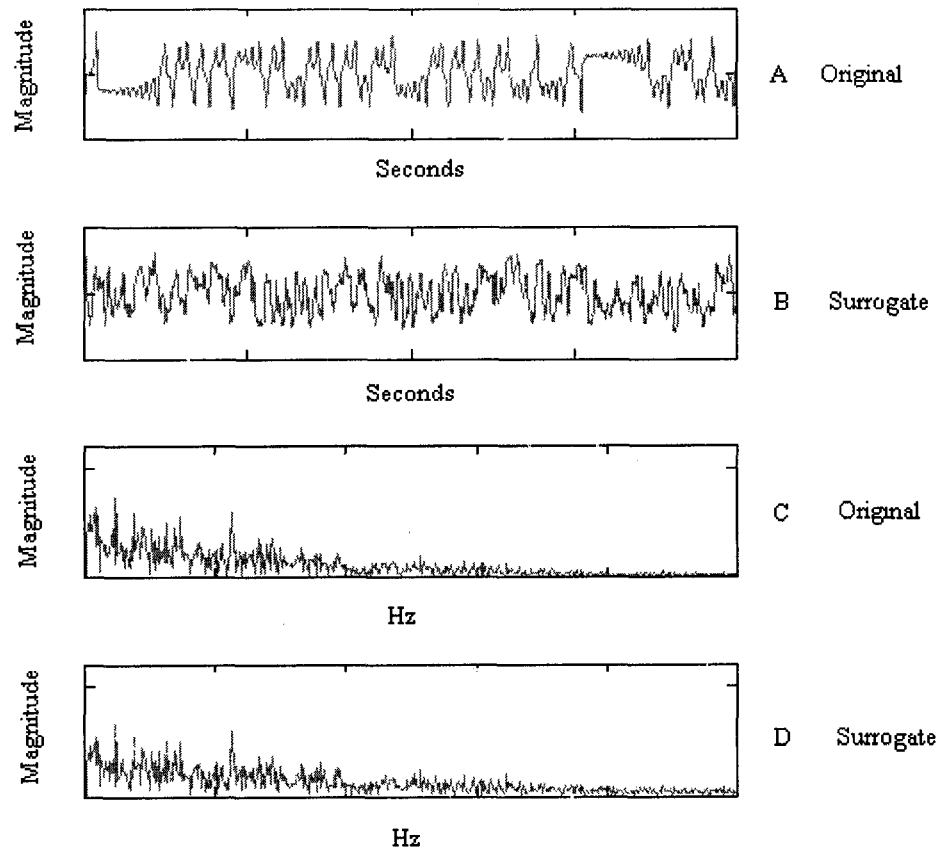


**Figure 3.4:** A) Displays the original signal. B) Displays a surrogate for the original signal. The surrogate signal was constructed such that both the mean and power spectrum is commensurate to that of the original signal, as evidenced by the graphs in C) and D). So if any other structure existed (e.g., in the Fourier phase relations), it was intentionally destroyed via this transformation.

**Table 3.1:** Surrogate data analysis results for the Lorenz system.

	<u>Fractal dimension</u>	<u>Lyapunov exponent</u>	<u>Kolmogorov entropy</u>	<u>%R</u>	<u>%D</u>
<i>Original (n = 1)</i>	2.23	3.02	0.96	45.09	99.34
<i>Surrogates (n = 1000)</i>	6.41 ± 0.35	8.78 ± 1.27	13.49 ± 2.63	23.18 ± 4.69	18.64 ± 2.71
<i>P<sub>MC</sub> (100 replicates)</i>	100%	100%	100%	100%	100%

For the Lorenz system, all corresponding  $p_{MC}$  (one per NDQ) values equaled 100%. So, we have very strong evidence in support of rejecting the null hypotheses. Therefore, we conclude that the Lorenz system is something beyond linearly filtered

noise as assessed by the corresponding NDQs. Of course, we know this to be the truth because the governing equations are, in fact, nonlinear and deterministic. Next, a surrogate analysis will be performed upon signal acquired from a system whose governing equations are unknown, the human brain.

### 3.5.3 - Surrogate Data Analysis of Human EEG

Recurrence plots constructed from 2 seconds of baseline human EEG (Figure 3.5) were similar to the complex two-dimensional patterns typical of physiological time series [17, 33, 37, 53, 63, 75, 80, 81, 83, 84] and chaotic deterministic systems such as the Lorenz system [85]. The essential feature of the plots was that their texture resulted directly from the dynamical electrical activity of the brain. The structure in the EEG was reduced in the corresponding EEG surrogates (Figure 3.5). The surrogate data analysis results for each NDQ reveal that %R and %D are able to consistently detect changes in the baseline EEG that are different than those in the surrogates (Table 3.2). A surrogate data analysis of baseline rabbit EEG produced similar results (i.e., %R, %D were the optimal NDQs). All statistical calculations were performed using MINITAB (Minitab, State College, PA) and custom MATLAB code (see APPENDIX B).

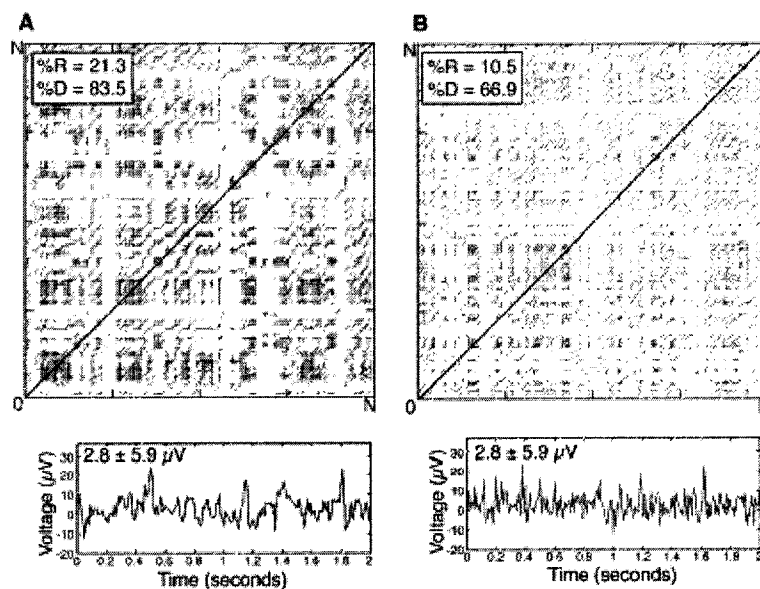


**Figure 3.5:** Recurrence plots produced from 2 s of human EEG data derived from an occipital electrode. The plots are symmetrical about the diagonals, which were added. (A) Original EEG (bottom) and associated plot (top). (B) Signal formed by randomizing the EEG (bottom); the recurrence plot (top) of the randomized signal is less deterministic than the plot for the original EEG (A, top). Recurrent points form distinct patterns characterized by %R and %D which, unlike the mean and standard deviation, are sensitive to nonlinear determinism present in the signal. N is number of recurrent points.

**Table 3.2:** Surrogate data analysis results for 100 baseline EEG epochs.

	<u>Fractal dimension</u>	<u>Lyapunov exponent</u>	<u>Kolmogorov entropy</u>	<u>%R</u>	<u>%D</u>
<i>Original (n = 1)</i>	4.21	8.19	21.41	29.3	34.97
<i>Surrogates (n = 1000)</i>	6.41 ± 2.78	9.34 ± 3.93	23.17 ± 5.63	26.18 ± 2.45	31.38 ± 3.62
<i>P<sub>MC</sub> (100 replicates)</i>	46%	31%	53%	94%	91%

### 3.6 - Nonlinear Dynamical EEG Evoked Response Model

#### 3.6.1 - The Experimental Model System

The biological processes responsible for producing the EEG will be viewed as a nonlinear dynamical system. Dynamical systems are completely characterized by their trajectory in phase space, the axes of which are the independent variables necessary to define the state of the system. The EEG time series is a combinatory description of the brain under its evolutionary rules, and the multi-dimensional behavior manifests itself in the convoluted one-dimensional measurement. It will be assumed that the EEG is the result of a deterministic response due to a complex set of inputs (stimuli) (Figure 3.6). These inputs are comprised of a finite set of internal and external variables that have the ability to influence the EEG. The variables, which are unascertained in identity and number, are assumed to interact in a time-dependent manner according to unknown (but certain) nonlinear, governing laws, thereby determining the observed signal. Under this model, a stimulus can affect the brain's electrical activity by affecting either one or more of the relevant variables or by affecting the way the variables interact.

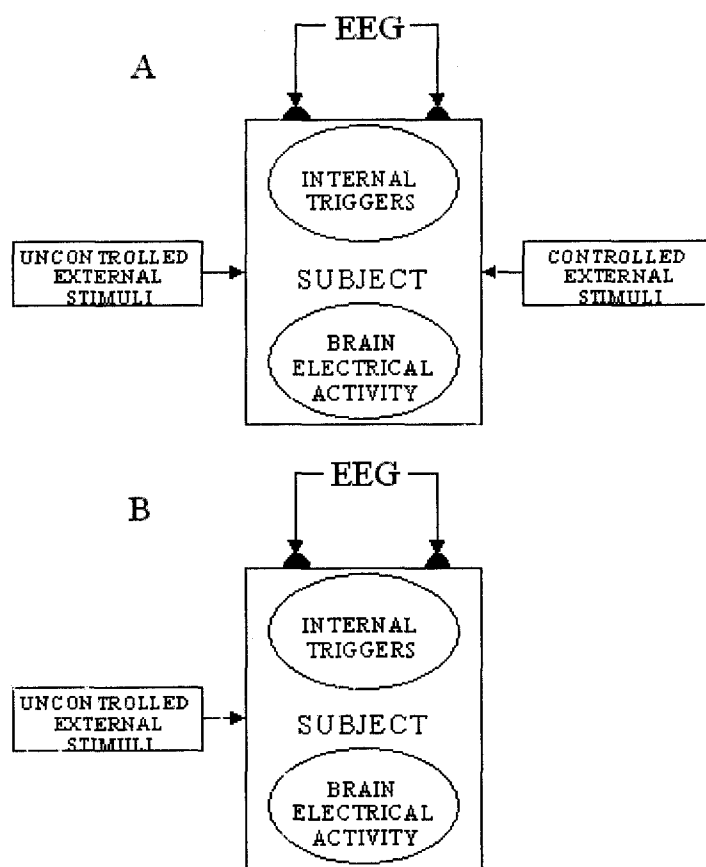


**Figure 3.6:** A) EEG response during application of controlled external stimuli (EMF). B) EEG response during the absence of controlled stimuli (EMF).

### 3.6.2 - The Basic Hypothesis

EMFs are detected by the body and their effects demonstrate themselves as alterations in the ongoing electrical activity of the central nervous system. The baseline EEG is regarded as a combination of contributions from different brain regions. The conjecture that a power-line field or a cell-phone field cause a change in the EEG, by altering one or more of its components, will be tested by comparing %R and %D measured in the presence and the absence of the field (Figure 3.7). This method differs from those used by others (Reiser et al., 1995; Mann and Roschke, 1996; Röschke and

Mann, 1997; Vorobyov et al., 1997; Eulitz et al., 1998; Freude et al., 1998; Wagner et al., 1998; Borbély et al., 1999; Krause et al., 2000; Wagner et al., 2000) principally in that it is designed to capture any deterministic structure that might exist in the EEG, not simply linear structure.

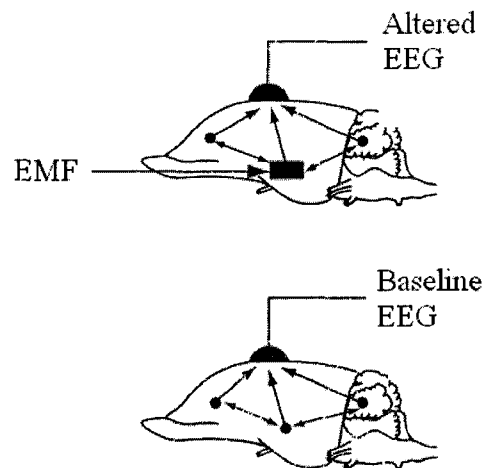


**Figure 3.7:** The baseline EEG is viewed as a complex combination of signals from many regions of the brain. The combined signal, as characterized by recurrence quantification analysis, is altered as a consequence of field transduction.

## CHAPTER 4

# CHANGES IN RABBIT BRAIN ELECTRICAL ACTIVITY DUE TO 60 HZ ELECTROMAGNETIC FIELDS

### 4.1 - Methods

#### 4.1.1 - Exposure System

During an experiment (Figure 4.1), the rabbit was restrained in an acrylic box, which was positioned inside a light-tight wooden box to minimize environmental influences and standardize the rabbit's sensory environment. For global exposure, using a four-coil unit, the wooden box was centered in the unit such that its axis and the rabbit's rostral-caudal axis were parallel. To produce localized exposure, the circular coils were positioned at appropriate locations inside the wooden box. The magnetic field was a subliminal stimulus as judged by the absence of any somatic response when the field was switched on or off; presentation of the field was not accompanied by any sensory cues to the rabbit.

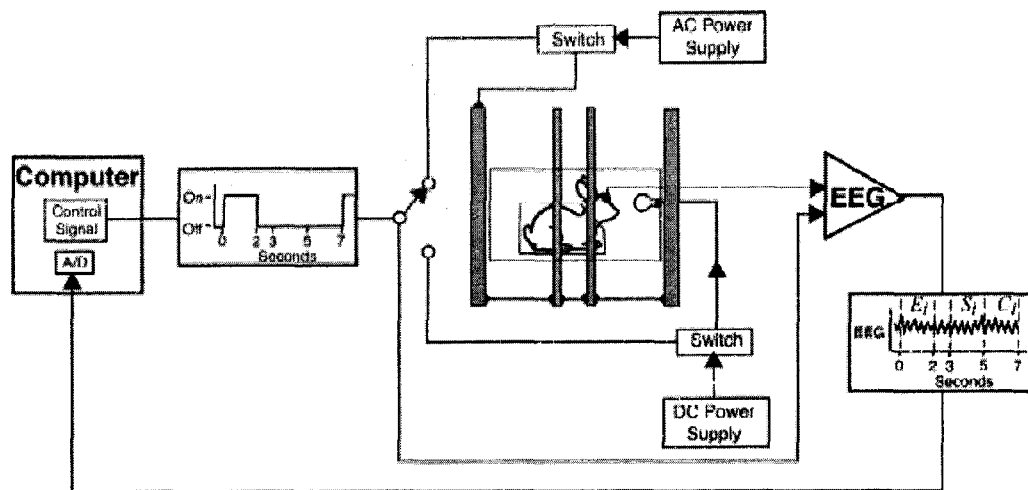


**Figure 4.1:** Schematic representation of the experimental system. A computer-generated timing signal controlled switching of the stimulus. The timing signal was also fed into one of the channels of the EEG amplifier to facilitate identification of the exposed (*E*), sham (*S*), and control (*C*) epochs of the EEG in each trial (the *i*th trial is illustrated). The location of the rabbit relative to the field-producing coils (shaded bars) is shown.

Global (full body exposure) magnetic fields were obtained using multiple-turn coils of 12-gauge magnet wire (Figure 4.2) [7, 54]. The outer coils (85 turns each) were 33.4 cm from the unit's centerline; the inner coils (35 turns each) were at 8.5 cm. Each coil was dipped in epoxy to minimize potential vibration effects due to interaction between the coil turns, and then wrapped with aluminum foil that was grounded to eliminate the possibility of effect on the animals due to electric fields. A coaxial configuration of four square coils, each 66 cm on a side, was used to produce full-body exposure to a field that was homogeneous to within 5% throughout the region occupied by the rabbit (Figure 4.3). In some experiments, the magnitudes and phases of the coil currents (3–8 A, depending on the experiment) were chosen such that the two halves of the rabbit's body were exposed to fields having predetermined differences (Figure 4.4). The four-coil unit

produced no detectable change in temperature at the location of the rabbit ( $< 0.01$  degrees Celsius). The rise times of all the coils were  $< 1$  As.

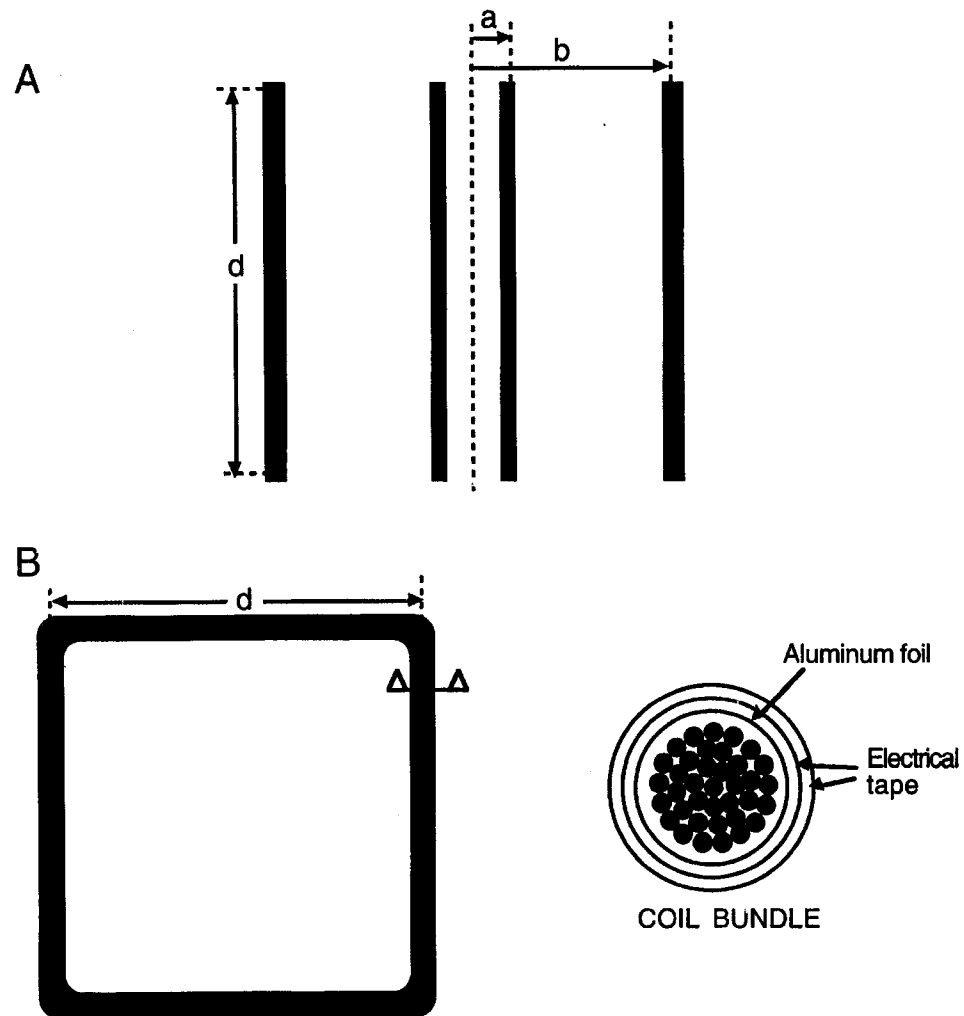


**Figure 4.2:** Four multiple-turn coils used for global EMF exposure ( $b = 33.4$  cm;  $a = 8.5$  cm;  $d = 66$  cm).

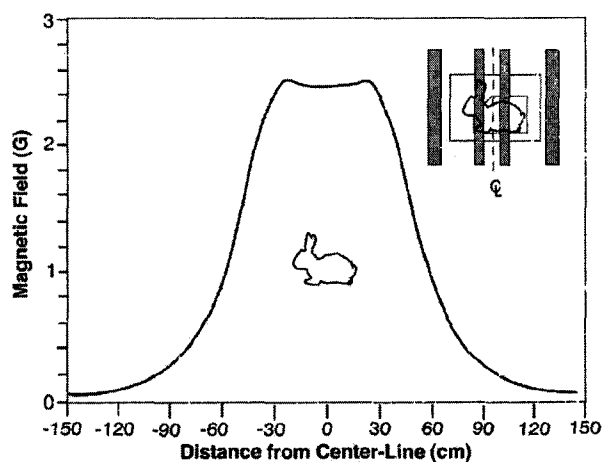


**Figure 4.3:** Magnetic field used for full-body exposure. The coils (shown in a side view as shaded bars) were energized to produce a homogeneous field in the region occupied by the rabbit (drawn approximately to scale).

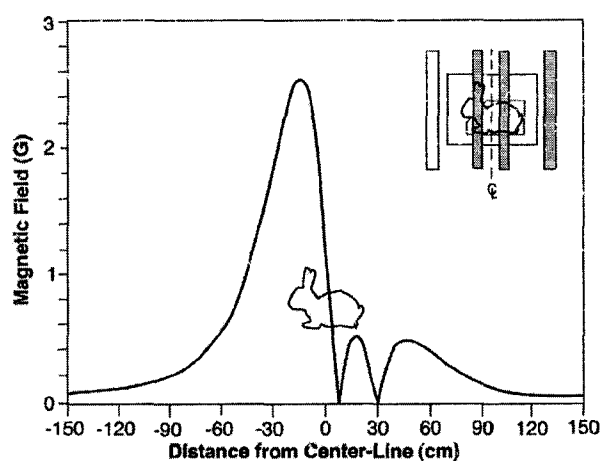


**Figure 4.4:** Magnetic field used for half-body field exposure. The coils were energized (shaded) to maximize the difference in average field between the halves of the body. For exposure of the cranial half-body region, the rabbit was positioned in the coil unit as shown. For exposure of the caudal region, the box containing the rabbit was reversed (drawn approximately to scale).

Localized exposure of the brain was produced using a pair of 14-turn circular coils, each 5 cm in diameter and located 9 cm apart (2.86 A). Localized exposure of the eye was produced using a 24-turn circular coil, 2 cm in diameter (1.45 A). All

coil fields were calculated using commercial software (MF3D, ERM, Pittsburgh, PA), and measured with a three-axis magnetic field sensor (Bartington MAG-03, GMW, Redwood City, CA). The circular coils produced temperature changes of 0.1–0.2 degrees Celsius at the location of the rabbit. As a control, coils were wound such that the current flowed in opposite directions in adjacent turns; when energized in the same way as the conventionally wound circular coils, the control coils produced the same heat as the conventionally wound coils, but no field. The rise times of all the coils were  $<1$  As.

A weak red light from a light-emitting diode was used as a positive control; the diode was mounted inside a tight-box 10 cm from the rabbit, and produced approximately 50 lumens at the corneal surface of the eye.

The average geomagnetic field at the location of the rabbit was 305 mGauss, 22.6 degrees below the horizontal. The geomagnetic component along the direction of the 60-Hz field was 239 mGauss.

#### 4.1.2 - Animals

Five female and five male New Zealand rabbits were used in the study. All animal procedures were approved by the Institutional Animal Care and Use Committee. During the experiments the rabbit was restrained in an acrylic box. To minimize environmental influences and standardize the rabbit's sensory environment, the box was mounted inside a wooden box designed to eliminate the entry of light and minimize the entry of sound and odor, while providing for ventilation and for passages of measurement and control signals (Figure 4.5).

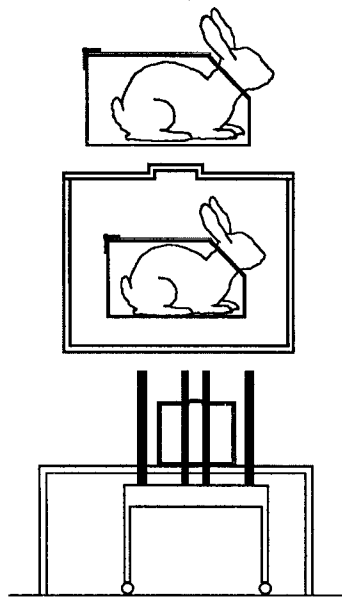


**Figure 4.5:** Sensory deprivation apparatus.

#### 4.1.3 - Procedure

The EEG was measured using gold-plated surface electrodes, .5 cm in diameter (Grass Instrument Co., Quincy, MA). The recording electrode was placed over the occipital region which was under the suture of the parietal and interparietal cranial bones, a location that was easily palpable. The indifferent electrode was placed 2.5 cm rostral along the midline, and the ground electrode was placed 2.5 cm rostral to the indifferent electrode, also along the midline. The electrodes were attached to the shaved scalp using conducting paste (EC2, Grass Instruments Co., Quincy, MA). Electrode impedances were less than  $3\text{ k}\Omega$ ; they were measured before and after each experiment (EZM 5 Electrode Impedance Meter, Grass Instruments, Quincy, MA). The EEG was measured using an amplifier (Nihon Kohden, Model 4400, Irvine, CA) that was capable of resolving source voltages of  $0.1\ \mu\text{V}$ . The signal was filtered to pass 0.3

-35 Hz, amplified, digitized at 512 Hz (12-bit), and then stored on a computer hard drive. Ten minutes of artifact-free EEG was obtained from each rabbit.

Multiple independent experiments were performed on each rabbit to allow a determination of its ability to detect the fields produced by the various coil arrangements, as assessed on the basis of deterministic changes in the EEG. Presentation of the stimulus (either light or field) commenced 5 minutes after the rabbit was placed in the light-tight box. A trial consisted in the application of a stimulus for 2 seconds, followed by an interstimulus period of 5 seconds. The first 5 trials were discarded, and the next 50 artifact-free trials were used for analysis of the EEG. Every experiment was replicated at least once. The EEG measured during the last 2 seconds of each trial was used as a control for the EEG measured during the corresponding stimulation epoch. The EEG measured during the 2 seconds that preceded the control epoch was defined as the sham epoch. As an additional control, it was analyzed statistically relative to the control in a manner identical to the analysis of the exposed epoch (Figure 4.6).

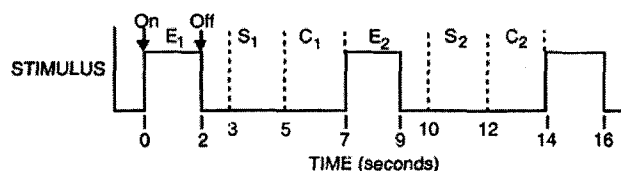


**Figure 4.6:** The EEG is recorded continuously. The stimulus is applied for 2-second intervals, separated by 5 seconds. The exposed epoch consists of the 2-second epoch during which the stimulus is applied, and the corresponding control epoch is the 2-second interval that commences 3 seconds after termination of the stimulus.

As an additional control procedure, after the rabbits were killed (Beuthanasia-D, Schering, Co., Kenilworth, NJ), the magnetic fields were applied as previously, and

voltage measurements (EEG) were made from the scalp electrodes to evaluate the possibility of passive electrical interactions with the electrodes.

#### 4.1.4 - EEG Analysis

Movement artifacts were identified by inspection of the EEG while blinded to the type of epoch in which they occurred, after which the trials that contained the artifacts were removed from the recorded voltage; movement artifacts occurred approximately equally in exposed, control, and sham epochs. The resulting scalar time series was embedded in a five-dimensional phase space using a time delay of 1; the values were chosen because they resulted in the most sensitive characterization of the EEG, as determined during preliminary studies. The local recurrence plot was obtained from the state vector  $X$  by plotting a point in two-dimensional space at the location addressed by  $(i,j)$  whenever  $X_j$  was near  $X_i$ . Two states were defined as near when they were within a five-dimensional hypersphere having a radius less than 15% of the minimum radius such that all points were near. The plots were quantified using percent recurrence (%R) and percent determinism (%D), defined respectively as the number of recurrent points divided by the possible number of recurrent points, and the number of recurrent points located on lines parallel to the main diagonal of the plot divided by the number of recurrent points. Calculations of %R and %D were carried out using software provided by Webber [82] and independently verified using custom MATLAB code (Mathworks, Natick, MA).

#### 4.1.5 - Statistics

In each experiment, the first five trials were discarded and the next 50 artifact-free trials were used to compare the values of the nonlinear quantifiers, using the Wilcoxon signed-rank test [37]. The statistic was presented for each comparison to more clearly illustrate the ability of the test to detect small differences between exposed and control conditions. The quantifiers were regarded as independent planned comparisons, and therefore no corrections were made even though two tests were performed on each rabbit in each experiment [37, 41]. The data is presented in terms of the mean  $\pm$  SD of the quantifiers, and the mean  $\pm$  95% confidence limits of the Wilcoxon signed-rank test metric (MINITAB, Minitab, State College, PA

and custom MATLAB code in APPENDIX B),  $\left[ \sum_{i=1}^{50} 2(E_i - C_i)^2 / (\bar{E} + \bar{C}) \right]^{\frac{1}{2}}$ , where  $E_i$

and  $C_i$  are respectively the quantifier values in the exposed and control epochs, and  $\bar{E}$  and  $\bar{C}$  are the corresponding epoch means. To minimize the potential consequences of nonstationarity in the EEG, the data is analyzed in a paired fashion. The RQA quantifiers were each evaluated for statistical significance at  $P < 0.05$ .

#### 4.2 – Results

Female rabbit number 1 was exposed to 2.5 G, 60 Hz, during 50 consecutive trials and the EEG was recorded continuously and unfolded in phase space. For each trial, the percent determinism as a function of time was calculated at minimum

resolution (80 time series points), and the results were averaged across all the trials. We found an apparent time-dependent increase in %D that occurred about 250 msec after the field was applied (Figure 4.7).

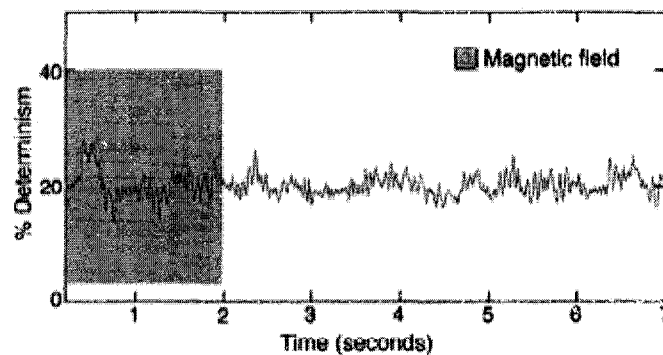
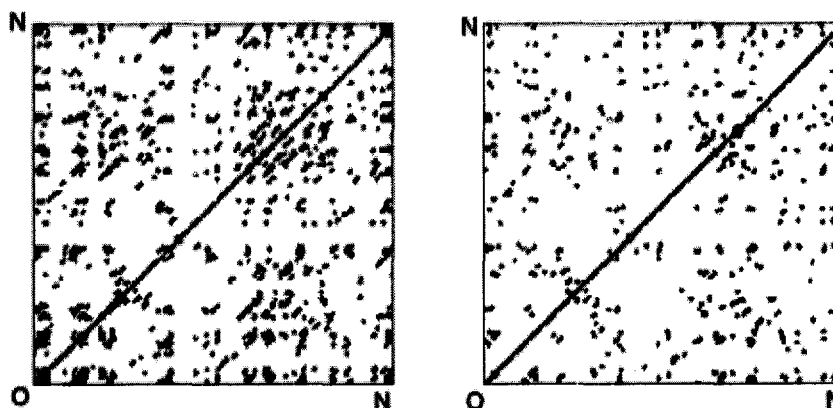


Figure 4.7: Percent Determinism in the EEG of rabbit no. 1, average over 50 trials.

To facilitate statistical analysis, the portion of the EEG signal in each exposure epoch identified with the increase in percent determinism (a segment of the time series centered at 250 msec and having a width of 250 msec) was unfolded in phase space. A local recurrence diagram was calculated for each exposure segment, and the corresponding average %D and %R were determined. Similar procedures were carried out for the sham segments (centered at 3.25 seconds, width of 250 msec) and for the control segments (5.25 seconds, 250 msec). The result for %D was  $37.1 \pm 2.7\%$  for the exposed segments, compared with  $13.3 \pm 2.2\%$  for the controls ( $p < .05$ ); the %D in the sham segments,  $14.1 \pm 2\%$ , did not differ from the controls. The values for %R were  $10.1 \pm .5\%$ ,  $2.7 \pm .7\%$ ,  $2.6 \pm .6\%$ , for the exposed, control, and sham segments, respectively. The local recurrence diagrams from which %D and %R (Figure

4.8) were calculated clearly revealed that quantitative differences had occurred in both variables.



**Figure 4.8:** Local recurrence plots from rabbit no. 1 obtained by concatenating the field (left) and corresponding control (right) segments. The recurrent points are shown as regions of increased density that occur symmetrically about the diagonal. N is the point index number.

The procedure developed for female rabbit number 1, as described, was applied to 4 additional female rabbits, and the overall results for all 5 female rabbits are shown in Figure 4.9. We found a statistically significant difference in percent determinism and percent recurrence in all animals tested. There were no cases of a false positive result, as assessed by comparing the sham and control segments (data not shown).

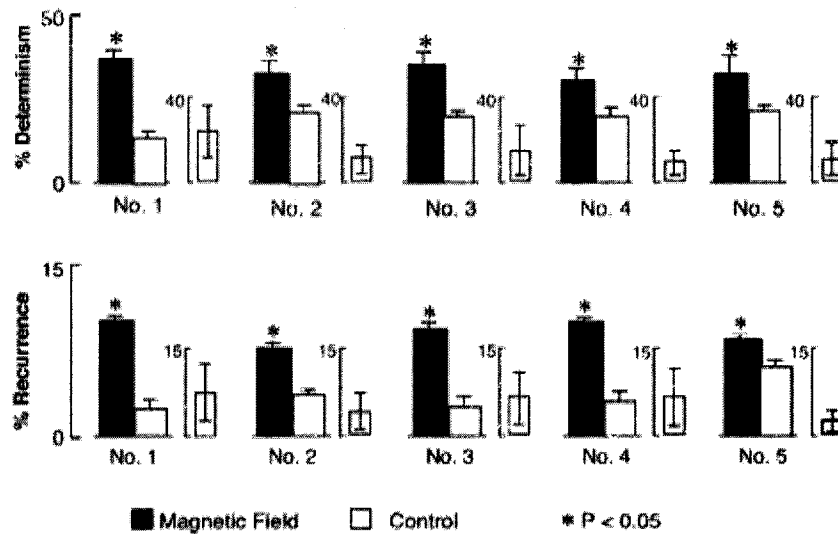


**Figure 4.9:** Effect of 2.5 Gauss, 60 Hz in five female rabbits, as assessed using two RQA quantifiers. For each rabbit and each quantifier, the difference between the exposed and control EEG epochs was evaluated using the Wilcoxon signed-rank test. EEG window centered at 250 ms, with width of 250 ms. The average values of the quantifiers ( $\pm$ SD) and the 95% confidence limits of the test metric are presented for each rabbit.

The effect of the light on the EEG was analyzed similarly to the effect due to the field. The average induced change in %D in female rabbit no. 1 (Figure 4.10) was stronger than that due to the field (Figure 4.7), and it occurred earlier (175 msec after presentation of the light, compared with 250 msec after the presentation of the field). The results for all 5 rabbits are shown in Figure 4.11. Again, the local recurrence diagrams clearly revealed the increased structure induced by the stimulus (Figure 4.12).

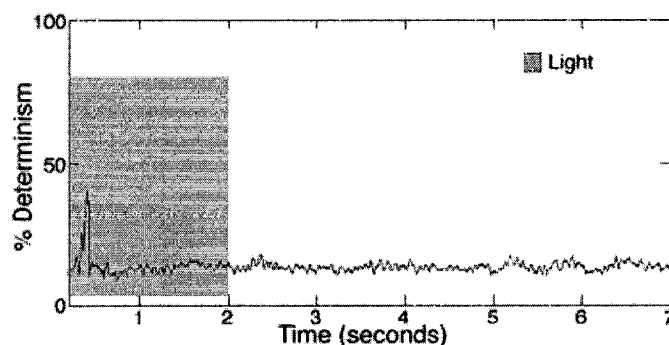


**Figure 4.10:** Percent Determinism in the EEG of rabbit no. 1, average over 50 trials.

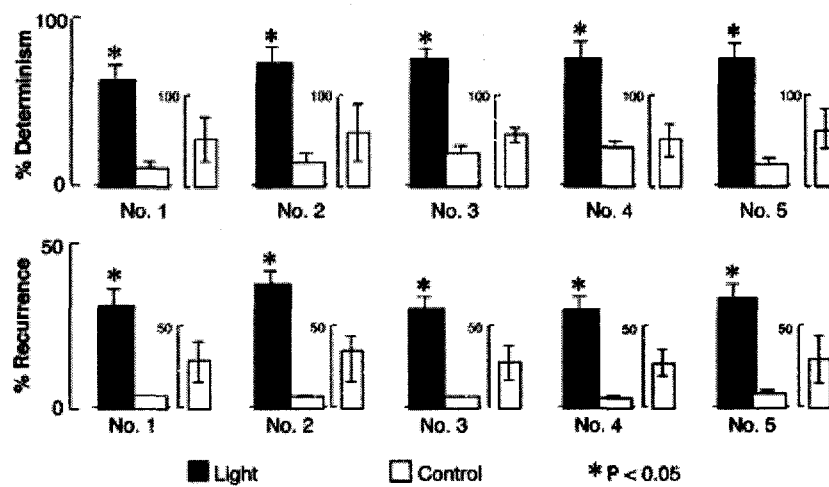


**Figure 4.11:** Effect of light on the EEG in five female rabbits, as assessed using two RQA quantifiers. For each rabbit and each quantifier, the difference between the exposed and control EEG epochs was evaluated using the Wilcoxon signed-ranked test. EEG window centered at 175 ms, with width of 266 ms. The average values ( $\pm$ SD) and 95% confidence limits of the test metric are presented for each rabbit.

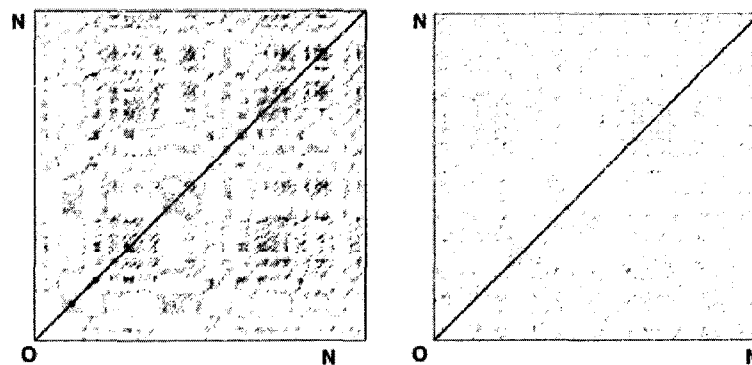


**Figure 4.12:** Local recurrence plots from rabbit no. 1 obtained by concatenating the light (left) and corresponding control (right) segments. The recurrent points are shown as regions of increased density that occur symmetrically about the diagonal.  $N$  is the point index number.

We evaluated the reproducibility of the effect of the field by repeating the experiments for each rabbit, and in every instance %D and %R were statistically significantly greater during the field-exposed segment. The results for all replicates in rabbit 1 are shown in Figure 4.13. Again, there were no cases of a false positive result when the sham and control segments were compared.

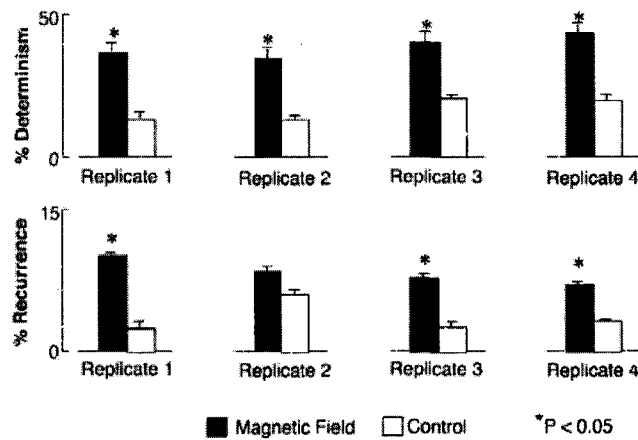


**Figure 4.13:** Reproducibility of the effect of 2.5 Gauss, 60 Hz on two RQA quantifiers of brain electrical activity in rabbit no. 1. EEG windows centered at 250 ms, with width of 250 ms. The average values of the quantifiers ( $\pm$ SD) and the 95% confidence limits of the test metric) are presented for each rabbit.

The experiments described above were repeated using 5 male rabbits. The effects of both the field and the light were evaluated using the windows widths and locations determined using female rabbit no. 1. As found previously using females, exposure of male to 2.5 G significantly increased %D and %R (Figure 4.14), the effect of light on the EEG was identical to that found previously for the female rabbits (data not shown). Consistent with the female rabbit results, the sham exposure did not result in any false positives (Figure 4.15). Again, the results were reproducible (data not shown).

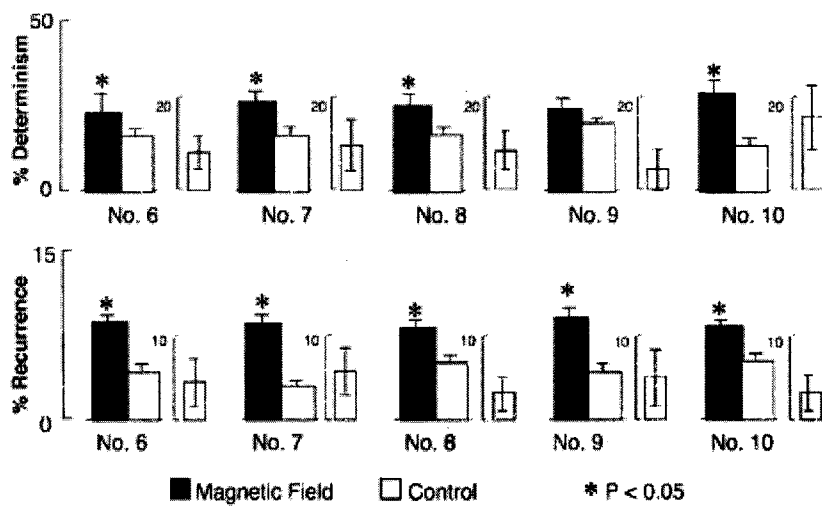


**Figure 4.14:** Effect of 2.5 Gauss, 60 Hz on the EEG in five male rabbits, as assessed using two RQA quantifiers. For each rabbit and each quantifier, the difference between the exposed and control EEG epochs was evaluated using the Wilcoxon signed-rank test. EEG window centered at 175 ms, with width of 266 ms. The average values ( $\pm$ SD) and 95% confidence limits of the test metric are presented for each rabbit.

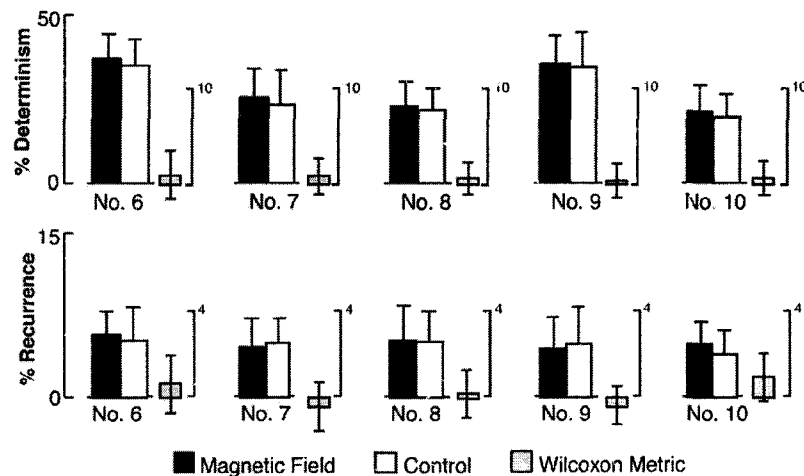


**Figure 4.15:** Sham exposure of the brain of rabbits (temperature control). The current through the coils was identical to that used in Figure 14, but it resulted in no detectable magnetic field ( $< 0.01$  Gauss). For each rabbit and each quantifier, the exposed and control EEG epochs were compared using the Wilcoxon signed-rank test ( $n = 50$  trials). A 250-ms segment of the data from each epoch (centered at 250 ms from the beginning of the epoch) was evaluated. The average values ( $\pm$ SD) of the quantifiers are shown. The average and 95% confidence limits of the test metrics are shown for each rabbit in the third bar.

Next, the question of where in the body the detectors of the field were located was considered. One possibility was that they were located throughout the body, as, for

example, receptors for somatosensory perception. Alternatively, they might have been localized, such as the primary detectors of the special senses. Calculations were performed in which the magnitude and direction of the current through each coil was systematically varied, and the particular combination that gave the maximum attenuation and greatest slope from 2.5 Gauss was determined. Then, each of the female rabbits were positioned in the field so that the cranial half was exposed to an average field of 2.0 Gauss, and the caudal half was exposed to a field that was never greater than about 0.4 Gauss (Figure 4.16). Exposure under these conditions resulted in changes in the EEG in each rabbit (Figure 4.17). When the experiment was repeated with the cranial half in the low-field region and the caudal half in the high-field region, no effect on the EEG was observed (Figure 4.18).

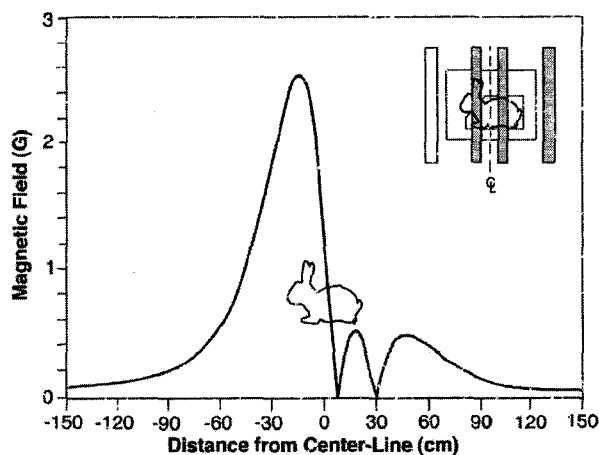


**Figure 4.16:** Magnetic field used for half-body field exposure. The coils were energized (shaded) to maximize the difference in average field between the halves of the body. For exposure of the cranial half-body region, the rabbit was positioned in the coil unit as shown. For exposure of the caudal region, the box containing the rabbit was reversed (drawn approximately to scale).

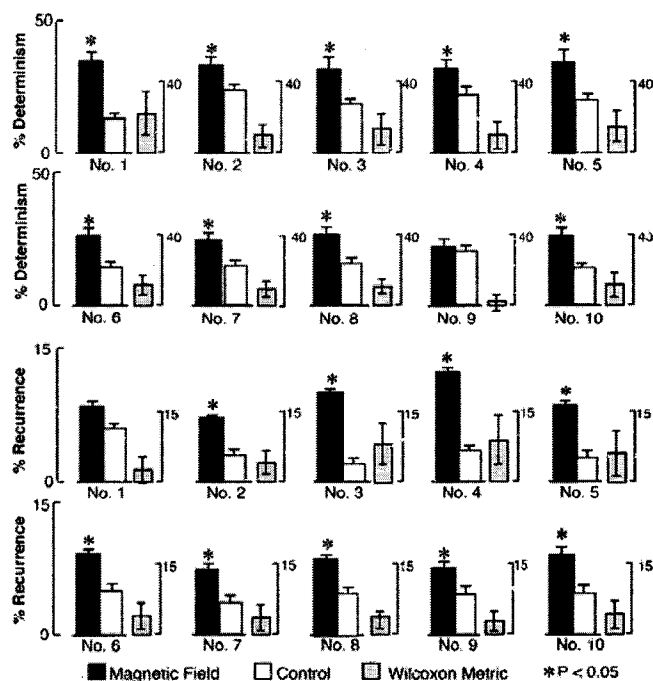


**Figure 4.17:** Effect of exposure to 60-Hz magnetic field such that the cranial and the caudal half-body regions were exposed to  $2.2 \pm 0.6$  and  $0.5 \pm 0.3$  Gauss, respectively (see Figure 3). For each rabbit and quantifier, the exposed and control EEG epochs were compared using the Wilcoxon signed-rank test ( $n = 50$  trials). A 250-ms segment of the data from each epoch (centered at 250 ms from the beginning of the epoch) was evaluated. The average values ( $\pm$ SD) of the quantifiers are shown. The average and 95% confidence limits of the test metrics are shown for each rabbit in the third bar.

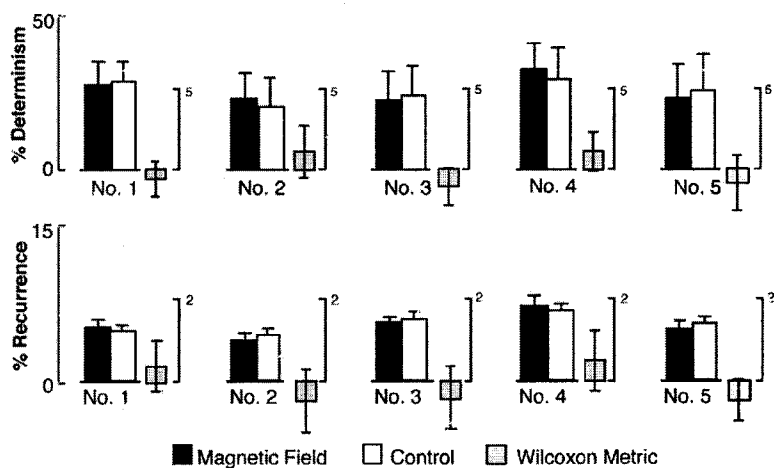


**Figure 4.18:** Effect of exposure to 60-Hz magnetic field such that the cranial and the caudal half-body regions were exposed to  $0.5 \pm 0.3$  and  $2.2 \pm 0.6$  Gauss, respectively (see Figure 3). For each rabbit quantifier, the exposed and control EEG epochs were compared using the Wilcoxon signed-rank test ( $n = 50$  trials). A 250-ms segment of the data from each epoch (centered at 250 ms from the beginning of the epoch) was evaluated. The average values ( $\pm$ SD) of the quantifiers are shown. The average and 95% confidence limits of the test metrics are shown for each rabbit in the third bar.

On the basis of these results, we hypothesized the field transduction occurred in the eye or the brain, and additional experiments using the male rabbits were performed to test the hypothesis. A coil 2 cm in diameter was constructed, and used to expose the right eye of each rabbit (Figure 4.19). We found no effect on the EEG under this condition (Figure 4.20).

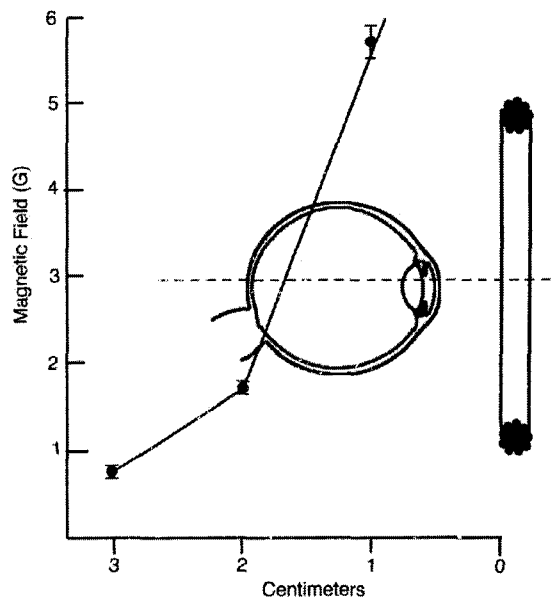


**Figure 4.19:** Magnetic field used for exposure of rabbit eye. The field was produced using one coil (shown on the right). The field (averaged over a circular area in the transverse plane 1 cm in diameter centered on the coil axis) is shown as a function of distance from the coil. The average field over the retina (assumed to be at 1.5–2 cm) was  $2.8 \pm 0.5$  Gauss, 60 Hz.

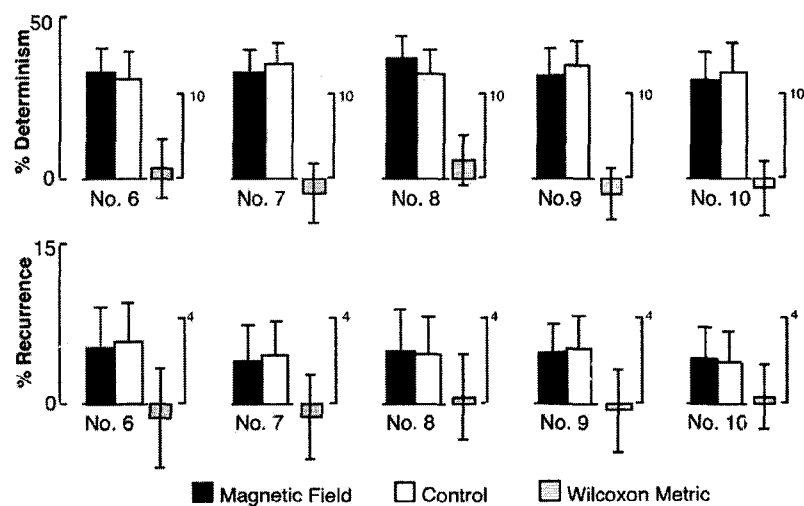


**Figure 4.20:** Effect of exposure to a 60-Hz field of  $2.8 \pm 0.5$  Gauss, averaged over a transverse plane through the retina. For each rabbit and quantifier, the exposed and control EEG epochs were compared using the Wilcoxon signed-rank test ( $n = 50$  trials). A 250-ms segment of the data from each epoch (centered at 250 ms from the beginning of the epoch) was evaluated. The average values ( $\pm$ SD) of the quantifiers are shown. The average and 95% confidence limits of the test metrics are shown for each rabbit in the third bar.

The possibility of a direct effect on the brain was evaluated in five rabbits, using a pair of coils positioned beside the head so that the field in the brain was  $2.5 \pm 0.3$  Gauss (Figure 4.21). Significant effects on the EEG were found (Figure 4.22). The effects were not seen when the experiment was repeated using coils that generated no field but the same amount of heat as the coils used previously. In both experiments, the previous window parameters were used, and there were no false-positive results (Figure 4.23).

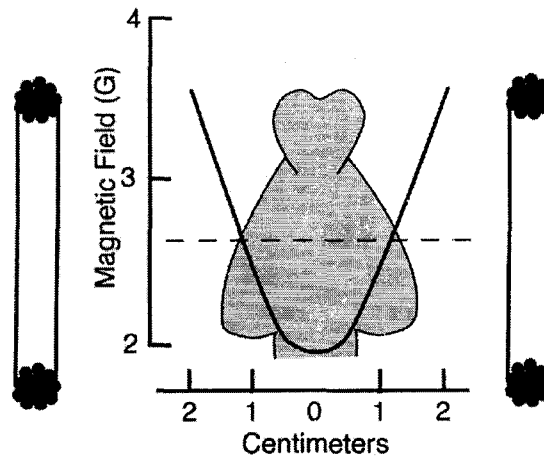


**Figure 4.21:** Magnetic field used for exposure of rabbit brain (shaded outline). The field (averaged over a circular area in the sagittal plane 4 cm in diameter centered on the coil axis) is shown as a function of distance from the mid-point between the generating coils. The average field in the brain (assumed to be at 1.5 to 1.5 cm) was  $2.5 \pm 0.3$  Gauss, 60 Hz. Common axis of coils is shown as a dashed line.

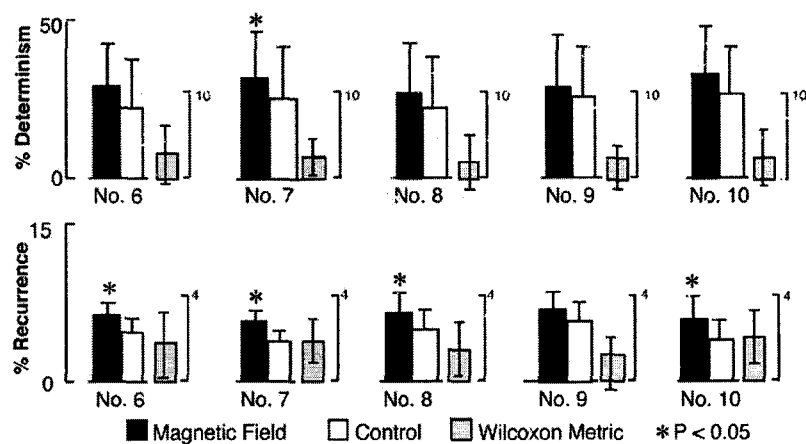


**Figure 4.22:** Effect of exposure of the brain to  $2.5 \pm 0.3$  Gauss, 60 Hz ( $n = 5$ ) (see Figure 6). For each rabbit and quantifier, the exposed and control EEG epochs were compared using the Wilcoxon signed-rank test ( $n = 50$  trials). A 250-ms segment of the data from each epoch (centered at 250 ms from the beginning of the epoch) was evaluated. The average values ( $\pm$ SD) of the quantifiers are shown. The average and 95% confidence limits of the test metrics are shown for each rabbit in the third bar.

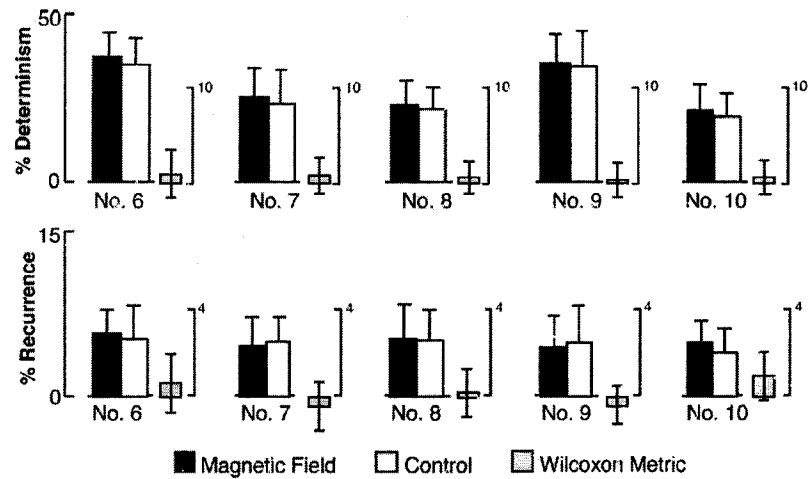


**Figure 4.23:** Sham exposure of the brain of rabbits (temperature control). The current through the coils was identical to that used in Figure 22, but it resulted in no detectable magnetic field ( $< 0.01$  Gauss). For each rabbit and each quantifier, the exposed and control EEG epochs were compared using the Wilcoxon signed-rank test ( $n = 50$  trials). A 250-ms segment of the data from each epoch (centered at 250 ms from the beginning of the epoch) was evaluated. The average values ( $\pm$ SD) of the quantifiers are shown. The average and 95% confidence limits of the test metrics are shown for each rabbit in the third bar.

After the animals were euthanized and cessation of heart activity was verified, each rabbit was exposed to a full-body field of 2.5 Gauss, and the input signal to the amplifier was analyzed as previously to evaluate the possibility of passive field interactions with the electrodes. We found that the RQA parameters were essentially zero, and independent of the presence of the field (data not shown).

#### 4.3 – Discussion

We studied the question whether electroreception in the rabbit, assumed to be a neurogenic process, could be consistently detected and, if so was the detection due to global or local exposure. In each of 10 rabbits, the EEG measured while the animal was exposed to a 2.5 Gauss full-body field differed significantly from the EEG measured in the absence of the field, as assessed statistically on the basis of changes in the %R and %D in the signal. The results were not due to some

unrecognized aspect of our analytical method because there were no false-positive results when the same method was used to compare two control epochs (S vs. C). The effect of the field was undoubtedly physiological in origin because no changes were seen in the input signal to the EEG amplifier when the field was applied to the rabbits after they had been euthanized. In addition, the observed delay of 125 ms between application of the field and the onset of the change in the EEG also indicated that the change was physiological in origin. We infer, therefore, that the field was transduced somewhere in the body, leading to the observed changes in the EEG, as expected under the neurogenic theory.

The possibility that transduction occurred throughout the body was evaluated by applying a field of comparable strength to only the front or back half of the animal in separate experiments, while minimizing the average field applied to the other half of the animal (about 0.5 Gauss). In the former experiment, we found an effect due to the field; in the latter experiment, no effects on the EEG were found.

Taken together, the two experiments showed that field detection occurred somewhere in the front half of the animals. When the brain was exposed to an average field of 2.5 Gauss, the EEG was altered in four of five rabbits studied; the effect could not be explained on the basis of heat produced by the coils.

The possibility that the transduction was mediated at least partly by retinal cells was evaluated by exposing that region, using a coil that produced an average field of 2.8 Gauss at the retina, and a much lower field at more proximal locations. Application of the field to the eye did not affect brain activity, suggesting that the photodetectors in the eye were not the locus of transduction of the field.

Taken together, these results can be interpreted to indicate that EMF transduction occurred somewhere in the head, probably the brain, although the methods used did not permit discrimination between specific brain structures that could have been the site of transduction. Central neurons interact strongly via synapses, and neuronal processes are often arranged in parallel, thereby enhancing ephaptic interactions. It is possible that the dense interconnectivity in the rabbit brain amplified transmembrane potential changes induced by the EMF, thereby altering the EEG. Other explanations are also possible. For example, the conditions of exposure and the anatomy of the rabbit's head were consistent with the possibility that transduction occurred in the hair cells of the ear (where the average field was greater than 2.5 Gauss). We did not address the problem of identifying the particular cell or process by which the field was actually detected.

In studies on hippocampal slices [3, 22, 38, 76], low-frequency fields produced immediate changes in electrical activity. The field used in the present study was 1-4 orders smaller than that induced in the brain slices. One possibility, among many, is that the brain electroreceptors inferred in the present study were located in the hippocampus. Another possibility is that more sensitive electroreceptors elsewhere in the brain could have been responsible for the effects reported here.

In summary, the results showed that the presence of transient deterministic brain states induced by an EMF signal could be documented using methods derived from nonlinear dynamical analysis, thereby allowing us to infer the approximate anatomic location of the signal's transduction.

## **CHAPTER 5**

# **CHANGES IN RABBIT BRAIN ELECTRICAL ACTIVITY DUE TO CELL PHONE ELECTROMAGNETIC FIELDS**

### 5.1 - Methods

#### 5.1.1 - Exposure System

EMF exposure of rabbits to the signal from a cellular telephone was produced using a standard commercial telephone (Nokia 5120) operating on a digital network (TDMA technology) in the 824-849 MHz band. The nominal maximum radiated power was 600 mW; the actual radiated power, which was determined by the distance between the telephone and the base-station antenna, was not measured. The presence or absence of the signal, however, was observed directly using a field detection meter (CellSensor, Tech International, Hallandale Beach, FL). After a call connection was established, the transmission path of the signal was alternated between two antennas, using a computer-controlled radiofrequency switch. One antenna was placed horizontally along the

rabbit's midline, 1 cm above its head (head antenna); the other antenna (distant antenna) was 3 meters distant (Figure 5.1). The switching occurred instantaneously ( $<1 \mu\text{sec}$ ).

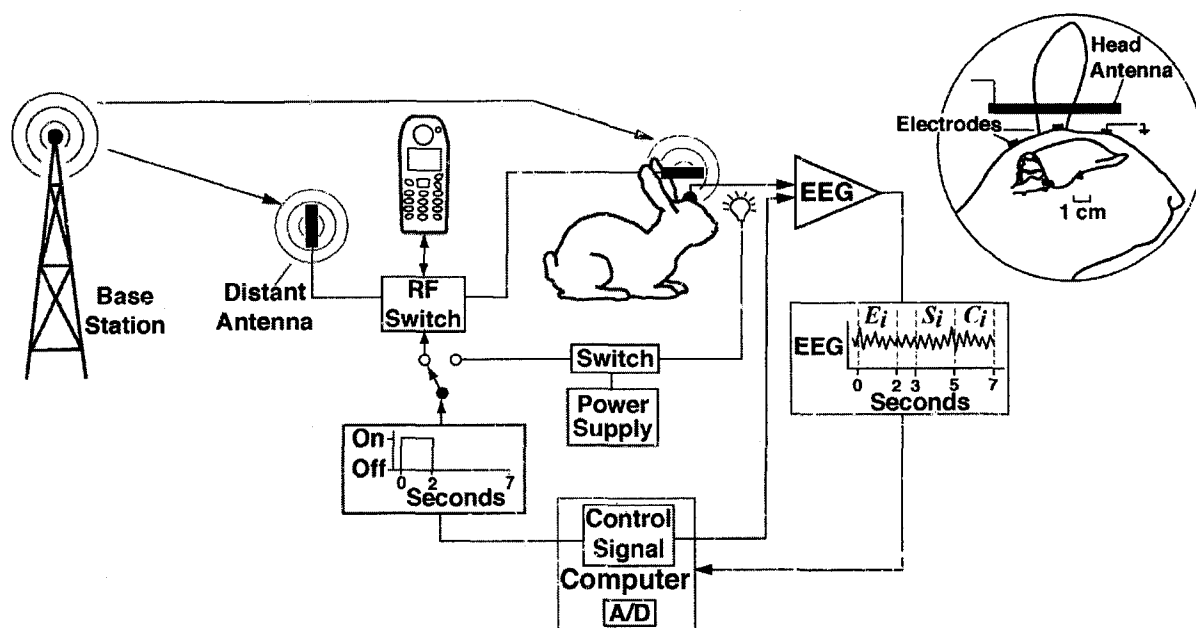


**Figure 5.1:** Schematic representation of the experimental system. The detail shows the location of the EEG electrodes relative to the head antenna. A computer-regulated RF switch controlled the connection with the base station. In each trial, the connection was maintained through the head antenna during 0-2 sec and through the distant antenna during 2-7 sec. The effects on the EEG were ascertained by comparing exposed ( $E$ ) and control ( $C$ ) epochs in each trial, using the Wilcoxon signed-rank test ( $N=50$ , the  $i^{\text{th}}$  trial is illustrated). Sham ( $S$ ) and control epochs were compared as a control procedure. Light was used as a positive control stimulus.

The rabbit was restrained in an acrylic box during the experiment. To minimize environmental influences and standardize the sensory environment experienced by the rabbit, the box was mounted inside a wooden box. It eliminated the entry of light and minimized the entry of sound and odor, while providing for ventilation and for the passages of measurement and control signals.

The cell-phone field at the head electrode was a subliminal stimulus to the rabbit as judged by the complete absence of a behavioral response when the field was

presented; its presentation was not accompanied by any sensory cues to the rabbit (the telephone was 2.5 m from the rabbit and 0.5 m from the distant antenna). A weak red light from a light-emitting diode was used as a positive control; the diode was mounted inside the light-tight box, 10 cm from the rabbit, and produced approximately 50 lumens at the corneal surface of the eye. The rise-time of the currents in the diode circuit was less than 1  $\mu$ sec.

The average geomagnetic field at the location of the rabbit was 305 mGauss, 22.6 degrees below the horizontal. The geomagnetic component along the direction of the 60-Hz field was 239 mGauss.

#### 5.1.2 - Animals

Five female (nos. 1-5) and five male (nos. 6-10) New Zealand rabbits were used in the study. All animal procedures were approved by the Institutional Animal Care and Use Committee. The electroencephalogram (EEG) was recorded over the occipital region, which was under the easily palpable suture of the parietal and interparietal cranial bones. The indifferent and ground electrodes were respectively 2.5 cm and 5 cm rostral. The electrodes (0.5 cm in diameter) were attached to the shaved scalp using conducting paste (EC2, Grass, Quincy, MA); the impedance (1-3 k $\Omega$ ) was measured before and after each experiment (EZM 5, Grass). At the conclusion of the experiments, the rabbits were sacrificed by intravenous injection of pentobarbital.

#### 5.1.3 – Procedure

The EEG was measured continuously after the rabbit was placed in the wooden box, using an amplifier (Model 4400, Nihon Kohden, Irvine, CA) capable of resolving

source voltages of  $0.1 \mu\text{V}$ . The signal was filtered to pass 0.3-35 Hz, amplified, digitized at 512 Hz (12-bit), and stored on a hard drive.

Independent experiments were performed on each rabbit to allow a determination of each animal's ability to detect the field. Presentation of the telephone signal commenced 5 min after the rabbit was placed in the light-tight box. A trial consisted in the application of the field to the rabbit for 2 seconds (*E* epoch), followed by a field-free period of 5 seconds produced by switching the transmission path of the signal to the distant antenna (Figure 5.1). A minimum of 60 trials were run, and then the call was terminated. Occasionally a call ended prematurely because the handshake between the telephone and the network was lost. In these cases the data was discarded and the experiment was repeated. In separate sessions, the experiments were repeated using light as the stimulus.

The voltage from the last 2 seconds of each trial was used as the control (*C* epoch) for the corresponding *E* epoch. The voltage from the 2 seconds preceding the *C* epoch was defined as the sham (*S* epoch); it was used as a control for our statistical procedure. Some experiments were performed with the head antenna repositioned parallel to one side of the rabbit, 1 cm from the thoracic region. As an additional control, after the rabbits were killed, the cell-phone field was applied using the head antenna, and voltage measurements were made from the scalp electrodes to evaluate the possibility of passive, electrical interactions with the electrodes.

#### 5.1.4 - EEG Analysis

Trials containing movement artifacts were removed from the recorded voltage. The artifacts were identified by visual inspection of the analog record of the signal,

where they appeared as brief (usually 1-2 seconds) discontinuous change. The artifact-free trials were sent through a series of filters (described below) designed to attenuate specific frequencies; the aim was to maximize the possibility of observing an effect of the cell-phone field by removing frequencies that did not contribute to the discrimination between the exposed and control epochs. The frequency-filtered trials constituted a scalar time series,  $S_t$ , consisting of voltages at discrete times  $t=1,2,3\dots N$ .  $S_t$  was time-delay embedded in a five-dimensional state space using a time delay of one; an embedding dimension of 5 and a time delay of 1 were chosen during preliminary analysis of the data on the basis that they resulted in the most sensitive characterizations of the EEG epochs. Portions of the attractor not within a fixed distance of its center of mass were removed. Our purpose was to increase the sensitivity of the analysis by removing portions of the attractor that were not responsive to the presence of the field. The removal of some system states interrupted the trajectory in phase space, and was equivalent in the time domain to removing the voltage at specific time points (five time points removed for each five-dimensional state vector that was removed). The resulting trajectory described the evolution of the dynamical system's state vector  $X$  for all remaining time points.

A local recurrence plot was obtained for each  $E$ ,  $C$ , and  $S$  epoch in each trial, as follows. A point was plotted in two-dimensional space at the location addressed by  $(i,j)$  whenever  $X_j$  was near  $X_i$ . Two states were defined as near only if both were contained within a hypersphere having a radius less than 15% of the minimum radius such that all points were near. The recurrence plot was quantified using percent recurrence (%R) and percent determinism (%D), defined respectively as the number of recurrent points

divided by the possible number of recurrent points and the number of recurrent points located on lines parallel to the main diagonal of the diagram divided by the number of recurrent points. %R is a measure of the extent to which the signal is correlated with itself in phase space. %D characterizes the tendency of the system to re-visit the same area of the attractor, and is therefore a measure of the amount of rule-obeying structure in the signal. Calculations of %R and %D were carried out using software provided by Webber [13] and independently verified using a custom MATLAB code (Mathworks, Natick, MA).

### 5.1.5 - Statistics

In preliminary studies involving only rabbit no. 1 we followed an iterative procedure to maximize the probability (P) of detecting a difference between the *E* and *C* epochs, using %R. Various portions (windows) of the epochs were considered, in combination with various combinations of frequency and phase-space filters, using the Wilcoxon signed-rank test to evaluate *E* versus *C*, and *S* versus *C*. The window and filter parameters that yielded the lowest P's for *E* versus *C* when  $P > 0.05$  for *S* versus *C* were then applied prospectively to evaluate the effect of the cell-phone field on %R and %D in the remaining nine rabbits.

In each statistical test, the first 5 trials were discarded, and the next 50 artifact-free trials were used in the analysis. The data is presented in terms of the mean  $\pm$  SD of the quantifiers, and the mean  $\pm$  95% confidence limits of the Wilcoxon signed-rank test metric (MINITAB, Minitab, State College, PA and custom MATLAB code in

APPENDIX B),  $\left[ \sum_{i=1}^{50} 2(E_i - C_i)^2 / (\bar{E} + \bar{C}) \right]^{\frac{1}{2}}$ , where  $E_i$  and  $C_i$  are respectively the

quantifier values in the exposed and control epochs, and  $\bar{E}$  and  $\bar{C}$  are the corresponding epoch means. The RQA quantifiers were regarded as independent planned comparisons, and were each evaluated for statistical significance at  $P < 0.05$ .

A Durbin Watson test (MINITAB, Minitab, State College, PA) was performed to check for serial correlations across the pairs used in the Wilcoxon signed-rank test. No significant correlations were found.

### 5.2 – Results

Using rabbit no. 1, we systematically compared portions of the signal in the *E* and *C* epochs (using the Wilcoxon signed-rank test) after the signal had been filtered in the frequency domain and in phase space. All reasonable combinations of epoch segment length (window) and location, frequency filtering, and filtering in phase space were considered. We found that %R and %D differed significantly between the *E* and *C* epochs when the frequency filter was set to remove 3, 4, and 8-12 Hz, the EEG window was 300 msec, centered at 250 msec from the beginning of the epoch, and only 85% of the attractor volume was included in the calculation of the recurrence plot. When the conditions thus obtained were applied to rabbit no. 1 the average ( $\pm$ SD) result for %D was  $18.3 \pm 4.6\%$  for the *E* segments (centered at 250 msec, width of 300 msec), compared with  $19.9 \pm 3.4\%$  for the controls (5.25 sec, 300 msec) ( $P < 0.05$ ); the %D in the sham segments ( $20.1 \pm 3.6\%$ , 3.25 sec, 300 msec) did not differ from the controls.

When the portion of the *E* epoch between 0.1-0.4 sec was compared with the similar portion of the *C* epoch (5.1-5.4 sec) in the remaining 9 rabbits using the frequency and phase-space filters identified from the signal of rabbit no. 1, we found that the cell-phone field affected the EEG in every rabbit except rabbit no. 9 (Figure

5.2). The direction of the effect was always to reduce the amount of determinism in the EEG. There were no cases of a false positive result when the *S* (3.1-3.4 sec) and *C* epoch segments were compared using the same filter settings employed for *E* vs. *C*. Each of the experiments was replicated and the results were essentially the same as those found initially, including the failure to find an effect in rabbit no. 9 and the absence of false positive results when *S* and *C* segments were compared.

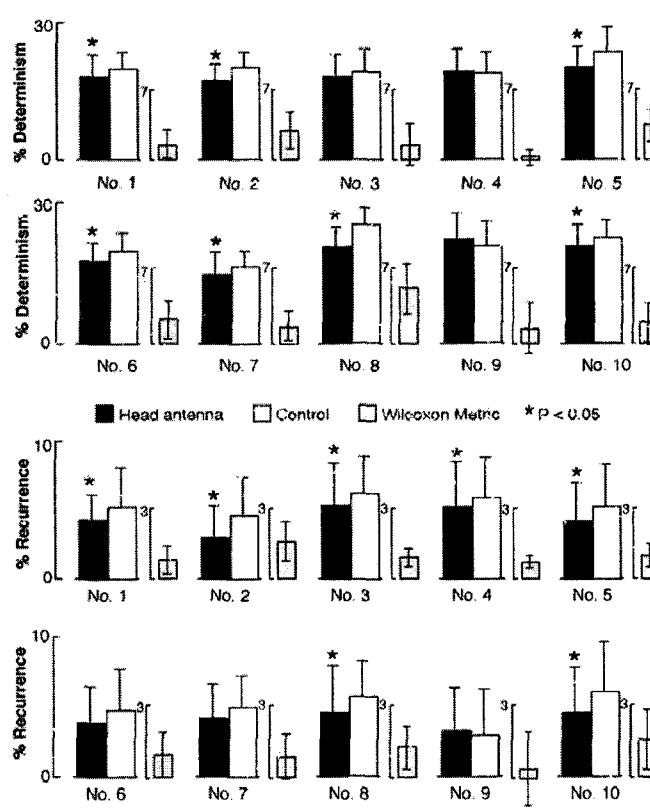


**Figure 5.2:** Effect of cell-phone field on the EEG in 10 rabbits, as assessed using the nonlinear quantifiers, %Determinism and %Recurrence. For each rabbit, a 250-msec segment of the data from each *E* epoch (centered at 250 msec from the beginning of the epoch) was compared with the similar segment of the control epoch in the same trial (N=50). The data was filtered in the frequency domain and in phase space after which the nonlinear quantifiers were calculated from the recurrence plots and compared using the Wilcoxon signed-rank test. The average values ( $\pm$ SD) of the quantifiers are shown. The average and 95% confidence limits of the test metrics are shown for each rabbit in the third bar.

When light was applied as the stimulus, a robust, consistent increase in %D and %R was found in every experiment, using a window of 250 msec centered at 175 msec (Figure 5.3); the frequency and phase-space filters were unnecessary. Again, there were no false positive results.

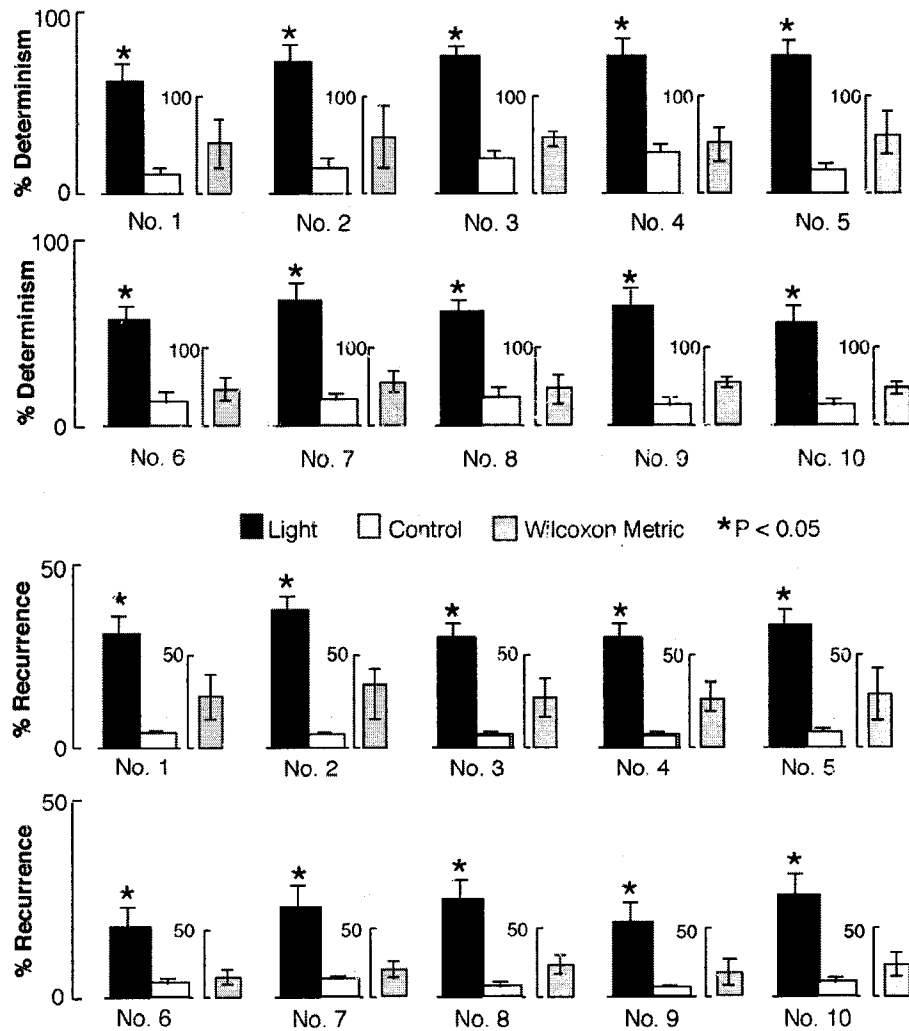


**Figure 5.3:** Effect of light on the EEG in 10 rabbits, as assessed using the nonlinear quantifiers, %Determinism and %Recurrence. For each rabbit, a 250-msec segment of the data from each *E* epoch (centered at 175 msec from the beginning of the epoch) was compared with the similar segment of the control epoch in the same trial ( $N=50$ ). The data was filtered in the frequency domain and in phase space after which the nonlinear quantifiers were calculated from the recurrence plots and compared using the Wilcoxon signed-rank test. The average values ( $\pm$ SD) of the quantifiers are shown. The average and 95% confidence limits of the test metrics are shown for each rabbit in the third bar.

When the head antenna was relocated to the thoracic region, no effect of the field on brain activity was observed (Figure 5.4). After the rabbits were killed and the absence of cardiac activity was verified, the experiments were repeated using the head antenna to evaluate the possibility that the results (Figure 5.2) were due to an interaction of the cell-phone field with the scalp electrodes. The baseline %D and %R measured under this condition essentially reflected the determinism of the output of the EEG amplifier in the absence of an input, which was near zero; no change was seen when the cell-phone field was presented (Figure 5.5).

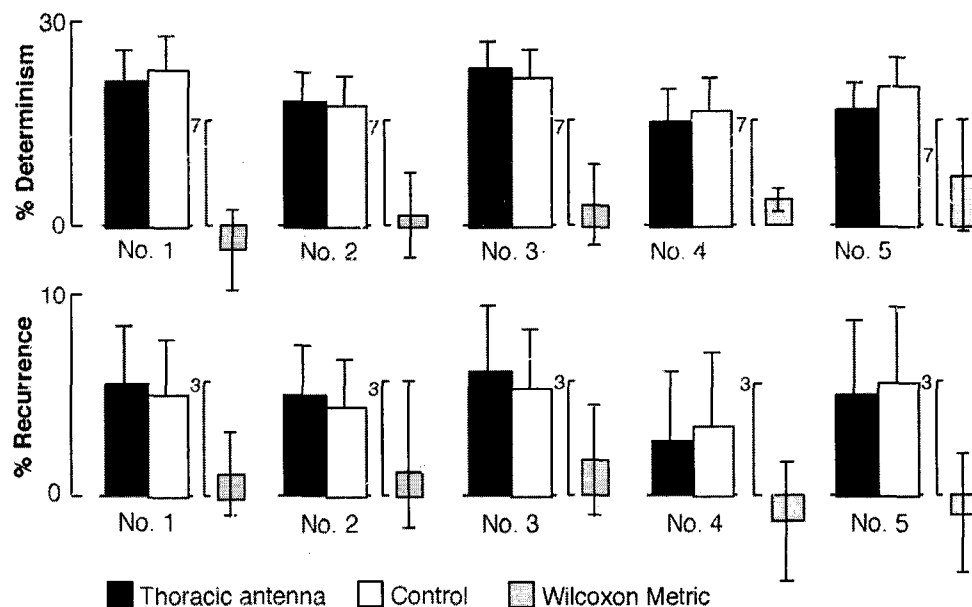


**Figure 5.4:** Effect of relocating the head antenna to the thoracic region, 1 cm from the rabbit, as assessed using the nonlinear quantifiers, % Determinism and % Recurrence. For each rabbit, a 250-msec segment of the data from each *E* epoch (centered at 250 msec from the beginning of the epoch) was compared with the similar segment of the control epoch in the same trial (N=50). The data was filtered in the frequency domain and in phase space after which the nonlinear quantifiers were calculated from the recurrence plots and compared using the Wilcoxon signed-rank test. The average values ( $\pm$ SD) of the quantifiers are shown. The average and 95% confidence limits of the test metrics are shown for each rabbit in the third bar.

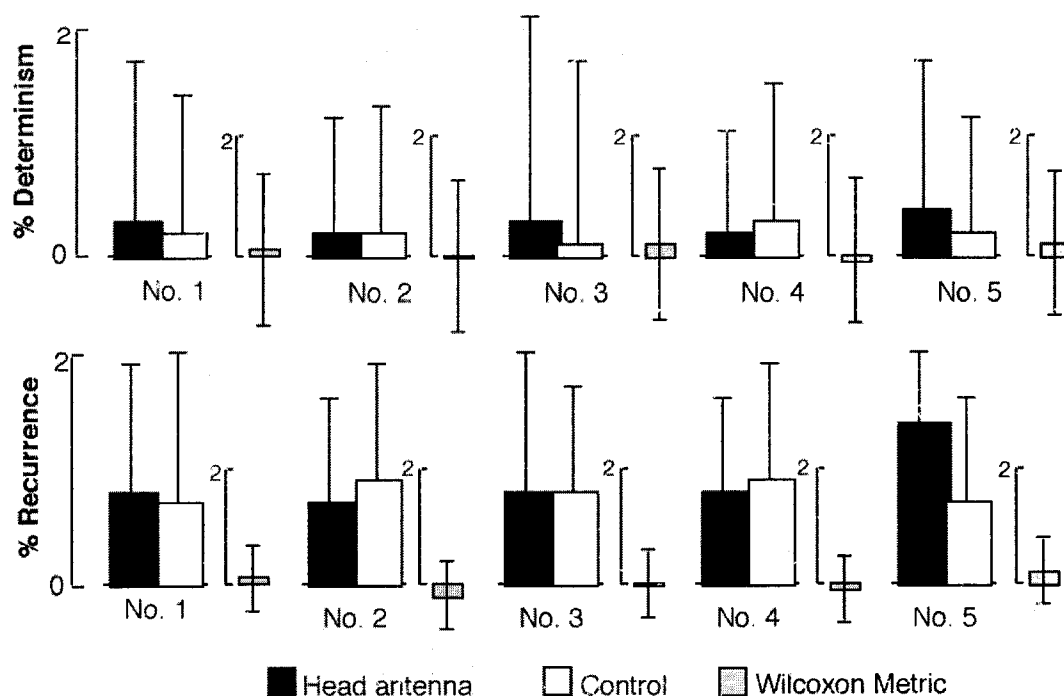


**Figure 5.5:** Results of control experiments performed on dead rabbits, as assessed, using the nonlinear quantifiers, %Determinism and %Recurrence. For each rabbit, a 250-msec segment of the data from each *E* epoch (centered at 250 msec from the beginning of the epoch) was compared with the similar segment of the control epoch in the same trial ( $N=50$ ). The data was filtered in the frequency domain and in phase space after which the nonlinear quantifiers were calculated from the recurrence plots and compared using the Wilcoxon signed-rank test. The average values ( $\pm$ SD) of the quantifiers are shown. The average and 95% confidence limits of the test metrics are shown for each rabbit in the third bar.

### 5.3 – Discussion

Because the brain is a dynamical organ, the earliest signs of impairment of its activity would be expected to be reflected in its functional properties, an outstanding example of which is the EEG. In nine of 10 independent experiments, the EEG recorded during exposure to the cell-phone field was found to differ significantly from the EEG recorded during field-free intervals (*E* versus *C*). No significant differences were found when two field-free intervals were compared (*S* versus *C*). It can therefore be concluded that the consistent pattern of differences between the *E* and *C* epochs was caused by the

field from the cell telephone, and was not somehow a consequence of our statistical method.

Several cogent considerations indicated that the effect on the EEG was a true physiological response, not a physical effect due to an interaction of the field with the electrodes. First, when the experimental conditions were duplicated after the rabbits had been killed, there was essentially no determinism in the voltage measured from the scalp (as expected), and no change in the determinism when the cell-phone field was applied. Any artifactual signal would have been detected under the conditions of the measurement. Second, the changes detected in the EEG were localized to a 300-msec window in the 2-sec exposure epoch. Differences were not observed when the window was located elsewhere. Further, the effects occurred only after a time delay following presentation of the cell-phone field. Both properties of the observations were far better explained under the assumption that they were true physiological responses, because pure physical effects would likely have occurred immediately upon presentation of the field and lasted throughout its presentation. Third, the cell-phone signal was designed by the manufacturer to function within the constraints of a particular digital system and was, therefore, nearly completely deterministic (%R=%D=100). Any putative electrode artifact would therefore have increased the determinism in the measured signal; thus, our observations that the RQA quantifiers decreased can better be attributed to a biological response to the field that manifested itself as a decrease in the determinism of brain electrical activity. We conclude that the field consistently affected brain electrical activity in the rabbits. It seems likely that a similar effect occurs when comparable cell telephones are used by human subjects because the exposure conditions used in the

study mimicked reasonably well those conditions associated with the normal use of a cell telephone.

The cell-phone stimulus resulted in increased randomness, which was opposite to the direction of change caused by light. One possible explanation is that the field was not detected by a specialized sensor as, for example, rhodopsin in the detection of EMFs at light frequencies [60]. EMF frequencies in the 800 MHz band did not exist during evolution (at levels remotely comparable to those in the modern environment), and consequently a specific mechanism to detect 800 MHz fields probably did not develop via natural selection. This may mean that the body's ability to detect cell-phone fields was a consequence of a vulnerability of one or more of the mechanisms evolutionarily chosen to detect other external or internal stimuli, or a vulnerability of one or more mechanisms evolutionarily chosen to process transduced signals. Looked at in this way, cell-phone fields can be said to interfere with normal brain function.

We assumed that the filter settings and window values for revealing a deterministic effect on brain function were identical for all animals. There is no good reason why this should be the case, and it could be argued that the assumption is more suited to a linear model than one derived from nonlinear dynamics. Our assumption might explain why an effect of the field was found in only nine of the 10 independent experiments. It is possible that the brain activity of the non-responding animal was sufficiently different from that of the others as to require individualized filter settings and window values. This is supported by our finding that the power spectrum of the non-responding rabbit was concentrated in the low-frequency region (Table 5.1). Tailoring the filters and window values to the baseline power spectrum of rabbit no. 9

might have revealed an effect of the field on the brain. (A suitable control for such an analysis would consist in the *S* versus *C* comparison.)

**Table 5.1:** Comparison of low-frequency spectral power in rabbit # 9 with that of the other male rabbits.

RABBIT #	SPECTRAL POWER ( $v^2$ )		
	< 3 Hz	< 4 Hz	< 5 Hz
9	14.1	17.0	19.5
6	8.2	10.7	13.0
7	6.7	9.2	11.5
8	7.3	9.6	11.7
10	9.3	11.7	13.7

The United States Federal Communications Commission (FCC) adopted the specific absorption rate (SAR) as a pertinent unit of measurement for assessing the safety of cellular telephones [1, 56, 69, 61]. Importantly, although only telephones operating below the FCC limit are lawful, the agency does not explicitly maintain that such telephones are safe, a term that presently is undefined. The FCC's choices of the SAR and a particular permissible numerical limit (1.6-W/kg) were based on the opinions of expert committees [1, 56]. The experts found no convincing evidence of biological effects due to cell-phone fields and recommended that the regulations be based on concepts of thermal physiology developed in the middle of the last century [13, 69]. It remains an open question whether an EMF that alters brain activity in the manner reported here is safe [1, 61].

The effect of the field was critically dependent on the type of tissue that absorbed the cell-phone energy, as determined by the different results found when the head antenna was relocated to the thoracic region. Under the present SAR regulation, if a gram of fat and a gram of hypothalamus absorb the same amount of energy in the same amount of time, they have the same SAR, irrespective of any physiological consequences [1, 29, 56, 61, 65, 68]. Our finding that the physiological consequences following the absorption of cell-phone energy depended on whether or not it was absorbed by the brain raises the question whether the FCC ought to use the SAR for gauging risk.

In summary, the results showed that radiation from a standard cellular telephone affected the brain electrical activity of rabbits exposed to the radiation under conditions that simulated normal human use of the telephone. The effect was not seen when the possible contribution of the brain to the SAR was minimized.

## CHAPTER 6

### CHANGES IN HUMAN BRAIN ELECTRICAL ACTIVITY DUE TO 60 HZ ELECTROMAGNETIC FIELDS

#### 6.1 - Methods

##### 6.1.1 - Exposure system

Magnetic fields were produced using a pair of coaxial coils, each 130 cm in diameter and consisting of 250 turns of copper wire; the coils were separated by 65 cm (the Helmholtz condition) by means of a wooden frame [7, 54]. The coil current was obtained from a function generator (Model 182A, Wavetek, San Diego, CA) and amplifier (Model 7500, Krohn-Hite, Avon, MA), and controlled by a computer-generated timing signal (Figure 6.1). The subjects sat on a comfortable plastic chair in a dark room with their eyes closed; their sagittal plane was perpendicular to the field produced by the coils. A magnetic field of 1 Gauss, 60 Hz was used; it was uniform to within 5% in the region of the head and upper chest (within 20% over the thorax and pelvis), as measured using a magnetometer (Bartington, MAG-03, GMW, Redwood City, CA). The field strength and frequency were chosen because they can be found in both the general and workplace environments, and are comparable to fields studied previously (Bell et al., 1991; Marino et al., 1996). The EMF was a subliminal stimulus; its presentation was not accompanied by any visual or auditory cues to the

subjects, and consequently the subjects were unaware of the precise times when it was applied. The equipment that controlled the coils and recorded the EEG was located in a room adjacent to that occupied by the subject.

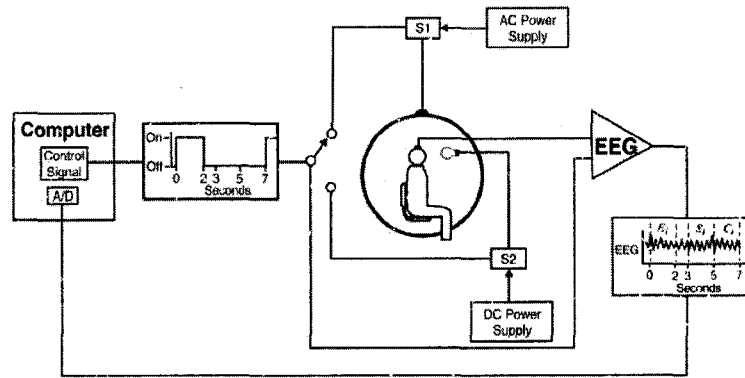


**Figure 6.1:** Schematic representation of the experimental system. A computer-generated timing signal controlled switches for the magnetic field and the light (S1 and S2, respectively). The timing signal was also fed into one of the channels of the EEG amplifier to facilitate identification of the exposed (E), sham (S), and control (C) epochs of the EEG in each trial (the  $i^{\text{th}}$  trial is illustrated). Circle, field-producing coils.

The average 60 Hz background magnetic field at the location of the subject was 0.1 mGauss. The average geomagnetic field at the location of the subject was 432 mGauss, 68.48 below the horizontal. The geomagnetic component along the direction of the 60-Hz field was 156 mGauss.

### 6.1.2 - Human Subjects

Eight clinically normal subjects were studied; their age in years and gender were 27/M, 34/F, 31/M, 18/F, 23/M, 45/F, 29/M, 28/F, for subjects 1--8, respectively. All procedures involving human subjects were reviewed and approved by the Institutional Review Board at our institution, including written informed consent. Scalp electrodes (Grass Instruments Co., Quincy, MA) were attached at C3, C4, P3, P4, O1, and O2 (International 10–20 system) and referred to linked ears; the ground was placed on the

forehead. The electrode impedances (measured before and after recording the EEG (EZM5, Grass Instruments)) were always less than 3 k $\Omega$ .

### 6.1.3 - Procedure

The EEG was detected using an amplifier capable of resolving 0.1  $\mu$ V (Model 4400, Nihon Kohden, Irvine, CA), subjected to analog filtering to pass 0.5 – 35 Hz, digitized at 512 Hz (12 bit), and stored on a computer hard-drive. Frequencies above 35 Hz were at least 40 db below the strongest frequency in the 0.3 – 35 Hz range.

We chose an intra-subject design because of its greater sensitivity, compared with an inter-subject design. The subject underwent a series of trials, each of which consisted of the application of the field for 2 s (E epoch), followed by a stimulus-free period of 5 s. The EEG signal was measured throughout each trial; the portion of the signal from the last 2 s of each trial was used as the control (C epoch) for the corresponding E epoch, and the existence of an effect due to the EMF was determined by comparing E versus C. In addition, as a control procedure, the signal from the 2 s preceding the C epoch was defined as the sham (S epoch) and was analyzed (S versus C) to evaluate the possibility of false positive results attributable to our analytical method. A minimum of 60 trials were run. As a positive control procedure, a second set of identical trials was carried out during the same experimental session using light as the stimulus (2 s on, 5 s off during each trial). The light source was mounted at eye level and produced less than 50 lumens at the corneal surface of the eye; it could be seen by the subjects even though their eyes were closed. The rise-times of the current through the coils and the light source were approximately 1 ms.

#### 6.1.4 - EEG Analysis

Trials that contained any movement artifacts as assessed by visual inspection of the graphical record were removed from the recorded signal. The remaining time series, which consisted of voltages at discrete times, was embedded in phase space; an embedding dimension of 5 and a time delay of 1 were chosen during preliminary analysis of the data on the basis that they resulted in the most sensitive characterizations of the EEG epochs. The result of the embedding procedure was a geometrical representation of the evolution of the system's state vector.

To quantify the phase-space appearance of the state vector, we produced 2-dimensional recurrence plots consisting of points that each corresponded to a pair of state vectors that were near one another; two states were defined as near only if both were contained within a 5-dimensional sphere having a radius less than 15% of the minimum radius such that all points were near. The recurrence plot was quantified using percent recurrence (%R) (which is the correlation sum evaluated at the chosen scale (15%)) and percent determinism (%D). %R was defined as the number of recurrent points divided by the possible number of recurrent points. %D was defined as the number of recurrent points located on lines parallel to the main diagonal of the plot, divided by the number of recurrent points. Calculation of %R and %D was carried out using software provided by Webber [82] and independently verified using a custom code MATLAB (Mathworks, Natick, MA).

#### 6.1.5 - Statistics

In preliminary studies we observed that the effect of the stimuli did not occur uniformly throughout the 2 s intervals in which they were presented. To maximize

the likelihood of detecting a difference between corresponding E and C epochs, we followed a systematic procedure aimed at isolating the epoch segments most affected by the stimulus. Using the EEG from subject no. 1, corresponding epoch segments (windows) were used to compare E versus C, and S versus C. Essentially all possible window parameters were considered, and those that yielded the lowest probability (P) for the comparison (using the t test) of E versus C when  $P > .05$  for S versus C were then applied prospectively to evaluate the effect of the stimuli on %R and %D in the remaining 7 subjects. In instances where 6 statistical tests were performed on the subject (calculation of %R for each of 6 electrodes), the criterion for accepting the conclusion that an event-related change in scalp potential actually occurred was that the MF resulted in at least two significant differences ( $P, 0:05$ ). It can be shown using the binomial theorem that this condition was sufficient to eliminate ( $P = .05$ , overall) the possibility of a family-wise error regarding rejection of the null hypothesis; all statistical calculations done with MINITAB (Minitab, State College, PA).

In each statistical test, the first 5 trials were discarded and the next 50 artifact-free trials were used to compare the values of the nonlinear quantifiers, using the t test. The data are presented in terms of the mean  $\pm$  SD of %R and %D; the tests involving the two quantifiers were regarded as independent planned comparisons.

A Durbin Watson test (MINITAB, Minitab, State College, PA) was performed to check for serial correlations across the pairs used in the two independent sample test. No significant correlations were found. Because of concerns regarding violation of the

independence assumption the two independent sample t-test, a Wilcoxon signed-rank test was later performed on the data. The results of each test were equivalent.

## 6.2 – Results

Recurrence plots constructed from the EEG (Figure 6.2A) were similar to the complex two-dimensional patterns typical of physiological time series [17, 33, 37, 53, 63, 75, 80, 81, 83, 84] and chaotic deterministic systems such as the Lorenz system [85]. The essential feature of the plots was that their texture resulted directly from the dynamical electrical activity of the brain; when the dynamical correlations in the EEG were reduced by randomizing the signal (Figure 6.2B), the mean and standard deviation of the resulting signal were unchanged but %R and %D decreased, indicating that the parameters characterized the determinism in the EEG more completely than did the mean and standard deviation.

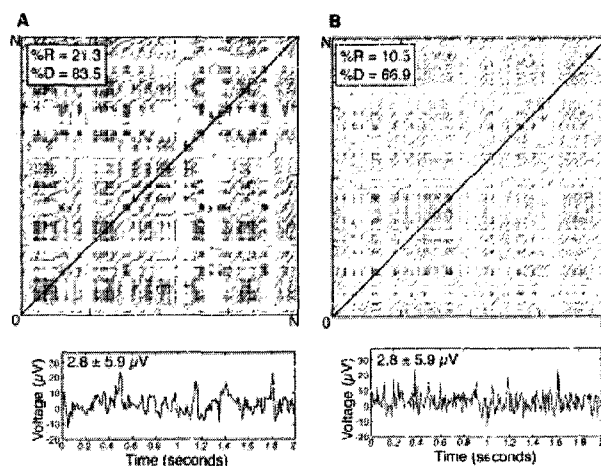


**Figure 6.2:** Recurrence plots produced from 2 s of EEG data derived from an occipital electrode. The plots are symmetrical about the diagonals, which were added. (A) Original EEG (bottom) and associated plot (top). (B) Signal formed by randomizing the EEG (bottom); the recurrence plot (top) of the randomized signal is less deterministic than the plot for the original EEG (A, top). Recurrent points form distinct patterns characterized by %R and %D which, unlike the mean and standard deviation, are sensitive to nonlinear determinism present in the signal. N is the recurrent point index.

The EMF was detected by each subject as evidenced by the occurrence of statistically significant changes in %R calculated from at least two electrodes in each subject (Figure 6.3). First, the EEG from subject no. 1 measured during the magnetic-field trials was unfolded in phase space, and %R was calculated for corresponding portions of the E and C epochs in each trial. We found that a 190 ms window centered at 215 ms after commencing application of the field yielded the lowest significant P value for E versus C (window centered at 5.215 s, width of 190 ms) when P was not significant for S (3.215 s, width of 190 ms) versus C. When the 190 ms window was shifted to earlier or later times by more than 30 ms, the E versus C comparison was not significant, indicating that the subject's response started at about 160 ms. The window width and location thus determined were then applied prospectively to 7 additional subjects, in 7 independent experiments, to ascertain the effect of exposure to the EMF, and statistically significant differences in %R were found in each experiment (Figure 6.3). Significant differences were also found in %D for each subject, particularly at the occipital electrodes (Figure 6.4), again indicating that the EMF was detected by each subject. There were no false positive differences (S versus C) from any electrode for either %R or %D (data not shown). Also, during sham experiments in which the coils were not energized during the E epochs, there were no significant differences in sham E versus C (not shown).

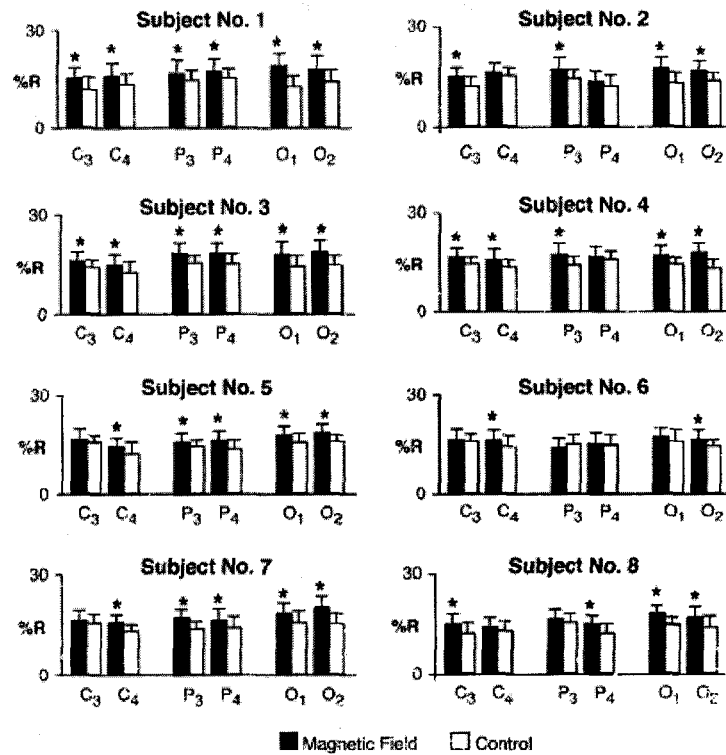


**Figure 6.3:** Effect of magnetic-field exposure on the EEG derived from central, parietal, and occipital electrodes, assessed using %R. The window (width of 190 ms) for comparison of the exposed and control epochs was centered at 215 ms from the beginning of the epoch. The average values ( $\pm$ SD) of the quantifiers are shown, \*P < .05

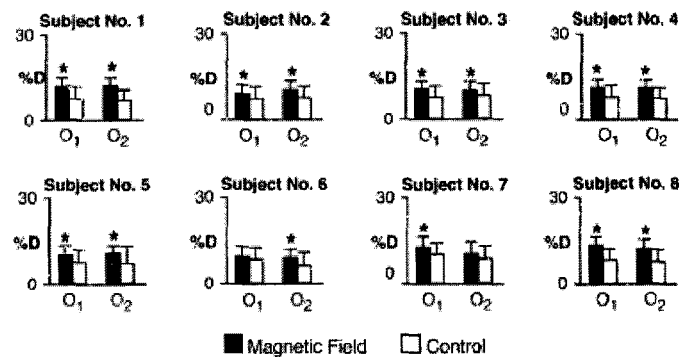


**Figure 6.4:** Effect of magnetic-field exposure on the EEG derived from occipital electrodes, assessed using %D. The window (width of 190 ms) for comparison of the exposed and control epochs was centered at 215 ms from the beginning of the epoch. The average values ( $\pm$ SD) of the quantifiers are shown, \*P < .05.

Light was also detected by the subjects, as evidenced by the large increases in %R and %D that occurred at each occipital electrode during the presentation of the stimulus. As previously, the optimal window parameters were determined using subject no. 1 (190 and 175 ms for width and center-location, respectively) and were used prospectively for the remaining subjects, all of which reacted strongly to presentation of the light. Representative results from two subjects are shown in Figure 6.5; there were no cases of a false positive result (not shown).

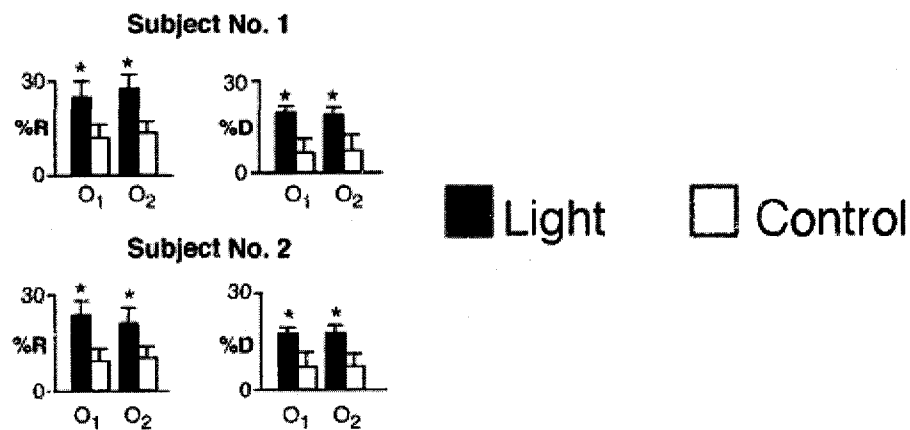


**Figure 6.5:** Effect of a light stimulus on the EEG derived from occipital electrodes, assessed using %R and %D. The window (width of 190 ms) for comparison of the light and control epochs was centered at 175 ms from the beginning of the epoch. The average values ( $\pm$ SD) of the quantifiers are shown, \*P < .05

### 6.3 - Discussion

We assumed that a method of analyzing the EEG that did not parse its activity into linear and nonlinear parts but rather characterized the determinism actually present in the signal would facilitate detection of the effects of EMFs. Based on that assumption, we used a novel analytical method to compare the EEG within individual subjects in the presence and absence of the field. In each subject, %R and %D calculated from the occipital EEG at 120–310 ms from the onset of

field presentation were altered, compared with the respective controls. No false positive comparisons were found when the same mathematical procedures were used to compare sham-exposed and control segments, indicating that neither our analytical method nor nonstationarity in the EEG could explain the results.

Several lines of evidence indicated that the field-induced alterations in the EEG reflected a true physiological response, and not solely a physical effect due to the interaction of the field with the electrodes. First, any physical effect would have been expected to begin at  $t \sim 0$  sec, because the rise-time of the current that produced the magnetic fields was practically nil. However, the observed response commenced 120 ms after the beginning of the E epoch; such a delay could be explained by a detection process in the nervous system that included an afferent signal, some processing of the information in the brain, and electrotonic propagation of that brain activity to the scalp electrodes. Second, the EEG changes induced by both the field and the light occurred only after a similar delay. Because of the great difference in frequency between the two stimuli, the occurrence of a similar delay was better explained by assuming that both changes were physiological, rather than by assuming that two electromagnetic fields which differed greatly in frequency had produced the same kind of physical effect. Third, field-induced EEG changes identical to those described here were observed in rabbits (Chapter 4), but the effect disappeared when the measurements were made after the animals had been killed, suggesting that a passive interaction with the field could not explain the statistical differences we found here between the EEG measured in the presence and absence of the field.

It could be argued that the effects of EMF exposure might persist beyond the 2 s exposure epoch, and that therefore the choice of the control was inappropriate. However, the E and C epochs differed significantly, indicating that any persistent effect due to EMF exposure did not prevent us from establishing the occurrence of an effect due to the field. Moreover, all comparisons of S versus C were statistically insignificant, implying that the EEG returned to its pre-exposure baseline within 3 s after termination of EMF exposure. Based on these considerations, and those above, we conclude that the 1 Gauss, 60 Hz field was transduced by each of the subjects, resulting in a change in brain electrical activity.

## CHAPTER 7

### CONSISTENT EMF EEG EFFECTS

The pattern of positive and negative reports is pervasive throughout all of EMF biology, as evidenced by the fact that no specific putative EMF-induced bioeffect has been conclusively proved or disproved [59]. It was conjectured that the pattern exhibited by the EMF reports could be understood as resulting from the use of linear methods to analyze activity governed by nonlinear laws. In particular, a mismatch between the dynamical activity of the system and the method used to analyze it could account for the lack of consensus regarding the effects of EMFs on the EEG.

The goal of this work was to show that detection of weak and environmentally-relevant EMFs occurred in each subject in a representative test group. To accomplish this purpose, the EEG was compared within individual subjects obtained during the presence and the absence of an EMF, using a new method of analysis that was capable of capturing both linear and nonlinear effects that might be present.

Other studies have described effects of electromagnetic fields on brain electrical activity [12, 21, 36, 50, 67, 45]. The novel aspect of our research is the consistency with which a deterministic response to the field in the EEG was detected. There are no previous reports of a similar consistent effect of a weak EMF on brain activity. This

suggests that the ability to detect low-strength, environmental EMFs is a universal property of the animal and human nervous system.

## APPENDIX A

### NUMERICAL INTEGRATION OF THE LORENZ SYSTEM

```
% Numerical integration of the Lorenz system
% Erik A. Nilsen, 9/13/2000

% Model parameters
sigma = 10;
r     = 28;
b     = 8/3;

% Initial conditions
x0    = -9;
y0    = -11;
z0    = 24;

% Length of integration
t_end = 40;

% Integrate the system using fourth-order Runge-Kutta
[t, v] = ODE45('lorenzsystemode', t_end, [x0,y0,z0], [], sigma, r, b);

% Split out the trajectory matrix into x,y,z vector variables
x = v(:, 1);
y = v(:, 2);
z = v(:, 3);

% Plot trajectory in 3D state-space
figure;
plot3(x, y, z, 'b-');
title('Lorenz state space');
xlabel('x(t)');
ylabel('y(t)');
zlabel('z(t)');
grid on;
rotate3d on;
```

```
view([37,26]);

% Display time series plots
figure;
subplot(3,1,1);
plot(t, x, 'b-');
title('Lorenz time series');
xlabel('t');
ylabel('x(t)');

subplot(3,1,2);
plot(t, y, 'b-');
xlabel('t');
ylabel('y(t)');

subplot(3,1,3);
plot(t, z, 'b-');
xlabel('t');
ylabel('z(t)');

% Now find next maxima to create next-maximum map of z(t)
max_points = find((z(2:end-1) > z(3:end)) & (z(2:end-1) > z(1:end-2))) + 1;
z_max      = z(max_points);
t_max      = t(max_points);

% Plot next-maximum map
figure;
plot(z_max(1:end-1), z_max(2:end), 'r. ');
title('Lorenz next maximum map');
xlabel('z_{max}(n)');
ylabel('z_{max}(n+1)');
```

## APPENDIX B

### CALCULATION OF THE WILCOXON SIGNED RANK STATISTIC

```
function [p, h] = signrankp(x,y,alpha)
%SIGNRANK Wilcoxon signed rank test of equality of means for
%comparing samples of unequal size.
%Erik A. Nilsen, 5/13/1999
% p = signrank(x,y,alpha) returns the significance probability
% that the means of two samples, x and y are equal.
% x and y need not be vectors of equal length. alpha is the desired
% level of significance and must be a scalar between
% zero and one.
%
% [p, h] = signrank(x,y, alpha) also returns the result of the
% hypothesis test, H. H is zero if the difference in means of
% x and y is not significantly different from zero. H is one if
% the two means are significantly different.
%
% p is the probability of observing a result equally or more
% extreme than the one using the data (x and y) if the null
% hypothesis is true. If p is near zero, this casts doubt on
% this hypothesis.
%
% Currently works for sample sizes > 25.

if nargin < 3
    alpha = 0.05;
end
```

```

[rowx, colx] = size(x);
[rowy, coly] = size(y);

if min(rowx,rowy) < 25
    error('SignRankP currently only works for sample sizes > 25');
end

if min(rowx, colx) ~= 1 | min(rowy,coly) ~= 1,
    error('SIGNRANK requires vector data.');
```

```

end
if rowx == 1
rowx = colx;
    x = x';
end
if rowy == 1,
    rowy = coly;
    y = y';
end

if rowx == rowy,
    [p, h] = signrank(x,y,alpha);
    return
end

CombinedSample = [x;y];
CombinedSample(:,2) = Order(CombinedSample,2); % returns rank adjusted for non-
uniqueness in 2nd col
RankedX = CombinedSample(1:rowx, 1:2);
RankedY = CombinedSample(rowx+1:rowx+rowy, 1:2);
if rowx < rowy
    T1 = sum(RankedX(:,2));
    T2 = rowx*(rowx + rowy + 1) - T1;
    T = min(T1,T2);
    MuT = rowx*(rowx+1)/4;
    SigmaT = (rowx*(rowx+1)*(2*rowx+1)/24)^.5;
    ZStat = (T-MuT)/SigmaT;
else
    T1 = sum(RankedY(:,2));
    T2 = rowy*(rowx + rowy + 1) - T1;
    T = min(T1,T2);
    MuT = rowy*(rowy+1)/4;
    SigmaT = (rowy*(rowy+1)*(2*rowy+1)/24)^.5;
    ZStat = (T-MuT)/SigmaT;
end
end

```

```

p = 1-normcdf(abs(ZStat));

if l==2 %this part from singrank is not used
diffxy = x - y;
nodiff = find(diffxy == 0);
diffxy(nodiff) = [];
n = length(diffxy);
[sd, rowidx] = sort(abs(diffxy));
neg = find(diffxy<0);

invr(rowidx) = 1:n; % invr is the inverse of rowidx.
w = sum(invr(neg));
w = min(w, n*(n+1)/2-w);

if n > 15,
    z = (w-n*(n+1)/4)/sqrt(n*(n+1)*(2*n+1)/24);
    p = 2*normcdf(z,0,1);
else
    allposs = (ff2n(n));
    idx = (1:n)';
    idx = idx(:,ones(2.^n,1));
    pranks = sum(allposs.*idx);
    tail = 2*length(find(pranks < w))+length(find(pranks == w)); % two side.
    p = tail./(2.^n);
end
end

if nargout == 2,
    h = (p<alpha);
end

```

## APPENDIX C

### COMPUTATION OF THE LOGISTIC MAPPING

```
% This program computes the evolution of the logistic map
% Erik A. Nilsen, 5/10/1999

% how many iterations
N = 100;

% how many iterations should be skipped to remove the transient effects
Ntrans = 25;

% in here we will store the computed values
s = zeros(1,N);

%initial condition of the map
s(1) = 0.5;

% this is the iteration of the map
for cnt= 2:N
    s(cnt) = R*s(cnt-1)*(1-s(cnt-1));
end;

% plot the sequence of the values
figure(1);
plot(s,'o-');

% and a recurrence plot ("transients removed")
figure(2);
plot(s(Ntrans:end-1),s(Ntrans+1:end),'.');
```

## BIBLIOGRAPHY

1. American National Standards Institute. *Safety levels with respect to human exposure to radio frequency electromagnetic fields, 3 kHz–300 GHz*. ANSI/IEEE 1992; C95.1-D69.62.
2. Babloyantz A, Destexhe A. *Low-dimensional chaos in an instance of epilepsy*. Proc Natl Acad Sci 1986; 83:3513–3517.
3. Bawin SM, Satmary WM, Jones RA, Adey WR, Zimmerman G. *Extremely-low-frequency magnetic fields disrupt rhythmic slow activity in rat hippocampal slices*. Bioelectromagnetics 1996; 17:388–395.
4. Bawin SM, Sheppard AR, Mahoney MD, Adey WR. *Influences of sinusoidal electric fields on excitability in the rat hippocampal slice*. Brain Res 1984; 323:227–237.
5. Bawin SM, Sheppard AR, Mahoney MD, Abuassal M, Adey WR. *Comparison between the effects of extracellular direct and sinusoidal currents on excitability in hippocampal slices*. Brain Res 1986; 362:350–354.
6. Becker RO, Marino AA. Electromagnetism & life. Albany: State University of New York Press 1982.
7. Bell GB, Marino AA. *Exposure system for the production of uniform magnetic fields*. J Bioelectricity 1989; 8:147–158.
8. Bell AA, Marino AA, Chesson AL. *Frequency-specific responses in the human brain caused by electromagnetic fields*. J Neurol Sci 1993; 123:26–32.
9. Bell GB, Marino AA, Chesson AL. *Alterations in brain electrical activity caused by magnetic fields: Detecting the detection process*. Electroencephalogr Clin Neurophysiol 1992; 83:389–397.
10. Bell GB, Marino AA, Chesson AL. *Frequency-specific blocking in the brain caused by electromagnetic fields*. Neuroreport 1992; 5:510–512.
11. Bell GB, Marino AA, Chesson AL, Struve F. *Electrical states in the rabbit brain can be altered by light and electromagnetic fields*. Brain Res 1992; 570:307–315

12. Bell GB, Marino AA, Chesson AL, Struve F. *Human sensitivity to weak magnetic fields*. Lancet 1991; 338:1521–1522.
13. Pattishall EG, editor. *Biological effects and exposure criteria for radiofrequency electromagnetic fields*. NCRP Report No. 86 1957; Bethesda, MD.
14. Borbely AA, Huber R, Graf T, Fuchs B, Gallmann E, Achermann P. *Pulsed high-frequency electromagnetic field affects human sleep and sleep electroencephalogram*. Neurosci Lett 1999; 275:207–210.
15. Bullock TH, Heiligenberg W, editors. Electroreception. New York Wiley Press 1986.
16. Carpenter DO, Ayrapetyan S, editors. Biological effects of electric and magnetic fields: sources and mechanisms. New York Academic Press 1994.
17. Censi F, Calcagnini G, Cerutti S. *Coupling patterns between spontaneous rhythms and respiration in cardiovascular variability signals*. Comput Methods Programs Biomed 2002; 68:37–47.
18. Cook CM, Thomas AW, Prato FS. *Human electrophysiological and cognitive effects of exposure to ELF magnetic and ELF modulated RF and microwave fields: a review of recent studies*. Bioelectromagnetics 2002; 23:144–157.
19. Cook MR, Graham C, Cohen HD, Gerkovich MM. *A replication study of human exposure to 60-Hz fields: effects on neurobehavioral measures*. Bioelectromagnetics 1992; 13:261–285.
20. Crasson M, Legros JJ, Scarpa P, Legros W. *50 Hz magnetic field exposure influence on human performance and psychophysiological parameters: two double-blind experimental studies*. Bioelectromagnetics 1999; 20:474–486.
21. Dobson J, St. Pierre TG, Schultheiss-Grassi PP, Wieser HG, Kuster N. *Analysis of EEG data from weak-field magnetic stimulation of mesial temporal lobe epilepsy patients*. Brain Res 2000; 868:386–391.
22. Duong DH, Chang T. *The influence of electric fields on the epileptiform bursts induced by high potassium in CA3 region of rat hippocampal slice*. Neurol Res 1998; 20:542–548.
23. Eckmann J-P, Kamphorst SO, Ruelle D. *Recurrence plots of dynamical systems*. Europhys Lett 1987; 4:973–979.
24. Elbert T, Ray WJ, Kowalik ZJ, Skinner JF, Graf KE, Birbaumer N. *Chaos and physiology: Deterministic chaos in excitable cell assemblies*. Physio Rev 1994; 74:1–47.

25. Eulitz C, Ullsperger P, Freude G, Elbert T. *Mobile phones modulate response patterns of human brain activity.* Neuroreport 1998; 9:3229–3232.
26. Fell J, Mann K, Roschke J, Gopinathan MS. *Nonlinear analysis of continuous EEG during sleep.* Biol Cybern 2000; 82:477–483.
27. Filligoi G, Felici F. *Detection of hidden rhythms in surface EMG signals with a non-linear time-series tool.* Med Eng Phys 1999; 21:439–448.
28. Fisher K, Coderre TJ, Hagen NA. *Targeting the N-methyl-D-aspartate receptor for chronic pain management: Preclinical animal studies, recent clinical experience and future research directions.* J Pain Symptom Manage 2000; 20:358–373.
29. Freude G, Ullsperger P, Eggert S, Ruppe I. *Effects of microwaves emitted by cellular phones on human slow brain potentials.* Bioelectromagnetics 1998; 19:384–387.
30. Gartzke J, Lange K. *Cellular target of weak magnetic fields: ionic conduction along actin filaments of microvilli.* Am J Physiol Cell Physiol 2002; 283:C1333–C1346.
31. Gavalas RJ, Walter DO, Hamer J, Adey WR. *Effect of low-level, low-frequency electric fields on EEG and behavior in Macaca nemestrina.* Brain Res 1970; 18:491–501.
32. Gluckman BJ, Neel EJ, Netoff TI, Ditto WL, Spano ML, Schiff SJ. *Electric field suppression of epileptiform activity in hippocampal slices.* J Neurophysiol 1996; 76:420–426.
33. Gonzalez JJ, Cordero JJ, Feria M, Pereda E. *Detection and sources of nonlinearity in the variability of cardiac R-R intervals and blood pressure in rats.* Am J Physiol Heart Circ Physiol 2000; 279:H3040–H3046.
34. Graham C, Cook MR, Cohen HD, Gerkovich MM. *Dose response study of human exposure to 60 Hz electric and magnetic fields.* Bioelectromagnetics 1994; 15:447–463.
35. Graham C, Cook MR. *Human sleep in 60 Hz magnetic fields.* Bioelectromagnetics 1999; 20:277–283.
36. Heusser K, Telschaft D, Thoss F. *Influence of an alternating 3-Hz magnetic field with an induction of 0.1 mT on chosen parameters of a human occipital EEG.* Neurosci Lett 1997; 239:57–60.

37. Ikegawa S, Shinohara M, Fukunaga T, Zbilut JP, Webber Jr. CL. *Nonlinear time course of lumbar muscle fatigue using recurrence quantifications.* Biol Cybern 2000; 82:373–382.
38. Jenrow KA, Zhang X, Renehan WE, Liboff AR. *Weak ELF magnetic field effects on hippocampal rhythmic slow activity.* Exp Neurol 1998; 153:328–334.
39. Jeong J, Chae J-H, Kim SY, Han S-H. *Nonlinear dynamic analysis of the EEG in patients with Alzheimer's disease and vascular dementia.* J Clin Neurophysiol 2001; 18:58–67.
40. Kamitani Y, Shimojo S. *Manifestation of scotomas created by transcranial magnetic stimulation of human visual cortex.* Nat Neurosci 1999; 2:767–771.
41. Kantz H, Schreiber T. Nonlinear Time Series Analysis. Cambridge University Press 1997.
42. Krause CM, Sillanmaki L, Koivisto M, Haggqvist A, Saarela C, Revonsuo A, Laine M, Hamalainen H. *Effects of electromagnetic field emitted by cellular phones on the EEG during a memory task.* NeuroReport 2000; 11:761–764.
43. Krystal AD, Greenside HS, Weiner RD, Gassert D. *A comparison of EEG signal dynamics in waking after anesthesia induction and during electroconvulsivetherapy seizures.* Electroencephalogr Clin Neurophysiol 1996; 99:129–140.
44. Lazeyras F, Zimine I, Blanke O, Perrig SH, Seeck M. *Functional MRI with simultaneous EEG recording: Feasibility and application to motor and visual activation.* J Magn Reson Imaging 2001; 13:943–948.
45. Lyskov E, Sandstrom M, Mild KH. *Provocation study of persons with perceived electrical hypersensitivity and controls using magnetic field exposure and recording of electrophysiological characteristics.* Bioelectromagnetics 2001; 22:457–462.
46. Lyskov EB, Juutilainen J, Jousmaki V, Partanen J, Medvedev S, Hanninen O. *Effects of 45-Hz magnetic fields on the functional state of the human brain.* Bioelectromagnetics 1993; 14:87–95.
47. Mann K, Roschke J. *Effects of pulsed high-frequency electromagnetic fields on human sleep.* Neurophysiology 1996; 33:41–47.
48. Marino AA, Nilsen E, Frilot II C. *Consistent magnetic-field induced changes in rabbit brain activity detected by recurrence quantification analysis.* Brain Res 2002; 951:301–310.
49. Marino AA, Nilsen E, Frilot II C. *Nonlinear changes in brain electrical activity due to cell-phone radiation.* Bioelectromagnetics 2003; 24:339–346.

50. Marino AA, Bell GB, Chesson A. *Low-level EMFs are transduced like other stimuli.* J Neurol Sci 1996; 144:99–106.
51. Marino AA, Wolcott RM, Chervenak R, Jourdeuil F, Nilsen E, Frilot C. *Nonlinear response of the immune system to power-frequency magnetic fields.* Am J Physiol Regul Integr Comp Physiol 2000; 279:R761–R768.
52. Marino AA, Wolcott RM, Chervenak R, Jourdeuil F, Nilsen E, Frilot C II. *Nonlinear dynamical law governs magnetic field induced changes in lymphoid phenotype.* Bioelectromagnetics 2001; 22:529–546.
53. Marwan N, Wessel N, Meyerfeldt U, Schirdewan A, Kurths J. *Recurrence-plot-based measures of complexity and their application to heart-rate-variability data.* Phys Rev E 2002; 66:202-208.
54. Merritt R, Purcell C, Stroink G. *Uniform magnetic field produced by 3, 4, and 5 square coils.* Rev Sci Instrum 1983; 54:879–882.
55. Micheloyannis S, Flitzanis N, Papanikolaou E, Bourkas M, Terzakis D, Arvanitis S, Stam CJ. *Usefulness of non-linear EEG analysis.* Acta Neurol Scand 1998; 97:13–19.
56. National Council on Radiation Protection and Measurements. New York Press 1986.
57. Mittleman RE, Hearn WL, Hime GW. *Xylazine toxicity-literature review and report of two cases.* J Forensic Sci 1998; 43:400–402
58. Mohr E, Langbein J, Nurnberg G. *Heart rate variability: a noninvasive approach to measure stress in calves and cows.* Physiol Behav 2002; 75:251–259.
59. Portier CJ, Wolfe MS. *Assessment of health effects from exposure to power-line frequency electric and magnetic fields.* NIH Health Report 1998.
60. Presman AS. Electromagnetic fields and life. New York Plenum 1970.
61. Proceedings of Tri-Service conference on biological hazards of microwave radiation. Report No. AD115603. Alexandria, VA: Documentation Center for Scientific and Technical Information, Cameron Station.
62. Reiser H, Dimpfel W, Schober F. *The influence of electro-magnetic fields on human brain activity.* Eur J Med Res 1995; 1:27–32.
63. Riley MA, Balasubramaniam R, Turvey MT. *Recurrence quantification analysis of postural fluctuations.* Gait Posture 1999; 9:65–78.

64. Rizzo JF, Miller S, Wyatt JL, Edell D. *Development of a silicon retinal implant: Reproducibility of electrically-evoked visual cortical responses in rabbits.* Invest Ophthalmol Vis Sci 1995; 36:42-64.
65. Roschke J, Mann K. *No short-term effects of digital mobile radio telephone on the awake human electroencephalogram.* Bioelectromagnetics 1997; 18:172-176.
66. Scheich H, Langner G, Tidemann C, Coles RB, Guppy A. *Electroreception and electrolocation in platypus.* Nature 1986; 319:401-402.
67. Schienle A, Stark R, Kulzer R, Klopper R, Vaitl D. *Atmospheric electromagnetism: individual differences in brain electrical response to simulated atmospherics.* Int J Psychophysiol 1996; 21:177-188.
68. Schonborn F, Burkhardt M, Kuster N. *Differences in energy absorption between heads of adults and children in the near field of sources.* Health Phys 1998; 74:160-168.
69. Schwan HP, Piersol G. *The absorption of electromagnetic energy in body tissues.* Am J Phys Med 1957; 33:371-404.
70. Sonnier H, Kolomytkin OV, Marino AA. *Resting potential of excitable neuroblastoma cells in weak magnetic fields.* Cell Mol Life Sci 2000; 57:514-520.
71. Sonnier H, Kolomytkin OV, Marino AA. *Action potentials from neuroblastoma cells in magnetic fields.* Neurosci Lett 2003; 337:163-166.
72. Terao Y, Ugawa Y. *Basic mechanisms of TMS.* J Clin Neurophysiol 2002; 19:322 - 343.
73. Theiler J, Rapp PE. *Re-examination of the evidence for low-dimensional, nonlinear structure in the human electro-encephalogram.* Electroencephalogr Clin Neurophysiol 1996; 98:213-222.
74. Theiler J, Eubank S, Longtin A, Galdrikian B, Farmer JD. *Testing for nonlinearity in a time series; the method of surrogate data.* Physica D 1992; 58:77-94.
75. Trzebski A, Smietanowski M, Zebrowski J. *Repetitive apneas reduce nonlinear dynamical complexity of the human cardiovascular control system.* J Physiol Pharmacol 2001; 52:3-19.
76. Vorobyov VV, Galchenko AA, Kukushkin NI, Akoev IG. *Effects of weak microwave fields amplitude modulated at ELF on EEG of symmetric brain areas in rats.* Bioelectromagnetics 1997; 18:293-298.

77. Vorobyov VV, Sosunov EA, Kukushkin KI, Lednev VV. *Weak combined magnetic field affects basic and morphine-induced rat's EEG*. Brain Res 1998; 781:182–187.
78. Wagner P, Roschke J, Mann K, Fell J, Hiller W, Frank C, Grozinger M. *Human sleep EEG under the influence of pulsed radio frequency electromagnetic fields*. Neuropsychobiology 2000; 42:207–212.
79. Wagner P, Roschke J, Mann K, Hiller W, Frank C. *Human sleep under the influence of pulsed radiofrequency electromagnetic fields: A polysomnographic study using standardized conditions*. Bioelectromagnetics 1998; 19:199–202.
80. Webber Jr. CL. *Rhythmogenesis of deterministic breathing patterns*. Haken H, Koepchen H-P, editors. Rhythms in biological systems. Berlin: Springer 1991; 171–191.
81. Webber Jr. CL, Schmidt MA, Walsh JM. *Influence of isometric loading on biceps EMG dynamics as assessed by linear and nonlinear tools*. J Appl Physiol 1995; 78:814–822.
82. Webber Jr. CL. 1998; <http://homepages.luc.edu/cwebber>.
83. Webber Jr. CL, Zbilut JP. *Dynamical assessment of physiological systems and states using recurrence plot strategies*. J Appl Physiol 1994; 76:965–973.
84. Zbilut JP, Webber Jr. CL. *Embeddings and delays as derived from quantification of recurrence plots*. Phys Lett A 1992; 171:199–203.
85. Lorenz E. *Deterministic non-periodic flow and extreme sensitivity of weather models*. J Atmos Sci 1969; 26:636–646.
86. Priestly MB. Time Series Analysis. Springer Press 1980.
87. Takens F. Dynamical Systems and Turbulence. Berlin: Springer 1981.